

Influence of biofilms on the transport of colloids and contaminants through porous media

Vom Fachbereich Chemie
der Universität Duisburg-Essen

zur Erlangung des akademischen Grades eines
Doktors der Naturwissenschaften
genehmigte Dissertation

von
Carlos Felipe Leon Morales
aus
Bogotá, Kolumbien

Datum der Einreichung: 21.12.2007
Tag der Prüfung: 08.04.2008

Referent: Prof. Dr. H.-C. Flemming
Korreferenten: Prof. Dr. U. Förstner
PhD Dr. I. Beech

to Mariël...

Acknowledgments

Here I would like to thank all the persons that in one way or another were involved with me during this investigation. First of all I'm very thankful to all the technicians and fellow PhD students from the Biofilm Centre for their patience and helpfulness when I needed to find my way in a completely new environment. It was hard at times, but overall, it was a wonderful experience to have shared an important part of my professional life with all of you.

To Prof. Hans-Curt Flemming I'm grateful for this great opportunity in a subject that was new for me but from which I learned a lot. I'm thankful for his trust and the continuous willing to count with me on new challenges.

I'm grateful to Prof. Ulrich Förstner for accepting the task of being my co-adviser and for friendly and useful discussion during the various project meetings all over Germany.

To Andrew Leis who was always interested, always available and who helped me so much at the beginning, thanks for introducing me to the project and for many hours of interesting discussion.

To Martin Strathmann I owe the idea of using rhodamine 6G as a fluorescent marker for laponite. His experience with CLSM and many quick, sharp and good ideas were invaluable for the preparation of this thesis. I appreciate having him as a supervisor.

Finally Mariël to whom this thesis is dedicated and who was my pillar during the ups and downs that represent writing a PhD thesis.

To all of you, a huge Thanks!

Table of Contents

1	Introduction	1
1.1	Subsurface environments and the importance of transport phenomena - an overview	1
1.2	Transport of solutes - mass transport in porous media	7
1.2.1	Darcy's law	7
1.2.2	Molecular diffusion	8
1.2.3	Advection	8
1.2.4	Advection and dispersion	9
1.3	Transport of colloids and microorganisms through porous materials	11
1.3.1	Colloids	11
1.3.2	Adaptations to ADE used to describe colloid transport - colloid filtration theory	11
1.4	Interactions between particles - the complexity of transport processes	13
1.5	Microorganisms as highly reactive particles - the foundation of biofilms	15
1.6	Biofilms in the subsurface	16
1.6.1	Biofilm basics	17
1.6.2	Distinguishing features of subsurface biofilms	17
1.6.3	Subsurface biofilms - the clogging factor	18
1.6.4	Ecological perspective	21
1.7	Retention capacity of biofilms - EPS and its impact on transport	24
1.8	Problem formulation and aim of the study	27

2	Materials and Methods	29
2.1	Bacterial strains and growth media	29
2.2	Buffers, solutions and colloidal suspensions	31
2.2.1	LRD-R6G staining protocol	31
2.2.2	Influent background solutions	34
2.3	Equipment	36
2.3.1	Optical measurements	36
2.3.1.1	UV-VIS spectrophotometry	36
2.3.1.2	Fluorescence spectrophotometry	36
2.3.1.3	Zeta potential measurements	36
2.3.1.4	Particle size distribution	37
2.3.2	Microscopy	38
2.3.2.1	Confocal Laser Scanning Microscopy	38
2.3.2.2	Fluorescence microscopy	38
2.3.2.3	Scanning Electron Microscopy	38
2.3.3	Electro-chemical equipment	38
2.3.4	General laboratory equipment	39
2.4	General experimental setting	40
2.5	Microbiological methods	40
2.5.1	Bacterial strains maintenance	40
2.5.2	Motility determination in agar media	41
2.5.3	Preparation of bacterial suspensions	42
2.5.4	Biofilm growth inside the porous medium	43
2.5.5	Effluent cell concentrations and bacterial mass determination	43
2.6	Biochemical and chemical analytical methods	43
2.6.1	Determination of dry weight	44
2.6.2	Determination of ash content / loss on ignition	44
2.6.3	Biofilm separation from the sand matrix	44
2.6.4	EPS isolation	44

2.6.5	Determination of carbohydrates	45
2.6.6	Determination of proteins	45
2.7	Transport methods	46
2.7.1	Column packing material	46
2.7.2	Sand columns	46
2.7.3	Sand-packed microscopy flow cells	47
2.7.4	Column hydraulic parameters	47
2.7.4.1	Hydraulic conductivity measurements	48
2.7.5	Calculation of colloid and biocolloid transport parameters	48
2.7.5.1	Colloid and biocolloid transport parameters obtained by CLSM	50
2.7.6	Colloid transport experiments in the presence of biofilms	52
2.7.7	Remobilization experiments	52
2.7.7.1	Remobilization of LRD from clean quartz sand columns	52
2.7.7.2	Colloid-facilitated remobilization of R6G from sand-packed microscopy flow cells as evidenced by CLSM	52
2.7.7.3	Natural colloids remobilization from SFM	53
2.8	Statistical methods	53
3	Results	54
3.1	Introduction	54
3.2	LRD physicochemical characteristics	55
3.2.1	Interaction between the colloid and R6G	55
3.2.2	Colloid aggregation and stability	58
3.2.3	LRD retention mechanisms in the porous medium	62
3.3	Quantification of LRD transport parameters	64
3.3.1	Influence of ionic concentration and type on LRD remobilization from water saturated sand	72
3.4	Transport of <i>P. aeruginosa</i>	72
3.4.1	Bacterial zeta potential measurements	74
3.4.2	Quantification of bacterial transport parameters	74

3.4.3	Retention at different columns depths as evidenced by CLSM	80
3.4.4	Remobilization of bacterial cells from sand matrices	80
3.4.5	Bacterial physiological states and transport	83
3.4.5.1	Bacterial survival	83
3.4.5.2	Impact of attachment on bacterial transport after remobilization .	83
3.5	Remobilization patterns from natural colloids at different ionic conditions .	87
3.6	Porous media biofilms	88
3.6.1	Growth of biofilms inside sand columns	88
3.6.1.1	Influence of biofilm growth on the saturated hydraulic conductivity of sand columns	90
3.6.1.2	Quantification of biofilm components in sand columns before the colloid transport experiments	92
3.7	Influence of biofilms on the transport of LRD through permeable sand	93
3.7.1	Influence of biofilms on LRD transport in the presence of monovalent cations	94
3.7.1.1	Biofilm quantification from Na ⁺ treated sand columns after colloid pulse injection	96
3.7.2	Influence of biofilms on LRD transport in the presence of divalent cations	96
3.7.2.1	Biofilm quantification from Ca ²⁺ treated sand columns after col- loid pulse injection	98
4	Discussion	101
4.1	Introduction	101
4.2	Field scale vs. laboratory scale approach	101
4.3	Discussion on the laboratory methods used	102
4.3.1	The use of CLSM sand-packed microscopy flow cells for transport exper- iments	105
4.4	Interaction between LRD and R6G	106
4.5	Factors determining the transport of LRD through porous media	109
4.6	LRD transport quantification	110
4.7	<i>P. aeruginosa</i> SG81 transport quantification	114

4.8 Laponite RD and bacterial transport	118
4.9 Biofilm formation and colloid transport	120
4.9.1 Distinguishing characteristics of sand-grown biofilms	122
4.9.2 LRD transport and the interaction between ionic composition and biofilm presence	123
4.10 Ecological perspective and concluding remarks	126
4.11 Conclusions	128
4.12 Outlook	130
Literature	147

List of Figures

1.1	Environmental relevance of the study	2
1.2	Redox zonation differences	3
1.3	Overview transport processes implicating colloids	5
1.4	Salt water intrusion into fresh groundwater scenarios	7
1.5	Tracer fronts resulting from advection, diffusion and dispersion	9
1.6	Flow paths in a porous medium	9
1.7	Iron oxides precipitated on bacteria	14
1.8	Time-dependent changes of <i>P. aeruginosa</i> biofilm thickness	20
1.9	Changes in hydraulic conductivity in columns inoculated with different bacterial strains	21
1.10	Liquid flow between two glass beads with accumulated biofilm	22
1.11	Schematic depiction of the binding sites in biofilms	26
2.1	Flow cells picture	39
2.2	Main experimental setting	41
2.3	Constant head permeameter	49
3.1	Rhodamine 6G absorbance spectra	56
3.2	Rhodamine 6G absorbance spectra in presence of laponite RD	56
3.3	Rhodamine 6G absorbance spectra at different laponite RD concentrations	57
3.4	Spectra from sedimented rhodamine 6G-stained laponite RD	57
3.5	Injection of rhodamine 6G to sand-packed microscopy flow cells	58
3.6	Detection of rhodamine 6G in sand grains	59

3.7	Remobilization of rhodamine 6G caused by laponite RD pulse injection	59
3.8	Remobilization of rhodamine 6G caused by colloidal pulses, CLSM	60
3.9	Remobilization of rhodamine 6G caused by colloidal pulses, sand columns	60
3.10	Aggregation process of rhodamine 6G-stained laponite RD	61
3.11	Interaction between rhodamine 6G and laponite RD	61
3.12	Laponite RD aggregation states	62
3.13	Laponite RD aggregates at high salt concentrations	63
3.14	Laponite RD coated quartz sand	63
3.15	Retention of 2000 mg L ⁻¹ laponite RD in porous media	64
3.16	Laponite RD CLSM image analysis of retention	65
3.17	Retention of 200 mg L ⁻¹ laponite RD in porous media	65
3.18	Retention of 20 mg L ⁻¹ laponite RD in porous media	66
3.19	Remobilization of 20 mg L ⁻¹ laponite RD from sand matrices	66
3.20	Image analysis of laponite RD retention and remobilization from sand matrices	67
3.21	Laponite RD transport profiles in non-inoculated sand columns	68
3.22	CLSM images of laponite RD transport at different salt concentrations	69
3.23	Laponite RD BTCs obtained from image analysis CLSM method	70
3.24	Image analysis from CLSM micrographs	71
3.25	Collision efficiencies for laponite RD as a function of ionic strength	71
3.26	Influence of fluid phase cation type and concentration on colloid remobilization	73
3.27	Zeta potentials from <i>P. aeruginosa</i> SG81 cells at different pH values	74
3.28	BTCs from bacteria in sand columns	75
3.29	CLSM micrographs with elution of a bacterial pulse at 0 mM salt concentration	76
3.30	CLSM micrographs with elution of a bacterial pulse at 1 mM salt concentration	76
3.31	CLSM micrographs with elution of a bacterial pulse at 10 mM salt concentration	77

3.32	CLSM micrographs with elution of a bacterial pulse at 140 mM salt concentration	77
3.33	Subtraction of non-attached bacteria from a CLSM micrograph	78
3.34	Image analysis from CLSM micrographs	79
3.35	BTCs of <i>P. aeruginosa</i> SG81 obtained from image analysis information, CLSM method	79
3.36	Collision efficiencies (α) for <i>P. aeruginosa</i> SG81 and SG81R1 as a function of ionic strength	80
3.37	Bacterial retention at different microscopy flow cell distances	81
3.38	Release of cells after a sudden change in ionic strength	82
3.39	Release of cells after increasing flow rate, CLSM	82
3.40	Release of cells after a sudden change in ionic strength, CLSM	83
3.41	Survival of bacteria after bacterial pulse preparation	84
3.42	Collection of detached bacteria populations	85
3.43	BTCs of planktonic and biofilm detached bacteria	85
3.44	Agar tests swimming results for planktonic and detached bacteria	86
3.45	Remobilization of natural colloids from slow sand filter material	88
3.46	Effluent samples at different influent salt concentrations	89
3.47	Particle size distributions for two example columns	90
3.48	Three-dimensional image of SYTO 9-stained biofilms growing on the surface of sand grains	91
3.49	SEM of biofilm containing sand grains	91
3.50	Changes in porous matrix hydraulic conductivity induced by biofilm growth	92
3.51	Biofilm components in sand columns before transport experiments	93
3.52	Absorbance and TCCs after colloid injection at low ionic strength	95
3.53	Column effluent after the introduction of 2000 mg L ⁻¹ laponite RD dispersed in 7 x 10 ⁻² M NaCl	95
3.54	Laponite RD breakthrough in Na ⁺ exposed columns	96
3.55	Breakthrough patterns of laponite RD when injected in natural columns	97

3.56	Biofilm components remaining in sand columns, Na ⁺ exposure	97
3.57	Laponite RD breakthrough in Ca ²⁺ exposed columns	98
3.58	Laponite RD breakthrough in slow sand filter material columns	99
3.59	Biofilm components remaining in sand columns, Ca ²⁺ exposure	99
4.1	Two common colloid injection techniques	105
4.2	Peclet number and advection/diffusion	111
4.3	Laponite RD BTCs with added Gaussian fit	112
4.4	Interactions between LRD and bacterial transport	121
4.5	Na ⁺ , Ca ²⁺ and biofilm influence on colloidal transport	126
4.6	Two extreme scenarios for biofilm development in the subsurface	128
4.7	Biogeochemical factors which might influence colloid transport	131

List of Tables

1.1	Colloid transport studies and their focus	12
2.1	Bacterial species used in the experiments	29
2.2	Nutrient media used for growing bacteria	30
2.3	Buffers, solutions and colloidal suspensions	33
2.4	Chemicals	34
2.5	Electrochemical equipment	39
2.6	Calculated column hydraulic parameters	47
3.1	Sand column and sand-packed microscopy flow cell packed characteristics	67
3.2	Laponite RD combined transport parameters at different ionic strengths . .	70
3.3	<i>P. aeruginosa</i> SG81R1 combined transport parameters at different ionic strengths	80
3.4	<i>P. aeruginosa</i> SG81 combined transport parameters at different ionic strengths	81
3.5	Assessment of swimming, swarming and twitching motility in agar media .	87
3.6	Transport parameters obtained from the colloid transport experiments . .	100
4.1	Common techniques in particle deposition kinetics	103
4.2	Zeta potentials for several bacterial strains	115

Glossary

ADE	Advection-dispersion equation, 9-12
APM	Alginate promoting medium, 30, 35
BSA	Bovine serum albumin, 35, 46
BTC	Breakthrough curve, 50, 65, 68, 71, 105
α	Collision efficiency, 13, 50, 71, 79
CER	Cation exchange resin, 35, 45
CEC	Cation Exchange Capacity, 33, 34, 109
CFT	Colloid filtration theory, 12, 55, 117
CFU	Colony forming units, 43
CLSM	Confocal Laser Scanning Microscopy, 21, 27, 44, 50, 55, 63, 65, 69, 79, 107, 111
d	Dispersivity, 9, 48
q	Darcy flux (L/T), 48
DAPI	4',6-diamidino-2-phenylindole, 35, 88
EDTA	Ethylenediaminetetraacetic acid, 35
EPS	Extracellular polymeric substances, 16, 17, 20, 23-27, 45, 46, 89, 93
D	Hydrodynamic dispersion coefficient, 9, 12, 48
K	Hydraulic conductivity, 8, 9, 19, 91, 93
v_x	Average linear velocity (L/T), 9, 10, 48
LB	Luria Bertani agar, 31

LRD	Laponite RD a synthetic hectorite, 32, 33, 37, 50, 52-56, 59, 62, 63, 65, 68, 69, 71, 73, 75, 76, 79, 91, 94, 95, 103, 107-111, 114, 119, 120
NA	Nutrient agar, 30
NB	Nutrient broth, 30
C	Suspended particle concentration in column effluent, 50, 71, 79, 94, 99
C_0	Suspended particle concentration in column influent, 50, 71, 79, 94, 99
Pe	Peclet number, 10, 48, 112
ε	Porosity, 9
k_d	Particle deposition rate coefficient, 12, 13, 50, 71, 79
pV	Total pore volume, 48
v	Colloid particle velocity, 12
PBS	Phosphate buffered saline, 34
PIA	Pseudomonas isolation agar, 30, 41, 43
η	Dimensionless colloid removal rate, 71, 79
R6G	Rhodamine 6G a cationic laser dye, 32, 33, 37, 50, 52-56, 59, 63, 73, 95, 109, 111, 120, 125
RhD	5×10^{-5} M rhodamine 6G in deionized water, 33
RhS	5×10^{-5} M rhodamine 6G in 0.7 M NaCl, 33
RhSca	5×10^{-5} M rhodamine 6G in 0.7 M CaCl ₂ , 33
SEM	Scanning Electron Microscopy, 39
SFM	Slow sand filter material, 47, 48, 54, 126
TCC	Total cell counts, 43, 44
TSB	Tryptic soy broth, 30, 43
Q	Volumetric discharge (L ³ T ⁻¹), 8, 48

YE Yeast extract, 31, 35

ζ Zeta potential, 37, 75

Abstract

The main objective of this thesis was to investigate the influence of biofilms on colloid transport in model sediment columns, at changing fluid ionic conditions. The transport of exogenous substances entering the subsurface is a subject of relevance for a wide variety of disciplines. In the field, particles such as clay particles, iron oxyhydroxides, natural organic matter and bacteria have been found as mobile colloids. Even though the influence of organic material accumulation on colloid transport has been taken into account to some extent, to the date of starting this thesis, no comprehensive studies on the influence of biofilm formation on the overall transport of colloidal particles in the subsurface were available.

Sand-packed columns and sand-packed microscopy flow cells subjected to constant liquid flow were used to determine colloid transport. The artificial clay colloid laponite RD (LRD), and the biofilm-forming bacterium, *Pseudomonas aeruginosa* SG81 were used as model colloid and biofilm forming microorganism, respectively. Changing ionic conditions were simulated by using Ca^{2+} and Na^{+} based solutions as influents and then switching to very low ionic strength solutions. Colloidal suspensions were injected to the columns as small volume pulses (10 % of total pore volume). This was done either in presence or in absence of microbial biofilms. Colloid transport parameters as well as microbiological parameters were obtained using a combination of online optical detection methods and offline microbiological and biochemical analytical methods. Confocal Laser Scanning Microscopy (CLSM), was used to obtain transport parameters from the sand-packed microscopy flow cells.

In absence of biofilms, a sodium chloride concentration of 7×10^{-2} M caused complete retention of LRD within the sand columns. Although at 2000 mg L^{-1} LRD, massive aggregation was observed and clogging occurred, aggregation alone was not responsible for LRD retention at lower concentrations (i.e., 200 or 20 mg L^{-1}). *P. aeruginosa* SG81 showed relatively low mobility at all ionic strengths tested and some (albeit reduced) mobility when introduced to the columns in 1 M NaCl, the highest concentration tested. In sterile columns, the presence of Na^{+} and Ca^{2+} ions in the influent followed by a low ionic strength solution did not cause LRD retention. The colloid was mobile with collision efficiencies from 0.05 to 0.08 ($\text{SE} \leq 20 \%$; $n = 9$).

In the presence of biofilms and after Na^{+} exposure, no colloid retention occurred but in some cases altered or enhanced colloid transport was observed. Colloid collision efficiency after 3 weeks of biofilm growth was 0.03 ($\text{SE} \leq 10 \%$; $n = 3$). In contrast, after Ca^{2+} ions exposure, colloid retention increased with biofilm age. After 3 weeks, almost complete retention was observed with a collision efficiency of 0.9 ($\text{SE} \leq 20 \%$; $n = 3$). Similar observations were made in columns packed with material from slow sand filtration units. Determination of EPS components remaining in the sand columns after the colloid transport experiments showed that, in the case of Na^{+} treated columns, cell/carbohydrate, cell/protein and carbohydrate/protein ratios remained constant even after a growing period of 3 weeks. In contrast, EPS analysis from Ca^{2+} treated columns, showed that colloid retention also increased with an increase in EPS content. Protein content was found to increase with time in relation to other EPS components and to be significantly correlated to colloid retention (0.999) at the established confidence level.

These data reveal the complex interactions between biofilms, ions and colloid transport. These observations suggest that while a reduction in ionic strength has a dominant influence on the mobilization of biological and inorganic colloids, the presence of laponite and biomass can have a distinct influence on their mobility. Changes in the electrolyte composition of water percolating the subsurface can frequently occur as well as changes in the relative abundance of microbial biofilms. This has to be considered when modeling colloid transport through the subsurface.

Chapter 1

Introduction

1.1 Subsurface environments and the importance of transport phenomena - an overview

Sediments and other subsurface environments are obvious sinks for a wide variety of contaminants in both dissolved and particulate form. They are also sinks and transformation pots for organic carbon. In fluvial environments for example, the interface between the major water body and the sediment (Figure 1.1), is a very active zone both in physicochemical and biological terms. The dynamic flux of energy, nutrients, metabolites and other substances is interdependent with local hydrodynamics (Huettel et al., 2003) and with local **biogeochemistry**. This is especially true in highly permeable sandy sediments, where advective transport, i.e., with the flowing water, contributes greatly to the movement of substances and energy (Janssen et al., 2005).

Traditionally, it has been believed that redox conditions determining organic matter oxidation, formed very well defined zones (Figure 1.2a). This might be true in low permeability, muddy, subsurface environments where diffusion is the dominating transport process but certainly it is not the case in coarse highly permeable sediments. Studies in marine benthic systems have demonstrated the importance of advective movement on the flux, mixing and exchange of metabolites and particles (Huettel and Rusch, 2000). Flow above the sediment, for example, by a river creates pressure differences throughout the sediment which are translated into advective and dispersive transport towards the depth of the sediment or towards the surface (Figure 1.2b). In other saturated subsurface environments, groundwater flow adds additional flow directions parallel to the surface. It is important to notice that river sediments and shallow coastal environments are generally coarse, with high hydraulic conductivity and low organic content. This

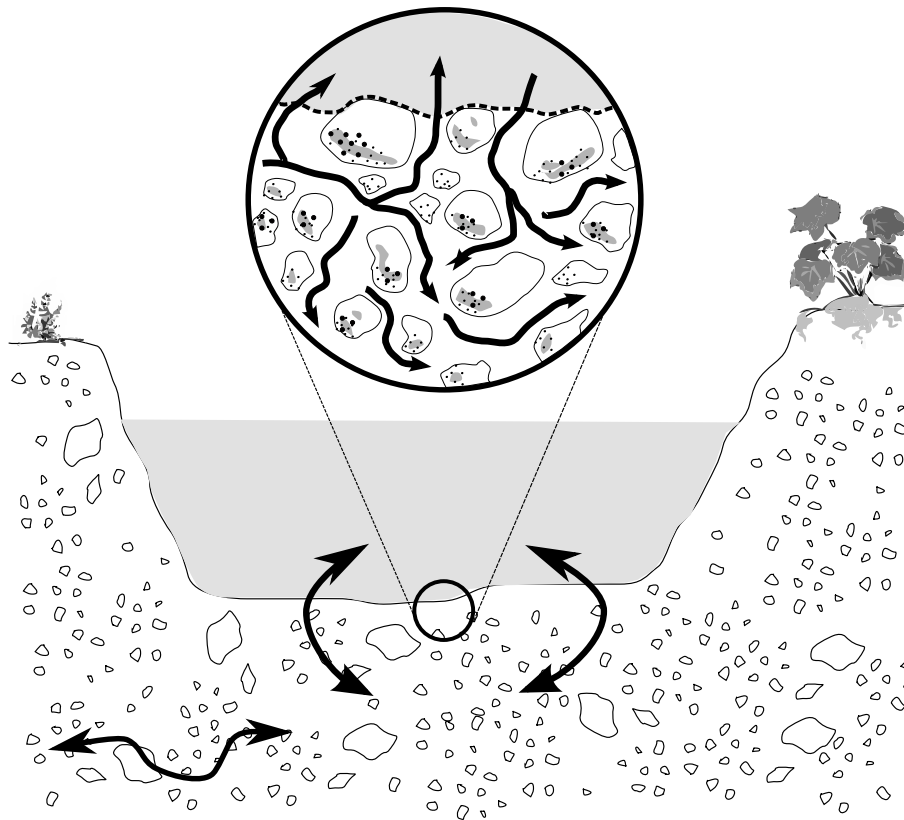


Figure 1.1: Environmental relevance of the study. Arrows represent possible flow directions.

does not mean, however, that they are not biogeochemically active (Huettel et al., 2003). Oxygen consumption in these environments has been found to occur at similar rates to that of fine-grained organic-rich sediments, suggesting their high mineralization capacity.

A wide variety of dissolved substances, including metals and other contaminants are effectively influenced by these advective pore water flows. Upwelling flows can be a source of reduced metals and many contaminants entering the water column in aquatic environments. In the other hand, groundwater flows parallel to the surface can result in these substances reaching drinking or irrigation water supplies.

Certainly, not only dissolved substances are affected by transport phenomena in porous environments. Advective movement largely determines the transport of Colloids in many environments. Colloids are particles with an average diameter between 10^{-9} and 10^{-6} m which can be formed by nucleation or precipitation among other processes (see Section 1.3.1). Their movement through the subsurface has been studied and modeled in detail, and several reviews are available (Ryan and Elimelech, 1996; Kretzschmar et al., 1999; McCarthy and McKay, 2004).

Scientific interest in the way colloids are transported through the intricate pores of sub-

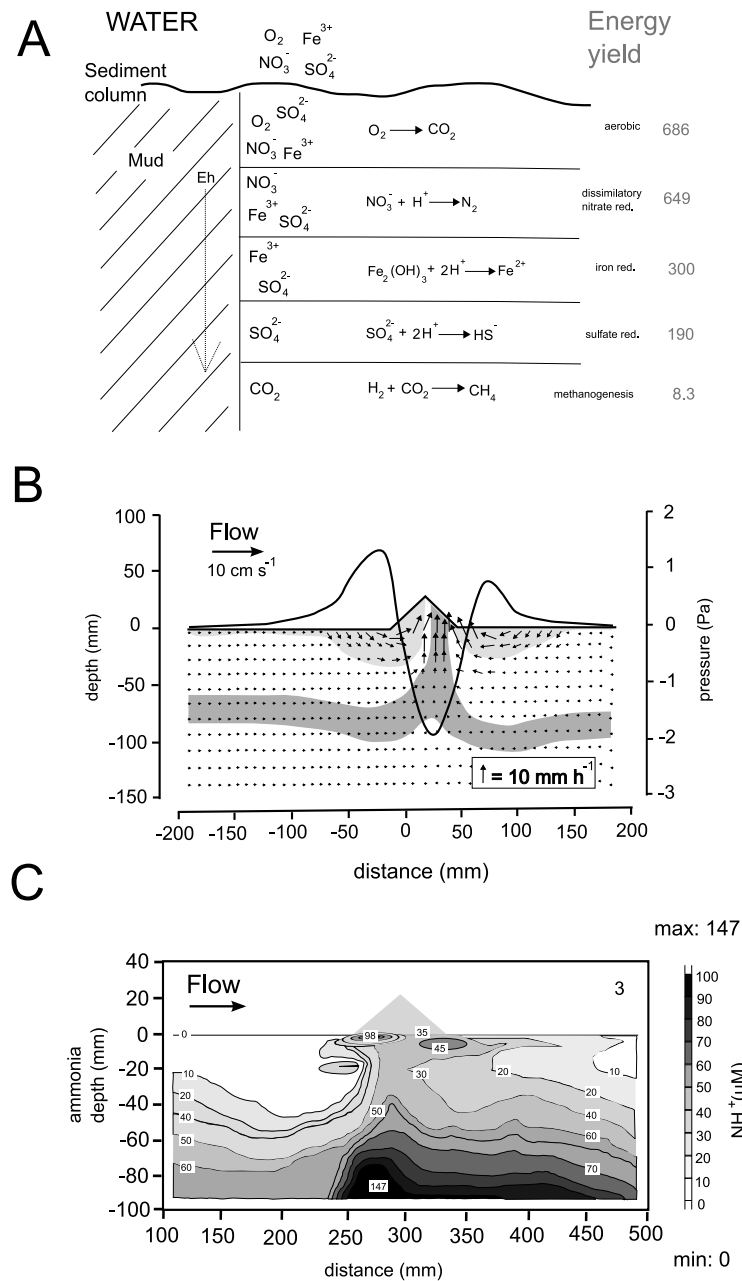


Figure 1.2: A: Redox zonation in subsurface environments as depicted traditionally. B: pressure distribution (thick line) at the sediment-water interface generating advective flow within the sediment. C: an example of this phenomenon in which pore water rich in ammonia is drawn to the surface due to pressure differences at the bed surface creating steep gradients between aerobic and anaerobic sediment zones. This is only one of the examples on the importance of transport processes, especially advection in highly permeable sediments. Figure modified from (Huettel and Rusch, 2000).

surface environments has been inspired by two facts affecting human health: colloids can be contaminants by themselves (bacteria, viruses, organics) and colloids can be carriers of contaminants (Kretzschmar et al., 1999). The awareness that colloids can act under certain conditions as contaminant carriers has motivated a great number of studies on colloidal transport in the subsurface throughout the last decade (Grolimund et al., 1996; Kim and Corapcioglu, 1997; Grolimund et al., 1998; Corapcioglu et al., 1999; Tatalovich et al., 2000; Cherrey et al., 2003).

It was clear then that a contaminant could be found in three regions: dissolved, sorbed to mobile colloids and sorbed to immobile surfaces (Figure 1.3). Certain conditions have been identified which must be met for the colloid transport to be important in terms of pollutant mobility. First of all colloids must be transported through the porous medium, there must be a strong association with the contaminant and they should travel sufficiently long distances, e.g., reaching drinking water abstractions (Ryan and Elimelech, 1996). Figure 1.3 depicts an overview of subsurface transport scenarios which implicate transport of colloids. The study of colloid movement and its influence on the fate of common subsurface contaminants is also a microbiological endeavor. This is true not only because many microorganisms fall into the size range of colloidal particles, but mainly because their active metabolisms will have an impact on the chemical and hydrodynamic characteristics of their habitats. The transport of microorganisms through porous media has therefore received considerable attention (Camesano et al., 1999; Deshpande and Shonnard, 1999; Jewett et al., 1999; Smets et al., 1999), although the focus of these studies has been varied. These include studies on preventing bacterial migration through aquifer systems (e.g. filtration of pathogens) (El-Masry et al., 1995; Tufenkji et al., 2002) to studies centered on enhancing microbial transport to a contaminated site for bioremediation (Li and Logan, 1999).

Microorganisms, regardless of being dead or alive, have been known for acting as accumulation sites for contaminants e.g. dissolved heavy metals, in a wide variety of environments including the subsurface (Ferris, 2000). Sorption of Uranium (VI) for instance has been used for the immobilization of this radioactive element (Hu et al., 1996). Bacteria can migrate long distances in porous media. Mobile bacteria can also be generated for example by detachment from biofilms. Thus microorganisms can be described as "bio-colloids", and as such, can participate in colloid facilitated transport of contaminants. Bacteria-facilitated cadmium transport for example has been observed in alluvial gravel aquifer media (Pang et al., 2005). In these column studies it was found that cadmium traveled 17 to 20 times faster in presence of bacteria than in bacterial-free controls.

Microbial deposition and colonization of porous media particles is a well observed phenomenon (Rijnaarts, 1994). **Biofilms** accumulating in these environments are impli-

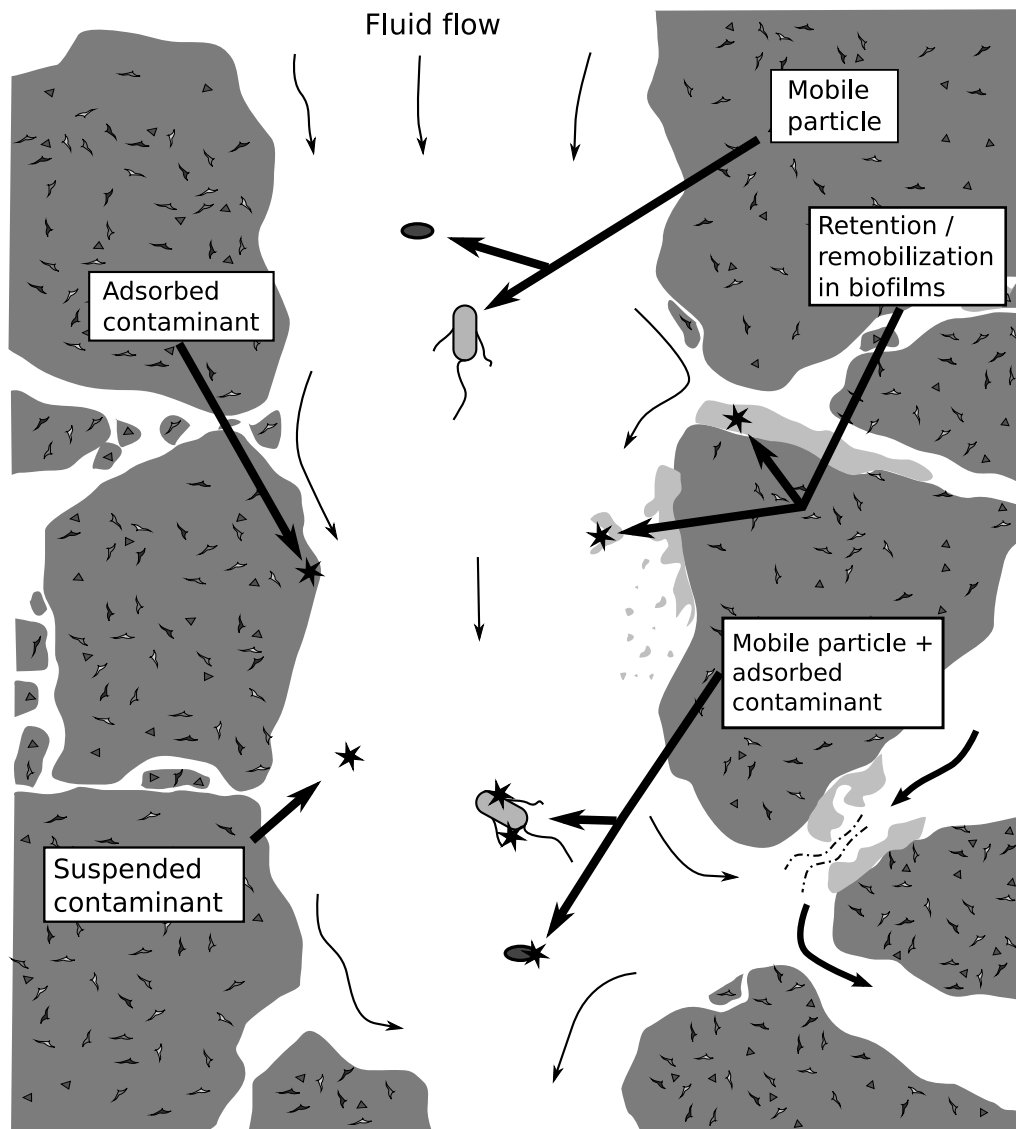


Figure 1.3: Overview of transport processes in the subsurface implicating colloid mobility.

cated in the biotransformation of contaminants, in hydrodynamic changes of the porous medium and importantly, on the transport of dissolved and particulate matter.

The amount and morphology of biofilms formed in porous media can be highly variable. This variability depends on the amount of biodegradable organic matter, and on electron donors and electron acceptors available (Anderson and Lovley, 1997; Bouwer et al., 2000).

In many subsurface environments, such as groundwater systems, pore water flow brings with it another important factor with profound consequences on the movement of dissolved substances, particles and on biofilm formation: **fluid ionic concentration and speciation**.

Many groundwaters are naturally rich in diverse ionic species. The type and amount of ions depend, besides groundwater flow, on salt type and concentration and on groundwater lithologic framework. Almost all of the dissolved solids in groundwater can be attributed to eight ions: Na^+ , K^+ , Ca^{2+} , Mg^{2+} , Cl^- , HCO_3^- , SO_4^{2-} and CO_3^{2-} (Fetter 1994). Obviously, these are not the only ions present but they are the ones generally found in higher concentrations. Moving groundwater bodies with distinct chemical compositions are known as hydrochemical facies. Generally, fresh hydrochemical facies are Ca^{2+} dominated. Calcium in groundwater comes from the decomposition of rocks and mainly from the dissolution of carbonate minerals which are important players in groundwater chemical equilibria (Chapelle, 2003). Na^+ plays also an important role in cation exchange processes mainly at coastal environments (Petalas and Diamantis, 1999; Allen and Suchy, 2001; Allen and Matsuo, 2002) where fresh hydrochemical facies are mixed with sea groundwater. Na^+ dominated salt water intrusion into fresh groundwater 1.4 has been identified as an influential factor on the partitioning of contaminants in groundwater (Westbrook et al., 2005). Na^+ rich water infiltration can also occur away from the coasts by for example NaCl stimulated street de-icing or by contamination. Several well controlled laboratory studies have investigated calcium and sodium influence on subsurface colloid transport and aggregation (Chen and Kojouharov, 1998; Kretzschmar and Sticher, 1998; Davis et al., 2001). Colloid stability and transport has been observed to be very sensitive to the presence of Ca^{2+} ions, resulting in colloid retention or aggregation even at relatively low Ca^{2+} concentrations.

It is not entirely clear however, how changes on fluid dominant ionic species and concentration influence biofilm formation and stability in subsurface environments. It is therefore unclear how these changes will affect the transport of colloidal particles and contaminants in the presence of biofilms. This is especially relevant in highly permeable subsurface environments such as sandy sediments, where advection and dispersion can represent an important mixing and transport mechanism.

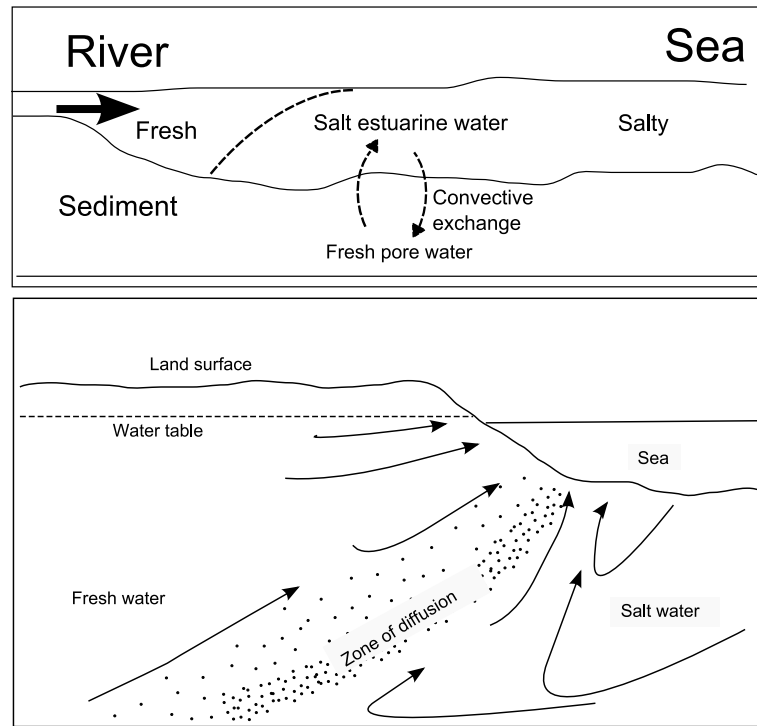


Figure 1.4: Salt water intrusion into fresh groundwater scenarios. A: in an estuary. B: in coastal environments (not in a fluvial system).

1.2 Transport of solutes - mass transport in porous media

1.2.1 Darcy's law

Henry Darcy provided the first systematic study of water flow through a porous medium. Darcy's main motivation was to find more effective ways for public water distribution. His contributions are a starting point for great part of the approach taken in this thesis.

Basically, Darcy's equation relates the flow of water through a porous medium Q , or volumetric discharge (L^3T^{-1}) to: A , or cross-sectional area (L^2) and h , hydraulic head which is a zero-order or scalar tensor (L). This relationship can be expressed as

$$Q = -KA \frac{dh}{dl} \quad (1.1)$$

where K is a proportionality constant known as hydraulic conductivity and dh/dl represents the gradient of hydraulic head.

Darcy's law was derived for flow in one dimension. In reality, several of these quantities, for instance the hydraulic conductivity and the hydraulic head, will have components in the three space dimensions x, y, z . The components in more than one dimension are significant only in situations where the diameter of the confinement space where water

is flowing is wide enough.

1.2.2 Molecular diffusion

Refers to transport of solutes by concentration gradients. At high permeability zones (e.g. organic low sands or fractured media) diffusion might not be a particularly rapid mean of dissolved solute transportation and can be in some cases of high advection transport be even ignored. In low-permeability hydrogeologic regimes (e.g clay rich environments), however, it might be the predominant transport system. Due to the reason that in our experimental setting, i.e., permeable sand columns, diffusion does not represent an important contributor to colloid transport, this concept will not be expanded in detail here.

1.2.3 Advection

Advection or convection occurs when dissolved solids are carried along with the flowing groundwater. The quantity of groundwater flowing and the solute concentration will determine the amount of solute being transported. For one-dimensional flow normal to a unit cross-sectional area of the porous media, the quantity of water flowing can be obtained by multiplying the average linear velocity (water flow rate through a cross-sectional area) times the effective porosity (porosity through which flow can actually occur).

$$v_x = \frac{K}{\varepsilon_e} \frac{dh}{dl} \quad (1.2)$$

where v_x is the average linear velocity (L/T), K is the hydraulic conductivity (L/T), ε_e is the effective porosity and dh/dl is the hydraulic gradient (L/L). The mass flux, F_x , due to advection is then equal to the quantity of water flowing times the concentration of dissolved solids as in;

$$F_x = v_x n_e C \quad (1.3)$$

Modeling advection returns a sharp concentration front. On the advancing side of the front, the concentration is equal to that of the invading water, whereas on the other side of the front it is unchanged from the background value (see long dashed line in Figure 1.5).

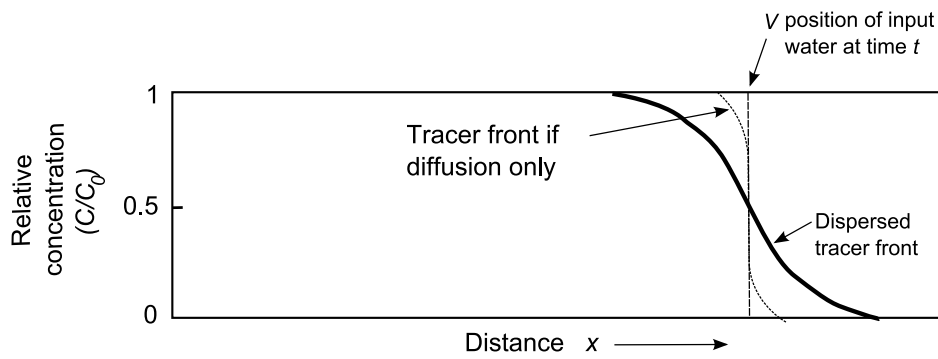


Figure 1.5: Resulting tracer fronts as affected by advection only, diffusion and dispersion in one-dimensional flow (Fetter, 1998).

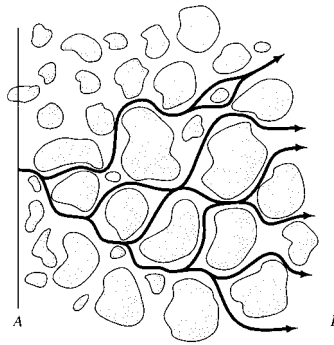


Figure 1.6: Flow paths in a porous medium and their influence on lateral hydrodynamic dispersion (Fetter, 1998).

1.2.4 Advection and dispersion

The transport of solutes through porous materials can be described by accounting for advection (or mechanical movement) and hydrodynamic dispersion (as a sum of molecular diffusion and mechanical dispersion). The equation describing these relationships is known as the advection-dispersion equation (ADE).

Due to the reason that geological materials are not homogeneous, transport of a solute results in different fronts, spreading at different rates. These rates are both greater and less than the average linear velocity. These differences are linked to wall effects (fluid particles travel faster in the center of the pores than along the edges), flow path lengths and pore size (Figure 1.6). The resulting effect of these velocity differences is a mixed solute front which is diluted at the advancing edge of flow (thick line in Figure 1.5). This is called mechanical dispersion and it can occur both along with the flow path and normal to it. Combining the processes of molecular diffusion and mechanical dispersion, results in **hydrodynamic dispersion**. Hydrodynamic dispersion uses an important hydraulic parameter known as the hydrodynamic dispersion coefficient, D , which is related to a property of the porous medium called dispersivity, d , and to the average linear

velocity, v ;

$$D_L = d_L v_i + D^* \quad (1.4)$$

$$D_T = d_T v_i + D^* \quad (1.5)$$

where D_L is the hydrodynamic dispersion coefficient parallel to the principal direction of flow (longitudinal), D_T is the hydrodynamic dispersion coefficient perpendicular to the principal direction of flow (transverse), d_L is the longitudinal dynamic dispersivity and d_T is the transverse dynamic dispersivity.

Mechanical dispersion and therefore, hydrodynamic dispersion can also be described using Fick's law for diffusion. This "diffusional" model of hydrodynamic dispersion predicts that the concentration curves will have a Gaussian distribution and can also be analyzed in terms of the mean and variance. A representation of what would happen with the relative concentration of a migrating solute when both advection and dispersion are included, is shown in Figure 1.5.

The combined effects of advection and dispersion are included in the derivation of the **ADE** for solute transport. The working assumptions are that the porous medium is homogeneous, isotropic, and saturated with fluid. For details on the derivation of this equation please refer to Bear (1972) or Ogata (1970). In its simplest form, ADE is

$$D_L \frac{\partial^2 C}{\partial x^2} - v_x \frac{\partial C}{\partial x} = \frac{\partial C}{\partial t} \quad (1.6)$$

where D_L represents the longitudinal hydrodynamic dispersion (L^2/T), and v_x the average linear velocity (L/T). The dispersion ADE component is located in the left side of the minus sign while the advection component is located after the minus sign. It would have been possible to separate the contributions of diffusion and mechanical dispersion in the hydrodynamic dispersion term used in equation 1.6. In most situations, however, representative of groundwater flow, the contribution of diffusion is insignificant and therefore is ignored. To corroborate that actually the influence of diffusion is minimal, a dimensionless number relating the effectiveness of mass transport by advection to that of diffusion has been defined. This number is known as the **Peclet number**, Pe and further details on its calculations can be found in the materials and methods section.

ADE as presented in this section, would be applicable only to situations in which dissolved solutes are totally conservative i.e., not interactive with the mineral grains (or any other material covering them) forming the porous medium. This situation occurs only rarely and even the most "conservative tracer" has certain degree of interaction with the porous medium. This interaction will result in mass removal from the groundwater, which can be temporal or permanent. The removal can be due to transformation,

retardation or attenuation.

1.3 Transport of colloids and microorganisms through porous materials

1.3.1 Colloids

Mass can be transported through the subsurface not only as solutes, but also as particulate matter. Colloidal phases are composed of particles not small enough to be considered "dissolved" and not big enough to be considered macroscopic. These colloidal phases constitute a wide border between dissolved matter and macroscopic aggregates. Colloidal suspensions are formed by a precipitation process in which nucleation processes are dominant and high amounts of small particles are formed (Shaw, 1980).

The stability of a colloid as small particles is due to the fact that all particles are charged either positively or negatively depending on the concentration and type of the electrolyte solution surrounding them. This makes it impossible for particles to come together, sorb, and form bigger particles. A colloidal particle in these conditions is maintained thanks to the presence of a double electrical layer that stabilizes the charge on the particle (Elimelech et al., 1995).

Colloid transport processes in subsurface environments, as said before, have a huge impact on the fate of pollutants in the environment. Because particles undergo similar processes of advection and dispersion besides retention processes as compared to solutes, their transport has been traditionally analyzed with the ADE as a starting point.

1.3.2 Adaptations to ADE used to describe colloid transport - colloid filtration theory

The presence of mobile colloids in the subsurface has been acknowledged already since several decades as reviewed in McCarthy and McKay (2004). The focus of the studies on these type of particles has been diverse, ranging from early studies on the control of microbial contamination to the migration of clay from the surface to deeper layers in soil diagenesis (McCarthy and McKay, 2004). In the field, particles such as clay particles, iron oxyhydroxides, silica, natural organic matter, viruses and bacteria have been found as mobile colloidal phases (Kretzschmar et al., 1997). The problem of deep bed filtration

in wastewater treatment and other chemical and engineering tasks encouraged most of the early research on colloid transport.

ADE can be adapted to describe colloid transport by including a term for particle retention. The concentration of suspended particles at a determined column depth and time, $c(x, t)$ can then be written as,

$$\frac{\partial C}{\partial t} = D \frac{\partial^2 C}{\partial x^2} - v \frac{\partial C}{\partial x} - kC \quad (1.7)$$

where v is interstitial colloid particle velocity, D is the hydrodynamic dispersion coefficient, and k is the particle deposition rate coefficient. Solutions of this equation have been used for modeling colloidal transport including microorganisms in many studies (Gross et al., 1995; Johnson et al., 1996; Kretzschmar et al., 1997; Grolimund et al., 1998; Li and Logan, 1999; Ryan et al., 1999; Bhattacharjee et al., 2002; Dong et al., 2002; Saiers and Lenhart, 2003). The influence of factors ranging from porous media particle charge to the influence of surfactants has been studied actively (Table 1.1).

Table 1.1: Colloid transport studies and their focus

Factor studied	Type of colloid	References
Porous media charge or charge heterogeneity	Latex particles, silica microspheres	Elimelech et al. (2000); Chen et al. (2001); Elimelech et al. (2003)
Surface charge and chemistry	Hematite particles, bacteria	Kretzschmar and Sticher (1998); Rijnaarts et al. (1999); Bolster et al. (2001); Becker et al. (2004)
Ionic strength and pH	Natural colloids, silica colloids, bacteria	Jewett et al. (1995); Grolimund et al. (2001); Bunn et al. (2002); Saiers and Lenhart (2003); Leon Morales et al. (2004); Redman et al. (2003)
Electrolyte type and concentration	Latex particles	Liu et al. (1995); Davis et al. (2001)
Hydraulic conditions of PM	Silica particles, bacteria	Fang and Logan (1999); Ren et al. (2000); Powelson and Mills (2001)
Porous media geometry and grain size	Bacteria	Bolster et al. (2001)
Influence of retained particles	Latex particles, bacteria	Song and Elimelech (1993); Camesano et al. (1999)
Influence of surfactants and other organics	Bacteria	Rogers and Logan (2000); Bolster et al. (2001); Dong et al. (2002)

Data obtained from well defined collectors and colloidal particles in model systems allowed for the development of what is now known as colloid filtration theory (CFT) (Yao et al., 1971). The conditions under which the set of equations composing the CFT ap-

proximately describes the problem of colloid transport are quite limited, i.e., the porous matrix is assumed to be initially free of colloidal particles (clean bed), there must be steady state, saturated flow conditions, there should be no ripening or blocking effects and there should not be preferential flow paths. Besides, the colloid retention regime should be that of "fast" retention conditions, i.e., at moderated to high ionic strengths. These conditions are met in well controlled laboratory column studies but not commonly in natural environments.

Colloid transport models developed over the years (see Ryan and Elimelech, 1996, for an extensive review) have been modified and adapted to heterogeneities found in sub-surface environments. It is already accepted that physicochemical conditions have great influence on the movement of colloids and from these the ionic strength and the type of cations composing the solution will excel as having a profound effect on the mobility of colloidal particles (Jewett et al., 1995; Liu et al., 1995; Grolimund et al., 1996; Li and Logan, 1999; Bunn et al., 2002; Saiers and Lenhart, 2003; Leon Morales et al., 2004).

Two types of deposition mechanisms can be observed depending on the size of colloid aggregates formed: (i) deposition by straining, in which the agglomerates are too big to pass through the medium pores, and (ii) deposition by interception, in which small aggregates or even individual colloids are retained on the surface of collectors subsurface matrix, e.g., sand grains, after collision. Interception mechanisms are dominated by physicochemical forces.

A common parameter used to measure the deposition of a colloidal particle, is the so-called **collision efficiency**. Collision efficiency, α , is defined as the probability of a migrating particle to attach, upon collision with sediment particles. It is obtained as the ratio between deposition rate constants (k term in 1.7) at increasing salt concentrations and those above certain salt concentration whereby deposition is independent of the salt concentration. Due to the reason that deposition is always higher at high salt concentrations, α values closer to 1 indicate high deposition while those closer to 0 indicate low deposition, for further details see section 2.7.5. At present, collision efficiency is difficult to predict and it must be obtained experimentally due to the fact that available colloid transport theories are unable to do so.

1.4 Interactions between particles - the complexity of transport processes

The interaction of cells with colloids constitutes an important aspect of global mineralization. In a great variety of environments cells contribute greatly to the total mineral



Figure 1.7: Iron oxides precipitated on bacteria in corrosion products of a drinking water pipe (from Flemming and Leis, 2002, modified).

deposition. This is particularly true in shallow, tropical marine environments, in rivers, and in lakes (Douglas and Beveridge, 1998).

The precipitation of metals on bacterial surfaces can trigger processes related with biomineralization (Figure 1.7). The initial metal complexation (binding with electronegative functional groups in cell walls, or additional layers) can serve as an additional nucleation site for more metal deposition that eventually will also be able to incorporate counter ions like OH^- , SO_4^{2-} , SiO_3^{2-} , etc. This metal ion bridging explains the high amount of silicate formation for example on microbial surfaces. Colloid-like particles bind mostly through this metal ion bridging effect, rather than through interactions with available amine groups. Carbonate formation in bacteria is another important sorption process mediated by bacterial surfaces. It happens due to the production of alkaline microenvironments near the cell surfaces as a consequence of physiological activities of the cell (for example, bicarbonate use as carbon source, yielding OH^- groups) and also due to the ability of S-layers to bind available Ca^{2+} which together allows gypsum ($\text{CaSO}_4 \cdot 2\text{H}_2\text{O}$) and/or calcite (CaCO_3) to precipitate.

Silicate formation by bacteria has been a very common phenomenon since the beginning of life. It is very likely that the direct participation of bacteria in the formation of these compounds rather than just a silicate after-formation binding with bacterial surfaces. The phenomenon of formation of microfossils is thought to be related to silicate interaction with bacteria (Schultze-Lam et al., 1996).

Colloidal substances naturally can sorb metals as well, these processes contribute to metal speciation in subsurface environments (Majone et al., 1998). This characteristic is interestingly not stopped when colloidal particles are associated with bacterial surfaces. They continue to bind metal ions which clearly enhances the overall metal binding capacity of bacterial surfaces. In fact it is not very usual to find bacterial-silicate precipitates lacking sorbed metals. Iron for example helps preserving structural characteristics of bacteria forming silicates.

The relationships of cells, colloidal fractions and metals have profound significance on several engineered biosorption processes like waste water treatment with immobilized cells, and more importantly it contribute to the understanding of complex transport

processes in soil. Understanding these complex transport processes is essential for more effective bioremediation strategies and for the prediction of contaminant fate in subsurface environments.

1.5 Microorganisms as highly reactive particles - the foundation of biofilms

As biocolloids, microorganisms have the highest specific surface of the living organisms. It is expected therefore a significant level of interaction between microbial cell surfaces and their environment. These interactions depend on the different types of cell walls, on their different molecular constituents and on the physicochemical conditions of the surroundings. Most cell surfaces have a net electronegative charge (Beveridge et al., 1997). At the most basic level bacterial cells can be classified according to their response to a stain used in light microscopy into Gram positive and Gram negative.

The cell wall of Gram positive bacteria is composed of a peptidoglycan matrix of about 20-30 nm with associated secondary polymers, teichoic or teichuronic acids (depending on the presence or absence of phosphate groups) and wall-associated proteins. The most common ionisable chemical groups in this type of cell wall are carboxylates (coming from the peptidoglycan, for example) and phosphates (coming from the teichoic acid). Studies with Gram positive bacteria such as *Bacillus subtilis* have demonstrated the presence of multiple cell wall depressions which enhances greatly its specific surface area (Beveridge et al., 1997).

Gram positive cell walls have an anionic nature which is reflected by their strong affinity for dissolved metal ions (Schultze-Lam et al., 1996). Metal binding on these types of cell walls is thought to occur in a two-step process. After the stoichiometric reaction of metal ions with the binding sites, these same sites initiate the deposition of larger amounts of metal (Beveridge et al., 1997). Metal binding can occur in different ways, e.g., by (i) ion exchange reactions, (ii) complexation, and (iii) precipitation, including redox reactions. The mechanisms can be both active and passive.

Active transport systems may allow the uptake of metals into the cytoplasm. This might be due to the inability of the cell to discriminate between essential metal ions such as calcium and toxic metal ions such as cadmium. Methylation and demethylation as well as oxidation and reduction are active processes altering the sorbed species and contributing to the overall sorption capacity of a biofilm (Brierley, 1990).

In the case of **Gram negative cell walls**, the major Gram positive cell wall component, peptidoglycan, is only present as a thin section located in a region called periplasm. The

periplasm is located between the cell membrane and the lipopolysaccharide, LPS bilayer. Embedded among the lipids, different types of outer membrane proteins can be found. These proteins are involved in several important processes such as transport or act as structural aids (lipoproteins).

The LPS in gram negative walls dictates to a great extent their binding capacity. It possesses an anionic net charge due to the exposed *phosphoryl* and *carboxyl* groups (Beveridge, 1999).

In both Gram positive and Gram negative bacteria, cell wall and membrane proteins participate not only in binding of solutes but also in local transport processes. Sorbed substances including particles can eventually reach the cytoplasm. In the cytoplasm, different types of transformations can occur, for example the reduction of poisonous heavy metals like mercury.

Although mainly negatively charged, some localized positive charges can be found in bacterial cell walls and membranes due to the presence of amine groups. This is one of the factors allowing the interaction with anions like SO_4^{2-} or SiO_2^{2-} . The interaction with silicates have important connotations for the colloid-sorption characteristics of bacteria.

Additional layers covering bacteria include capsules (most common), S-layers and sheaths (Schultze-Lam et al., 1996). Capsules and sheaths are composed mainly of acidic mucopolysaccharides or polypeptides. Capsules also interact strongly with metal ions (Parker et al., 1996).

1.6 Biofilms in the subsurface

Sections 1.4 and 1.5 highlight the importance of microbial complex surface characteristics on their capacity to interact with other particles and with surfaces. Once attached, microorganisms will tend to proliferate and to produce extracellular polymeric substances (EPS) (Wingender et al., 1999). This form of microbial life is known as biofilms (Flemming and Wingender, 2001a). Biofilms are found almost everywhere (wherever microbial life exists) and they can be located at different interfaces (Nivens et al., 1995). In natural soil and aquatic environments, on plant surfaces, on tissues of animals and man as well as in technical systems such as filters, pipes and reactors. The prerequisites of their occurrence are minimal: water, nutrients (even in traces), and microorganisms. Biofilms develop adherent to a solid substratum at solid-water interfaces, but can also be found at water-air and at solid-air interfaces. In this section, only the basic features that are shared by all biofilms are presented. The focus, however, is on biofilms growing in the confined spaces of sediment porous matrices and other subsurface environments.

1.6.1 Biofilm basics

Probably, the most common feature to all biofilms is that the microorganisms are embedded in a matrix of EPS which are responsible for their morphology, physicochemical properties, structure, coherence, and ecological features (Flemming and Wingender, 2001b; Allison, 2003; Flemming and Wingender, 2003). The existence of biofilms has been inferred for more than 60 years with pioneering works showing for the first time the affinity of microorganisms for surfaces (Zobell, 1943). However, the expression *biofilm* only became accepted by the end of the nineteen-seventies (Costerton et al., 1978).

A modern definition of biofilms was given by Donlan and Costerton (2002): "A biofilm is a microbially derived sessile community characterized by cells that are irreversibly attached to a substratum or interface or to each other, are embedded in a matrix of EPS that they have produced, and exhibit an altered phenotype with respect to growth rate and gene transcription".

The formation of biofilms starts with the first contact of a microorganism to a surface. Surfaces immersed into water become, within seconds, covered with a so-called conditioning film which consists of macromolecules such as humic substances, polysaccharides and proteins that are present in trace amounts in water. The cells do not need to be viable for adhesion, as the already present EPS are sufficient for adhesion (Flemming and Schaule, 1998). The organisms adhere to a surface for a certain period of time until they begin to multiply. A detailed model, defining five **stages in biofilm development**, using *Pseudomonas aeruginosa* as a model was proposed by Sauer et al. (2002). They divided the biofilm development into (i) reversible attachment, (ii) irreversible attachment, (iii) maturation-1 (log phase), (iv) maturation-2 (plateau phase), and (v) dispersion. The production of EPS serves, among other functions, as a structural aid for the consolidation of the mature biofilm. EPS helps in sequestering nutrients from the bulk water phase (sorption and other retention processes) and it is the main physical component of the biofilm that allow cells to be protected from "stressful" environments.

1.6.2 Distinguishing features of subsurface biofilms

Due to their porous nature, many subsurface environments have huge specific surface areas. Large surface areas are partly responsible for the tendency of nutrients and other metabolites to be filtered out by the porous medium. Accumulation of nutrients, with almost no exception, results in significant amounts of adhered microorganisms. Depending on the biogeochemical environment, these adhered microorganisms will grow

into biofilms or they will be remobilized. As it will be expanded later, there have been a great deal of research on biofilms developing in subsurface environments (Bouwer et al., 2000). There are several subsurface properties which determine biofilm formation in these environments in contrast to other types of interfaces and environments:

- High specific surface areas result in high nutrient accumulation and in high probability for microorganisms to be attached.
- The uneven distribution of pore sizes and the presence of dead-end paths make the porous medium a place where flow regimes change in relatively small spatial scales. This results in a wider range of localized flow regimes which has an impact on biofilm morphology and structure (Stoodley et al., 2005).
- Increased flow path tortuosity created by the porous medium geometry results in higher collisions of migrating particles and therefore, higher possibilities for microbial attachment as compared to flat surfaces, e.g., water distribution systems.
- With decreasing collector size (increasing specific surface area), bacterial size becomes an issue due to straining and clogging processes.
- High packing density of porous medium granules results in more drastic hydrodynamic alterations caused by biofilm accumulation as compared to flat surfaces. This can also limit nutrient distribution to biofilms close to the source of nutrients, e.g., water injection wells for bioremediation, underground leaking tanks, etc.

1.6.3 Subsurface biofilms - the clogging factor

The importance of "conservative solids" and microorganisms on the permeability and hydraulic conductivity loss found on many engineering operations was already recognized in the late nineteen forties (Allison, 1947). Many studies from the sixties and seventies dealing with engineering of filtration processes, investigated the loss of permeability caused by prolonged flow. Several of them came to the conclusion that these losses in permeability were caused by microorganisms. These investigations were done within the framework of soil science, water treatment and petroleum engineering (Taylor and Jaffe, 1990a). A great deal of effort was put on finding strategies to avoid the clogging of water injection wells in oil recovery procedures (Shaw et al., 1985). Strategies to selectively reduce the permeability of highly permeable regions were also investigated (Raiders et al., 1989). Water injection to oil bearing formations is a common strategy to enhance oil recovery. These and other studies during the eighties gave unequivocal evidence of the effects of biofilm formation on porous media hydrodynamics. Most

of the studies at this stage were only descriptive. No attempts were made to relate clogging data with biofilm growth dynamics and/or substrate utilization. More detailed information on subsurface biofilm growth dynamics (Taylor and Jaffe, 1990b) as well as changes in porous media hydrodynamic conditions (Cunningham et al., 1991) became available only as late as in the early nineties. The first modeling attempts (as reviewed in Rittmann, 1993) of biofilm growth in porous media, meant the beginning of a research subject that is still not completely explored.

Modeling of biofilm accumulation in these types of materials represents a huge computational challenge due to the multitude of processes involved: from microbe attachment to the kinetics of microbial growth and extracellular polymers production to biofilm detachment processes. These processes can be simulated separately with known models and then fed into more general biofilm models (Wanner et al., 1995; Chen and Kojouharov, 1998). For example microbial and therefore biofilm growth can be modeled using Monod kinetics:

$$\mu(c_n) = \frac{\mu_{max}c_n}{K_s + c_n} \quad (1.8)$$

where μ_{max} is the maximum specific growth rate, and K_s is the value of the concentration of nutrients, C_n , where the specific growth rate $\mu(c_n)$ has half its maximum value. The microbial death rate is assumed also to be proportional to the size of biofilm population (Chen and Kojouharov, 1998).

Changes in the saturated hydraulic conductivity can be used as an indirect indication of biofilm development. For example, the presence of bacterial extracellular polymers has been found to be responsible for saturated hydraulic conductivity reduction in sand columns (Vandevivere and Baveye, 1992). This is an indication of an active biofilm community. In saturated conditions, Darcy's law (see section 1.2.1) can be used to measure the hydraulic conductivity of the medium at any stage of biofilm development.

Cunningham et al. (1991) found that biofilm thickness acquired a quasi-stable state after about 5 days of growth under high load substrate conditions (Figure 1.8). Porous medium porosity decreased between 50 and 96 % and permeability decreased between 92 and 98 %. Vandevivere and Baveye (1992) found saturated hydraulic conductivity reduction due to the presence of bacterial extracellular polymers in the porous medium. They tested several mucoid strains and compared the results with non-mucoid mutants (Figure 1.9). The production of EPS had no effect on either cell multiplication within or movement through the sand columns; the reduction in permeability was therefore attributed to obstruction of pores with the polymers produced. All mucoid strains in this study caused strong clogging near the source of nutrients (column inlet).

In most cases a minimum permeability persisted after the biofilm reached its maximum

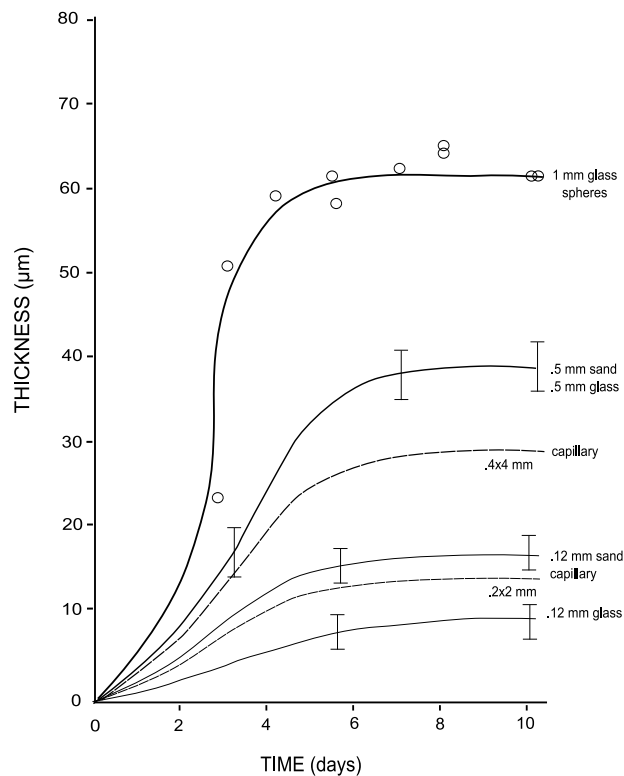


Figure 1.8: Time-dependent changes of *P. aeruginosa* biofilm thickness. Special porous media capillary reactors allowed for optical measurements of biofilm thickness throughout the experiment. A quasi-steady state in biofilm thickness is reached after about 5 days of operation (Cunningham et al., 1991).

thickness. This suggests a stabilization of biofilm accumulation and maintenance of a minimum nutrient transport within the porous medium. Polymer production decreases both the permeability and the porosity of the biofilm supporting porous medium. This fact however, does not exclude the possibility of patchy, localized biofilms affecting the hydraulic conditions of the medium. As explained in Rittmann (1993), patchy biofilms decrease permeability by accumulating in pore throats. Under these conditions, relatively low amounts of biomass accumulating at pore throats will cause great losses in permeability.

The conclusions obtained from many of the previously described experiments relied on indirect quantification of biofilm processes (e.g., rates of nutrient consumption in the effluent, dissolved oxygen concentrations in influents/effluents) or in destructive analytical techniques. New, advanced analytical tools for biofilm research such as the Confocal Laser Scanning Microscopy (CLSM), were not easily applied to biofilms in porous materials. There were, however, attempts to adapt the CLSM technology to study these types of biofilms by developing especially crafted porous media microscopy flow cells (Stoodley et al., 1994), and recently, using special transparent porous media analogues (Leis et al., 2005).

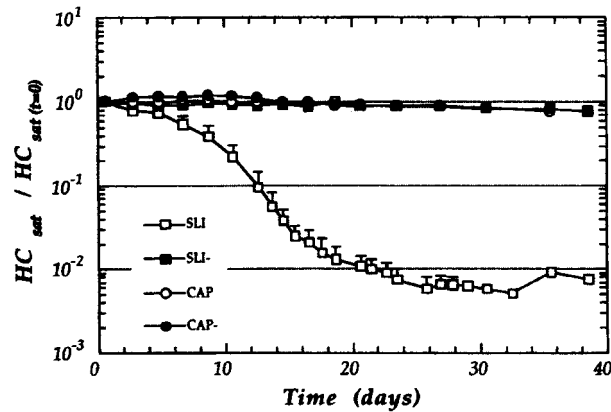


Figure 1.9: Changes in hydraulic conductivity in columns inoculated at a 2-cm depth with a slime-producing strain (SLI), with an encapsulated strain (CAP), or with their respective non-mucoid variants (SLI- and CAP-) (Vandevivere and Baveye, 1992).

At this stage, the main driving force for subsurface biofilm research was still the changes in the hydrodynamic conditions of the porous medium, e.g., permeability and hydraulic conductivity (Figure 1.10). The emerging field of bioremediation has provided ever since most of the data accumulated until today on subsurface biofilms. One of the most evident effects of subsurface biofilm formation is the drastic decreasing in pore liquid hydraulic conductivity. Losses in hydraulic conductivity combined with the ability to degrade a wide variety of contaminants is probably the reason behind the term “biobarriers” which is so commonly used in the literature.

1.6.4 Ecological perspective

Microorganisms are important soil components performing many processes associated with energy transfer and nutrient cycling (Horwath, 2002). These functions are critical to maintaining ecosystem productivity at all levels of the food web. The soil microbial biomass takes advantage of the multitude of soil niches providing different habitats and substrates. The most important function of soil biofilms is decomposition of organic material, thus generating nutrients for their own utilization or for other organisms or plants. In this respect, the soil biofilms act as a source and sink for nutrients in the soil. Another important by-product beyond nutrient cycling is the formation of stable organic matter. The soil organic matter, through its interaction with minerals, serves many functions that increase soil quality through enhancement of physical, chemical, and biological characteristics of the soil matrix.

It is clear now that the type of biofilm (patchy or confluent) will have an impact not only on the biodegradation of pollutants and on the movement of colloids but also on

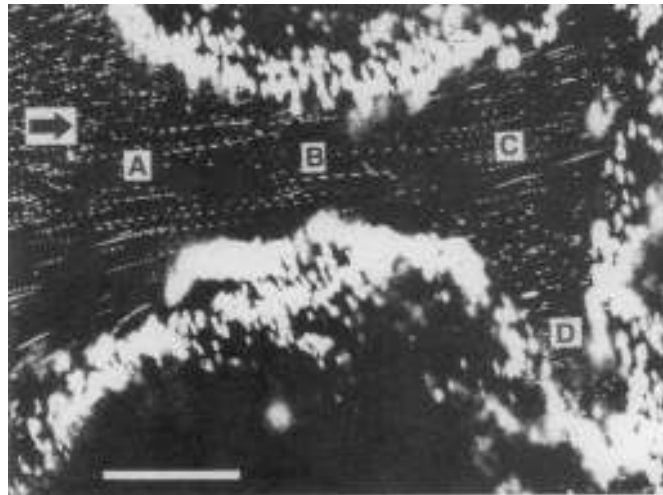


Figure 1.10: Liquid flow between two glass beads with accumulated biofilm, as visualized with latex particles (bright dashed tracks). Velocity profiles were determined across the channel at the entrance (A), throat (B), and exit (C) areas of the constriction. One of the pores was blocked by biofilm, creating a stagnant area (D). The direction of bulk fluid flow is indicated by the arrow. Bar = 100 μ m. (Stoodley et al., 1994).

porous media hydrodynamics. A great deal of the physical characteristics of porous media biofilms will be determined by the types of microorganisms composing the biofilm, their ecology and the geochemistry of the site (Anderson and Lovley, 1997). Most pristine subsurface environments are oligotrophic. This oligotrophic nature derives from the fact that there are small amounts of organic substrates available. Most easily degraded carbon sources are used by surface or close-to-surface biota before they can reach deeper layers within the surface (Anderson and Lovley, 1997). Even though microbial growth rates in subsurface environments are slower than in surface soils, there is a wide diversity of microbial life in many of them (Kieft and Phelps, 1997). There are also indications that the microbial community is adapted to these oligotrophic conditions. For example, when bacteria were transported by advection in high recharge zones to deeper layers of the subsurface, they displayed increased nutrient stress as compared with native communities (Balkwill et al., 1997).

On the contrary, contaminated environments display a rich variety of redox processes (Ludvigsen et al., 1998). In this type of environments, anaerobic microbial processes are of much more relevance than aerobic processes. This is because aerobic microorganisms can readily degrade most of the constituents of common aquifer pollutants removing in this way oxygen from the system. Due to the poor oxygen solubility, any traces of oxygen entering the system through diffusion from the surface or with recharge water will be quickly removed by these active aerobic microorganisms. Organic matter will be then utilized in a succession of electron accepting processes.

Currently, most of the data about subsurface biofilms is coming directly from bioreme-

diation studies. The so-called **biobarriers** are a subject of intense research in recent years. Biobarriers can be as diverse as their microbial constituents, with equally diverse degradation properties. Biobarriers are used heavily for groundwater bioremediation. A fair amount of effort has been directed to modeling (Wanner et al., 1995; Chen and Kojouharov, 1998; Chen-Charpentier and Kojouharov, 2001) and to biobarrier technology. The use of starved bacteria and controlled injection of nutrients for forming thick biofilms was (and still is) a promising strategy for the containment of subsurface contaminant plumes (Cunningham et al., 2003). These "redox-reactive" barriers as they are commonly known, expanded the concept of porous media biofilms from simple "biomass accumulations reducing permeability", to the whole range of redox conditions in which they can be found in natural and contaminated environments. From aerobic biofilms in oxygenated environments to methanogenic biofilms in anaerobic environments, many are subject of active research. Examples include: biobarriers composed of dissimilatory metal-reducing bacteria (DMRB). DMRB bacteria are known to facilitate the degradation of many chlorinated organics and the precipitation of heavy metals (Gerlach et al., 1998); biobarriers used to contain nitrate groundwater plumes, using nitrate reducing bacteria (Dutta et al., 2005); or subsurface biofilm degradation of aromatic hydrocarbons (Zhang et al., 1995). For in depth reviews, especially on bioremediation of organic compounds refer to Holliger et al. (1997) or Anderson and Lovley (1997).

Many of these studies, however, underestimate the role of biofilms as complex multicellular structures. The physical alteration of the porous medium caused by biofilms (e.g., changes in hydraulic conductivity or permeability) is already a well observed phenomenon. The same is true for the characterization of biofilms thriving at several redox conditions including, nitrate reducing, sulphate reducing and methanogenic. Despite of this, a lot of information is still needed on several phenomena in which biofilms are clearly involved. These processes include transport of both dissolved and particulate matter; changes in pore water chemistry due to biofilm formation; degradation and transformation pollutants. In the case of degradation and transformation of pollutants, it is very common to find studies in which general conclusions are drawn from degradation properties of isolated bacterial species. As expanded in the next section, the EPS matrix in which many of these microorganisms are embedded in nature, can influence considerably their retention and transformation capacities. More studies are therefore required which take into account biofilms as a whole rather than as their isolated constituents. This should be done in order to resemble a bit closer conditions occurring *in situ*.

1.7 Retention capacity of biofilms - EPS and its impact on transport

A key feature of biofilms and their metabolic activities is their retention and transformation capacity (Flemming, 1995; Flemming and Leis, 2002; Flemming et al., 2005). Biofilms play a role both as sink and source for pollutants not only in the subsurface but in many other environments such as rivers and water distribution systems. Both transformation and retention are phenomena altering the migration of particles in subsurface environments. The work described in this thesis concentrates on retention-remobilization rather than on transformation (which usually involve longer time scales as those performed here).

Retention of solutes and particles has been described both as an equilibrium and as a kinetic process. In both cases it is common to utilize the term *sorption*. Sorption refers to both *adsorption*, *absorption* and *desorption*. *Adsorption* implies the retention of a solute on the surface of the particles of a material. *Absorption* in contrast involves the retention of a solute within the interstitial molecular pores of such particles (Skoog et al., 1996). The term *desorption* involves the release of sorbed materials to the surrounding solution.

Biofilms can sorb water, inorganic and organic solutes, colloids and other particles. The two main biofilm compartments with retention capacity are the microorganisms and the EPS matrix. The retention capacities of microorganisms including their cell walls, membranes and cytoplasm, as individual particles were presented in section 1.5. In this section, the retention capacities of the EPS matrix are presented.

The largest component in terms of volume in most biofilms is the highly hydrated extracellular polymeric matrix, understood as the network of EPS (Wingender et al., 1999) plus the accumulated material (Flemming and Leis, 2002). EPS which consists of polysaccharides, proteins, nucleic acids, and lipids, provide charged and non-charged areas, as well as hydrophobic regions of proteins and polysaccharides, where sorption can occur.

By definition, EPS are located at or outside the cell surface independent of their origin. The extracellular localization of EPS and their composition may be the result of different processes: active secretion, shedding of cell surface material, cell lysis, and adsorption from the environment. Microbial EPS are biosynthetic polymers (biopolymers) which consist mainly of polysaccharides and proteins, but can also contain substantial amounts of DNA, lipids, glycolipids and humic substances (Jahn and Nielsen, 1995; Nielsen et al., 1997). Most bacteria are able to produce EPS, whether they grow in suspension or in biofilms. Cell surface polymers and EPS are of major importance for the

development and structural integrity of flocs and biofilms. They mediate interactions between the microorganisms and maintain the three-dimensional arrangement. It must be pointed out that polysaccharides are not necessarily the main EPS component. In many cases of environmental biofilm samples, proteins prevail, and humic substances are also integrated in the EPS matrix, being considered by some authors as belonging to the EPS (Wingender et al., 1999). Although mostly a minor component, lipids can make up a significant proportion of the EPS in some cases. This has been shown in the case of strongly acidophilic organisms, colonizing and leaching pyrite (Gehrke et al., 1998).

Extracellular polysaccharides are believed to have the main structural function within biofilms by forming and stabilizing the biofilm matrix. The role of proteins, however, is mostly considered in terms of their enzymatic activity. Only a few authors speculate that extracellular proteins may also have structural functions. For example, the bridging of extracellular polysaccharides by lectin-like proteins is discussed (Dignac et al., 1998). Furthermore, the role of lectins (proteins with specific binding-sites for carbohydrates) in adhesion of bacterial cells and biofilm formation has been investigated (Tielker et al., 2005). A part of the extracellular proteins has been identified as enzymes. An overview about extracellular enzymes can be found in Wingender and Jaeger (2002).

It is obvious that each of these sites has different sorption mechanisms and capacities (Beveridge, 1989). Sorption characteristics in biofilms as composed of living organisms can change depending on a great number of factors (Langley and Beveridge, 1999). This is exemplified on studies in which a biofilm of *P. putida* was exposed to toluene. Exposure to toluene resulted in an increase of charged groups in the EPS providing more ionic binding sites (Schmitt et al., 1995). A comprehensive review on the sorption properties of biofilms can be found in Flemming et al. (2005).

In Figure 1.11 are represented different possibilities for sorption and desorption to and from a biofilm matrix (including microbes). Substances located initially at the water phase will have a strong tendency to interact with many of the sorption sites depicted in this figure.

Water retention is of highest importance for biofilm organisms. Biofilms are highly hydrated with most of the water retained by the EPS network. Only 1 - 10 % of the water in a biofilm is cytoplasmic whereas 90 - 99 % remains with the EPS. This can be demonstrated when considering that biofilm cell densities range between 10^{10} and 10^{11} cells mL^{-1} of biofilm volume and an average cell has a volume of approximately 10^{-12} ml with a water content of 85 %. This affinity for water gives a slimy consistency to biofilms. The mobility of this water seems to be very similar to that of the free water phase as concluded from NMR studies (Vogt et al., 2000). However, an FTIR-ATR study indicates discrete steps in the exchange kinetics of H_2O and D_2O , leading to the conclusion that

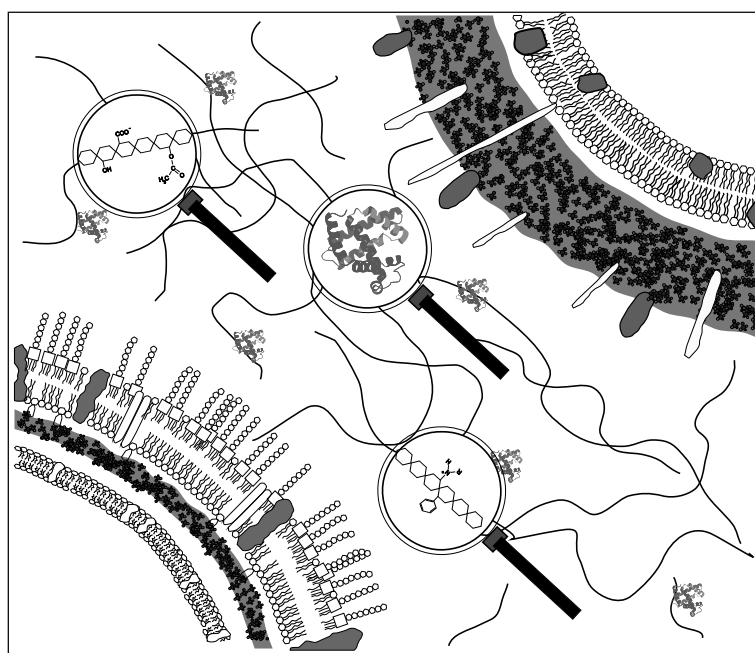


Figure 1.11: Schematic depiction of the binding sites in biofilms (Gram-positive and Gram-negative cell, and EPS including polysaccharides and proteins) (courtesy Martin Strathmann).

the EPS-retained water is organized in a differentiated structure (Schmitt and Flemming, 1999). **Metals.** Since EPS may contain anionic groups such as carboxyl, phosphoryl, and sulphate groups (Sutherland, 1994) as well as anionic peptides within proteins, they offer cation exchange potential.

Extensively studied for their metal-binding action are the EPS produced by bacteria in sewage treatment facilities (Flemming et al., 1996; Flemming and Leis, 2002). EPS bind a wide variety of metals such as Pb^{2+} , Sr^{2+} , Zn^{2+} , Cd^{2+} , Co^{2+} , Cu^{2+} , Mn^{2+} , Mg^{2+} , Fe^{2+} , Ni^{2+} , and Ag^+ . Theoretical predictions of EPS-binding capacities, based on estimated numbers of available carboxyl and hydroxyl groups, suggest a very high capacity, especially for acidic polysaccharides. This means that a small amount of EPS could theoretically bind a large amount of a given metal. Metal binding by EPS seems highly plausible from a mechanistic point of view, considering the charged groups of the EPS and their ionic binding capacity. However, in spite of the large body of references confirming this, Späth et al. (1998) separated EPS from cells after loading activated sludge with Cd^{2+} . Most of the metal was bound to the cell surfaces and not to the EPS as could have been expected considering the charged nature of many EPS components. The same was true for Ni^{2+} and Zn^{2+} . These findings coincide with the results of the research of Beveridge (1989) who demonstrated that bacterial cell walls can act as templates for metal deposition.

Organics. The sorption of organic substances to EPS is a well known phenomenon. The unwanted sorption of organic pollutants by biofilms is vastly documented, especially in

sewage treatment plants (Flemming et al., 1996).

Wolfaardt et al. (1998) investigated the spatial arrangement of EPS using fluorescent-labeled lectins and Confocal Laser Scanning Microscopy (CLSM) in presence of the herbicide diclofop. They found a nearly 1:1 correspondence between the distribution of regions that accumulated diclofop (and other chlorinated ring compounds) and regions with binding sites for the α -L-fucose-specific *Ulex europaeus* Type I lectin. These regions also bound polyanionic and cationic fluorochrome-conjugated dextrans, and a hydrophobic-specific dye, demonstrating the non-uniform distribution of charged and hydrophobic regions in the biofilm matrix.

EPS can contain significant amounts of proteins. These may as well provide apolar areas with a sorption potential for apolar organic molecules. However, the polysaccharide moiety, although hydrophilic by nature, must interact with hydrophobic molecules as well. This consideration is supported by the colonization of hydrophobic surfaces by means of the EPS of hydrophilic bacteria and by the performance of biofilm reactors which degrade hydrophobic organics. It is known that many EPS have surface active properties (Neu, 1996) which must play a central role in such processes.

1.8 Problem formulation and aim of the study

Three main environmental issues highlighted in section 1.1, justify the work that is described in this thesis: (i) The ubiquity of biofilms, which represent an important aspect of many sites biogeochemistry; (ii) the presence of mobile colloids with their role on contaminant transport and (iii) the common changes in pore water ionic composition and concentration. Hydrodynamic transport is the underlying phenomenon driving the interaction between all these issues.

As expanded in sections 1.2 and 1.3 many of these issues have been investigated in isolation with experiments aiming to prove fundamental principles or at highly defined experimental conditions. In terms of biofilms, it has been proven for example that their formation is interdependent with hydrodynamics (Cunningham et al., 1991) and electron donors and acceptors available. Accordingly, colloid and bacterial transport has been actively investigated already for several years. The influence of ionic concentration and speciation in combination with biofilm formation and colloid transport in highly permeable sediments remains, however, a vastly unexplored subject.

The model aerobic biofilm forming microorganism, in combination with a highly permeable porous medium (quartz sand) were chosen in order to resemble conditions found in highly permeable sediments. These types of sediments are found for instance in many

river beds and on water saturated zones just below the water table in many other subsurface environments. These are zones of complex hydrodynamic conditions in which transport processes are not diffusion limited but rather highly influenced by advective and dispersive processes. Sand column studies were chosen instead of static batch systems in order to reproduce as closely as possible, dominant advective conditions. Clay colloids on the other hand were chosen for being important soil constituents which interact actively with microorganisms and are implicated on the transport and transformation of many substances including contaminants. Finally, changing ionic conditions were simulated by using Ca^{2+} or Na^{+} based solutions as column and microscopy flow cell influents. Calcium and sodium ions were chosen due to their importance in many subsurface environments as highlighted in section 1.1.

The main aim of this work was to investigate the influence of biofilms on colloid retention-remobilization processes in model sediment columns, at changing fluid ionic conditions. Biofilm influence was expressed in terms of the relative contribution of two major EPS components: extracellular carbohydrates and extracellular proteins. The following set of research objectives were identified in order to achieve this main aim:

- To characterize the transport of Laponite RD as model clay colloid, including aggregation and interaction with a model contaminant.
- To characterize the transport of *Pseudomonas aeruginosa* SG81 including the impact of attachment and phenotypical changes on its mobility through saturated porous environments.
- To demonstrate interactions between both types of colloids and their impact on colloidal mobility through the porous medium at changing electrochemical conditions.
- To determine the influence of biofilms on colloid transport processes at two environmentally relevant pore fluid ionic compositions.

The results are expected to contribute to the understanding of complex interaction processes determining biofilm influence in colloid and contaminant transport as well as biofilm formation and stability in subsurface environments.

Chapter 2

Materials and Methods

2.1 Bacterial strains and growth media

Table 2.1: Bacterial species used in the experiments

Strain	Genotype/phenotype	Origin	Reference
<i>Pseudomonas aeruginosa</i> SG81	Mucoid	Isolate from a technical water system	(Grobe et al., 1995)
<i>Pseudomonas aeruginosa</i> SG81R1	Spontaneous, non-mucoid revertant	Derived from strain SG81	(Grobe et al., 1995)

The well characterized, biofilm-forming, EPS producing microorganism, *Pseudomonas aeruginosa* SG81 and its alginate deficient mutant, *P. aeruginosa* SG81R1 were used as a model microorganisms. *P. aeruginosa* SG81 is a mucoid, Gram-negative, motile bacterium which was originally isolated from a technical water system (Grobe et al., 1995). On agar plates, *P. aeruginosa* SG81 over-produces slimy and shiny colonies. This slime is composed of extracellular polymeric substances including polysaccharides and proteins among others (Wingender et al., 2001). This strain especially produces copious amounts of the acidic polysaccharide alginate. Biofilm developing conditions inside sand columns were not known for this organism yet.

All nutrient media were dissolved in deionized water and autoclaved for 20 min at 121°C. When necessary, the pH of the resulting solutions was adjusted to 7 using either HCl (0.2 M) or NaOH (0.2 M). Sterile agar media was spread in Petri dishes (20-25 mL) and used within 3 weeks (storage at 4°C) after preparation. For confluent biofilm-forming microorganisms, Petri dishes containing vents were used, in order to assure sufficient air exchange. Nutrient media used are compiled in Table 2.2.

Table 2.2: Nutrient media used for growing bacteria

Description/ reference	Solutions	Manufacturer	Components	Quantity per liter
Nutrient agar (NA)	Ready-to-use medium	Difco 0001-17	Bacto beef extract	3.0 g
			Bacto peptone	5.0 g
			Bacto agar	15.0 g
Tryptic soy broth (TSB)	Ready-to-use medium	Merck, Darmstadt	Peptone from Casein	17.0 g
			Peptone from Soja	3.0 g
			D-(+)-Glucose	2.5 g
			NaCl	5.0 g
			K ₂ HPO ₄	2.5 g
Pseudomonas isolation agar (PIA)	Ready-to-use medium	Difco 0927-17-1	Bacto peptone	20.0 g
			Bacto agar	13.6 g
			MgCl ₂	1.4 g
	+ Glycerin	Fluka 49770	K ₂ SO ₄	10.0 g
			Irgasan DP 300	25 mg
Nutrient broth (NB)	Ready-to-use medium	Difco 0003-17-8	Bacto beef extract	3.0 g
			Bacto peptone	5.0 g
Alginate promoting medium (APM) ^a	1		Na-D-Gluconate	2.181 g
	2		KNO ₃	1.011 g
	3		MgSO ₄ • 7 H ₂ O	0.492 g
	4		NaH ₂ PO ₄ • H ₂ O	17.15 mg
APM50	APM		K ₂ HPO ₄	48.84 mg
	Suppl. 1		+ Na-D-Gluconate	106.87 g
	Suppl. 2		Yeast Extract (YE)	0.5 g
Luria Bertani agar (LB)	Ready-to-use medium	Difco	NaCl	17.5 g
			Tryptone	10 g
			YE	5 g
M9-Medium ^b	1 2 3 4	Merck	Bacto-Agar	15 g
			D-Glucose	40 g
			MgSO ₄ • 7 H ₂ O	20 g
			CaCl ₂ • 2 H ₂ O	2 g
M9-Medium ^b	4		Na ₂ HPO ₄ • 2 H ₂ O	70 g
			KH ₂ PO ₄	30 g
			NaCl	5 g
			NH ₄ Cl	10 g

... continued on next page

... continued from previous page

Description/ reference	Solutions	Manufacturer	Components	Quantity per liter
	5	Difco	Bacto-Agar	20 g
	6		Glutamic acid	50 g
Swarming-agar (0.5 % agar)	M9-Medium-based		M9-Medium Sol. 1	90 mL
			M9-Medium Sol. 2	9 mL
			M9-Medium Sol. 3	9 mL
			M9-Medium Sol. 4	90 mL ^c
			M9-Medium Sol. 5	225 mL
			M9-Medium Sol. 6	9 mL
			Deionized water	468 mL
Swimming-agar (0.3 % agar)	M9-Medium-based		M9-Medium Sol. 1	90 mL
			M9-Medium Sol. 2	9 mL
			M9-Medium Sol. 3	9 mL
			M9-Medium Sol. 4	90 mL ^d
			M9-Medium Sol. 5	135 mL
			M9-Medium Sol. 6	9 mL
			Deionized water	567 mL

^aOhman and Chakrabarty (1981), ^bSambrook et al. (1989), ^cwithout NH₄Cl, ^dwith NH₄Cl

2.2 Buffers, solutions and colloidal suspensions

Laponite RD (LRD), a synthetic hectorite clay was chosen as a model colloid due to its high purity, monodispersity, and homogeneous dispersion properties in deionized water. LRD consists of 30 nm diameter plate-like particles with a thickness of 1-2 nm when hydrated (Nicolai and Cocard, 2001). LRD suspensions were used at the concentrations compiled in Table 2.3.

Rhodamine 6G (R6G) was used to facilitate the detection of LRD in presence of organic material. In sterile experiments similar aggregation and transport patterns were found for unstained suspensions. Thus, R6G does not influence the aggregation and transport of LRD. Other various chemicals used in the experiments are compiled in Table 2.4.

2.2.1 LRD-R6G staining protocol

The procedure described here is according to Tapia Estévez et al. (1994). It was observed that 5×10^{-6} M R6G worked well for concentrations between 2000 and 200 mg L⁻¹ LRD.

For lower concentrations, 5×10^{-7} M R6G worked better. LRD could be easily dissolved in deionized water at concentrations up to 10000 mg L^{-1} after being stirred for about half an hour. The pH of the resulting suspension depended on LRD concentration and it ranged from pH 10 for LRD concentrations of 2000 mg L^{-1} or more to pH between 6-7 for LRD concentrations lower than 200 mg L^{-1} . To adjust pH to 7, 0.2 M HCl was added to the colloidal suspensions ($750 \text{ }\mu\text{L}$ for 2000 mg L^{-1} , $75 \text{ }\mu\text{L}$ for 200 mg L^{-1}). For lower LRD concentrations no HCl was added.

The Cation Exchange Capacity (CEC) of the clay was not directly measured but a value of 0.73 meq g^{-1} was obtained from the literature (Cione et al., 1998). The milliequivalents of dye were obtained simply by: $\text{meq} = \text{mg} * \text{valence} / \text{molecular weight}$.

The following R6G stock solutions were used: 5×10^{-5} M R6G in deionized water (RhD), 5×10^{-5} M R6G in 0.7 M NaCl (RhS) and 5×10^{-5} M R6G in 0.7 M CaCl_2 (RhSca). Example procedure for 200 mg L^{-1} LRD and 5×10^{-6} M R6G corresponding to 3.5 % of the clay CEC:

- Weight 0.05 g powder LRD and put them in a 250 mL Erlenmeyer flask.
- Measure 250 mL deionized water and take out 25 mL from this volume.
- Mix the LRD with the water and use a magnetic stirrer to dissolve it for at least 30 minutes.
- Once the colloidal suspension is completely clear, add $75 \text{ }\mu\text{L}$ from 0.2 M HCl while stirring.
- While still stirring add:
 - 25 mL of RhD for no salt R6G-LRDsuspension.
 - 0.22 mL of RhS and 24.8 mL of RhD for 0.625 mM NaCl.
 - 0.45 mL RhS and 24.55 mL RhD for 1.25 mM NaCl.
 - 0.9 mL RhS and 24.1 mL RhD for 2.5 mM NaCl.
 - 1.8 mL RhS and 23.2 mL RhD for 5 mM NaCl.
 - 3.6 mL RhS and 21.4 mL RhD for 10 mM NaCl.
 - 12.6 mL RhS and 12.4 mL RhD for 35 mM NaCl.
 - 25 mL RhS and no RhD for 70 mM NaCl.
 - Replace RhS with RhSca when needed for CaCl_2 .
- The R6G containing solutions should be added drop wise while stirring with the help of a pipette.

- LRD-R6G suspensions can be dialyzed (for 24 h) against a bigger volume of deionized water so any free R6G is eliminated.

Even though suspensions at 0.35 % and 35 % of the clay CEC, were also prepared, these were not used for the main transport experiments.

Table 2.3: Buffers, solutions and colloidal suspensions

Description/reference	pH	Solution/suspension	Components	g L ⁻¹
NaCl based solutions	7.3	6.25 x 10 ⁻⁴ M		0.0365 ^a
	"	1.25 x 10 ⁻³ M		0.0730 ^a
	"	2.50 x 10 ⁻³ M		0.1461 ^a
	"	5.00 x 10 ⁻³ M		0.2922 ^b
	"	1.00 x 10 ⁻² M	NaCl	0.5844 ^b
	"	3.50 x 10 ⁻² M		2.0454 ^b
	7.9	7.00 x 10 ⁻² M		4.0908 ^b
	"	1.40 x 10 ⁻¹ M		8.1816
	"	1 M		58.44
CaCl ₂ based solutions	7.1	6.25 x 10 ⁻⁴ M		0.0919 ^a
	"	2.50 x 10 ⁻³ M		0.3675 ^a
	"	1.00 x 10 ⁻² M	CaCl ₂ • 2 H ₂ O	1.4702 ^b
	"	3.50 x 10 ⁻² M		5.1457 ^b
	7.3	7.00 x 10 ⁻² M		10.2914 ^b
EPS extraction buffer ^c	7	Single	Na ₃ PO ₄	0.76
			NaH ₂ PO ₄	0.552
			NaCl	0.526
			KCl	0.075
Phosphate buffered saline (PBS)	7.4	Single	NaCl	8
			Na ₂ HPO ₄ • 2 H ₂ O	1.805
			KCl	0.2
			KH ₂ PO ₄	0.24
Nigrosine	-	Single	Nigrosine	0.02
Laponite based solutions	7	2000 mg L ⁻¹	NaCl	0.1461 ^d
				4.0908 ^d
				8.1816 ^d
				0 ^d
				0.0365 ^d
				0.073 ^d
Laponite based solutions	7	200 mg L ⁻¹	NaCl	0.1461 ^d
				0.2922 ^d

... continued on next page

... continued from previous page

Description/reference	pH	Solution/suspension	Components	g L ⁻¹
				0.5844 ^d
				2.0454 ^d
				4.0908 ^d
		20 mg L ⁻¹	NaCl	0 ^e
				4.0908 ^e

^a+ 0.0084 g NaHCO₃, ^b+ 0.084 g NaHCO₃, ^cFrølund et al. (1996), ^d+ 2.4 x 10⁻³ g L⁻¹ Rhodamine 6G
^e+ 2.4 x 10⁻⁴ g L⁻¹ Rhodamine 6G

2.2.2 Influent background solutions

CaCl₂ or NaCl based solutions were used at the concentrations used for the transport experiments. For the biofilm influence experiments, these solutions were used at 70 mM concentration as background solutions either when Alginate promoting medium (APM) or the model colloid suspensions were not the influents. In order to keep pH between 7 and 8, 1 mM NaHCO₃ was added to the working solutions. Low ionic strength solutions were either deionized water or 0.1 mM NaHCO₃.

Table 2.4: Chemicals

Name	Formula	Molecular weight	Manufacturer	Order Nr.
Acetone	C ₃ H ₆ O	58.08	KMF	KMF.08-201
Bovine serum albumin (BSA)	-	-	Sigma	A-4503
Calcium chloride dihydrate	CaCl ₂ • 2 H ₂ O	147.02	Merck	21101
DAPI (4',6-diamidino-2-phenylindole)	-	-	Sigma	D-9542-50MG
DOWEX, 50x8	-	-	Fluka	44445
Ethanol absolute	C ₂ H ₆ O	46.07	KMF	KMF.08-205
Ethylenediaminetetraacetic acid-di-sodium salt-dihydrate (Titrplex III) (Na ₂ -EDTA)	C ₁₀ H ₁₄ N ₂ Na ₂ O ₈ • 2 H ₂ O	372.24	Merck	1.08418.0250
Fluorescein-sodium	C ₂₀ H ₁₀ Na ₂ O ₅	376.28	Merck	1.03992.0050
Folin-Ciocalteu phenol reagent	-	-	Sigma	F9252-500ML
Formaldehyde solution 37 %	CH ₂ O	30.03	Baker	7040

... continued on next page

... continued from previous page

Name	Formula	Molecular weight	Manufacturer	Order Nr.
D-gluconic acid, sodium salt	C ₆ H ₁₁ NaO ₇	218.1	Sigma	69005
Hydrochloric acid, 25 %	HCl	36.46	Fluka	84410
Lowry reagent	-	-	Sigma	L3540-1VL
Magnesium sulphate hepta-hydrate	MgSO ₄ • 7 H ₂ O	246.37	Merck	1.05886.1000
Methanol	CH ₃ OH	32.04	Merck	1.06009.2511
Nigrosine			Merck	1.15924.0025
Phenol	C ₆ H ₆ O	94.11	Riedel de Haën	33517
Potassium di-hydrogen phosphate	KH ₂ PO ₄	136.09	Fluka	60218
di-potassium hydrogen phosphate	K ₂ HPO ₄		Merck	1.05104.1000
Potassium hydroxide	KOH	56.11	Baker	0385
Potassium nitrate	KNO ₃	101.11	Merck	1.05063.1000
SYTO® 9	-	-	Molecular Probes	L7012
Propidium iodide	-	-	Molecular Probes	L7012
Rhodamine 6G	C ₂₈ H ₃₀ N ₂ O ₃ • HCl	479.02	Fluka	83698
Sodium acetate	C ₂ H ₃ NaO ₂	82.03	Merck	1.06268.1000
Sodium azide	NaN ₃	65.01	Merck	1.06688.0100
Sodium bicarbonate	NaHCO ₃	83.99	Riedel de Haën	31437
Sodium chloride	NaCl	58.44	Riedel de Haën	31434
Sodium di-hydrogen phosphate mono-hydrate	NaH ₂ PO ₄ • 2 H ₂ O	137.99	Merck	1.06346.1000
di-sodium hydrogen phosphate di-hydrate	Na ₂ HPO ₄ • 2 H ₂ O	177.99	Riedel de Haën	30412
Sodium hydroxide	NaOH	40	KMF	KMF.08-620.1000
Sulfuric acid, 95-97 %	H ₂ SO ₄	98.08	KMF	KMF.08-743
Tween 20 (polyoxyethylene sorbitan monolaurate)	-	-	Fluka	93773
YE	-	-	Merck	1.03753.0500

2.3 Equipment

2.3.1 Optical measurements

2.3.1.1 UV-VIS spectrophotometry

A UV-VIS photometer (Cary 50, Varian Inc) was used to monitor bacterial and contaminant concentrations in column effluents. The spectrophotometer is equipped with a xenon lamp and it is operated with the WinUV operating software. The equipment is able to perform a wide variety of spectroscopic analysis using the default software specifications. It was necessary, however, to develop a custom application in order to perform the online measurements used in this study. The Applications Development Language (ADL) was used for this purpose. An ADL shell script was written so the equipment could be programmed to perform time series measurements at the specified time intervals and wavelengths. The script is available here: http://lamaquina.de/thesis/scripts/caryUV/meas_winNT.ADL. Online measurements were performed in this way, by connecting the sterna flow cell to the outlet of the chromatographic columns.

2.3.1.2 Fluorescence spectrophotometry

Column effluent fractions were obtained using a fraction collector (Pharmacia FRAC-100). Fluorescence measurements were performed using a fluorometer (SFM 25, Kontron Instruments). The fluorescence of the same solution used for sediment column saturation was used to determine the relative fluorescence of collected effluent fractions. LRD-R6G complexes were detected in column effluents by fluorescence at an excitation wavelength of 480 nm, and emission wavelength of 551 nm.

2.3.1.3 Zeta potential measurements

The zeta potential of suspensions of *P. aeruginosa* SG81 was measured using the ZetaSizer 3000 (Malvern Instruments). This instrument, uses Doppler Laser anemometry to obtain data on electrophoretic mobility of colloidal particles. The zeta-potential can then be obtained by using the Henry equation:

$$\mu = \frac{2\varepsilon\zeta f(kr)}{3\eta} \quad (2.1)$$

where μ is the mobility, ζ is the Zeta potential, ε is the di-electrical constant, η is the Dynamic viscosity and $f(kr)$ is the Henry function. The following conditions were set for the instrument:

- Sample volume: 50 mL (of a 10^7 cells / mL suspension)
 - Cells were recovered from an overnight culture, washed by centrifugation or filtration and re-suspended in buffer at the specified concentration.
- Salinity: 0.14 M NaCl
- Titrator settings: 0.250 M HCl; 0.250 M NaOH (injection volume: 0.080 mL)
- The sample was split in two, the titration always started from the pH measured in the bacterial suspension without the addition of acid or base (around 5.6). In one part of the sample the titration was made with HCl towards low pH and in the other with NaOH towards high pH values.
- The data was combined and the zeta potential was plotted against pH.

2.3.1.4 Particle size distribution

These analysis were performed at the IWW Institute for water in Mülheim, using a Particle Measuring System Syringe (Markus Klotz GmbH). Particle size distributions were obtained from SFM effluent fractions at different salt concentrations. 50 mL from the intact fraction (around 400 mL) were concentrated in 0.5 M CaCl_2 . From this suspension, 18 mL were dialyzed against deionized water overnight and then further concentrated in 1 mL by freeze drying. The samples prepared in this way were submitted to the IWW for further analysis. Instrument conditions were as follows:

- Flow rate : 20 mL min^{-1}
- Flask volume : 10 mL
- Sample volume : 1 mL
- Dilution factor : 1:1000
- Density : 1 g mL^{-1}
- Number of measurements per fraction : 5

2.3.2 Microscopy

2.3.2.1 Confocal Laser Scanning Microscopy

A laser scanning module (LSM 510 - Carl Zeiss Jena) coupled to an inverted Axiovert 100 M BP microscope (Zeiss), was used. The system was equipped with an argon laser (possible excitation wavelengths: 458 nm, 488 nm and 514 nm at 25 mW), two helium-neon lasers (possible excitation wavelengths: 543 nm at 1 mW and 633 nm at 5 mW) and one argon-ions-UV-laser (possible excitation wavelengths: 351 and 364 at 80 mW). The microscope was equipped with the following objectives: Plan-Neofluar 10x / 0.30, Plan-Neofluar 20x / 0.50, Plan-Neofluar Multi-Immersion 25x / 0.8 Imm. corr., 40x / 1.30 oil, C-apochromat objective 40x / 1.20 W. corr., LD achroplan 40x / 0.6 corr., LD achroplan 63x / 0.75 corr., plan-apochromat 63x / 1.40 oil DIC and finally, plan-neofluar 100x / 1.30 oil. The microscope was operated through a PC with the software LSM 510 Release 3.2 (Zeiss). Basic visualization and image manipulation was done using the program Axio Vision (Version 3.1, Zeiss Vision). Further image analysis was done with the program ImageJ (see section 2.7.5.1 for more information on this).

2.3.2.2 Fluorescence microscopy

For epifluorescence imaging a Laborlux S (Leitz) microscope was used. The microscope comes equipped with the following objectives: PL Fluotar 10x / 0.30, 25x / 0.60, 40x / 0.70 and 100x / 1.32 oil. Pictures were taken using a digital camera (Pentax 5 M pixel).

2.3.2.3 Scanning Electron Microscopy

A LEO 1530 field emission scanning electron microscope (LEO Electron Microscopy Group) was used for obtaining the electron micrographs. Images were made using the secondary electron detector as well as the Inlens-detector at an acceleration voltage of 10-15 kV. The images were taken at the University of Duisburg-Essen, section Duisburg, in the Faculty of Material Science.

2.3.3 Electro-chemical equipment

A D230 multi-logging rack equipped with pH, conductivity and ion selective electrodes was used for off-line measurements of pH, conductivity and ion concentration. Online measurements were performed with the help of electrode flow cells (Figure 2.1)

Table 2.5: Electrochemical equipment

Item	Description	Manufacturer
Data-logger D230	Modular rack for simultaneous logging of a wide variety of electrochemical measurements	Consort nv - Belgium
Data-logger module D291	pH/mV/Ion/O ₂ /°C module with 4 channels	Consort nv - Belgium
Data-logger module D292	Conductivity/TDS/°C module with 4 channels	Consort nv - Belgium
pH electrode	Autoclavable - no temperature compensation	Cole Parmer
pH electrode	With temperature compensation	Novodirect
Conductivity electrode x 2	Standard cond. cell + ATC (Pt 1000), 1 cm ⁻¹ , 0.1 S cm ⁻¹ to 100 mS cm ⁻¹	Consort nv - Belgium



Figure 2.1: Flow cells used in combination with electrodes for effluent or influent online measurement.

2.3.4 General laboratory equipment

Freeze drying apparatus	Manuf. Christ, Type ALPHA 1-2
Water bath	Manuf. "Gessellschaft für Labor-Technik", type GFL 1013
Water bath - round shaker	Manuf. "Gessellschaft für Labor-Technik", type GFL 1092
Hot-plate / magnetic stirrer	Manuf. IKA, type RCT basic
Table-centrifuge	Manuf. Heraeus, type Biofuge fresco
Refrigerated-centrifuge	Manuf. Kendro, type Sorvall RC26Plus with rotor SS34
Ultra-sound disintegrator	Manuf. Branson, type Sonifier 250
Vortex apparatus	Manuf. Scientific Industries, Inc, type Vortex-Genie 2

Other small common laboratory equipment is not mentioned here.

2.4 General experimental setting

Two model setups were used for the experiments described in this thesis: experiments with sand columns and experiments with sand-packed microscopy flow cells. Figure 2.2 depicts the general column arrangement and main experimental setting of the work presented in this thesis. Organic-free sand (treated as described in Section 2.7.1) was packed in vertically positioned glass columns as well as in microscopy flow cells. These microscopy flow cells were used for direct visualization and quantification of transport processes inside the sediment porous matrix. The columns were connected using tygon tubing (Type R-3603, Novodirect, Kehl, Germany) to peristaltic pumps (Ismatec SA, Switzerland), to online measurement devices (UV-VIS flow cells, electrode flow cells) and to fraction collectors for off-line measurements (cells, EPS etc). Except when specifically stated, the flow rate for all experiments was constant and it was checked before each set of experiments. Colloid and bacterial mobility through the sand was assessed by the analysis of particle breakthrough curves, from which, deposition rate coefficients and collision efficiencies were obtained (as explained in Section 2.7.5).

To determine biofilm influence on colloid transport processes, experiments were performed in columns representing a subsurface porous matrix, in absence (sterile) and presence of biofilms (non-sterile). For biofilm influence and remobilization of natural colloids, colloid mobility was stimulated by decreasing the ionic strength of the background solution (see Section 2.7.6 and 2.7.7). Before decreasing ionic strength, the background solution was set, either as Ca^{2+} dominated, or Na^{+} dominated (see Sections 2.2.2 and 2.7.6). After the completion of the experiments (except for the microscopy flow cells), the remaining sand was removed from the column for further biofilm analysis (Section 2.6).

2.5 Microbiological methods

2.5.1 Bacterial strains maintenance

P. aeruginosa SG81 and SG81R1 were maintained on Pseudomonas isolation agar (PIA), which, by the presence of glycerine, stimulates alginate production. Representative colonies were inoculated in fresh agar media using a heat-sterilized loop. After incubation at 36°C for 24 h, the cultures were used, or they were stored at 4°C in a refrigerator. The maximum time of conservation was three weeks.

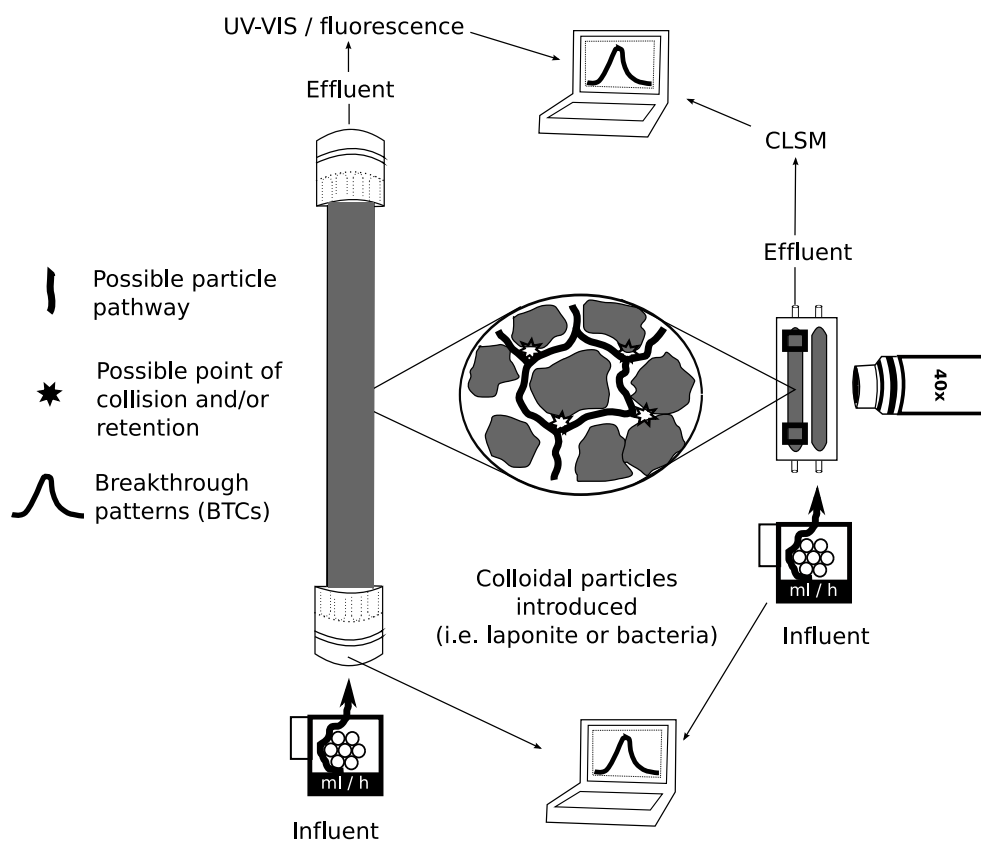


Figure 2.2: Main experimental setting

2.5.2 Motility determination in agar media

Swimming was determined in agar plates containing M9-minimal medium and 0.3 % agar. 5 μL of the bacterial suspension to be tested (10^8 cells mL^{-1}) were injected into the agar in the middle of the agar plate. The inoculated swimming test agar plates were incubated for 24 h at 36°C . A turbid zone around the inoculation point could be observed in positive plates. Swarming was determined in M9-minimal medium agar plates using solution 4 without NH_4Cl . Glutamate was used as only nitrogen source at a concentration of 0.05 % (w/v). The agar concentration was 0.5 % (w/v). 5 μL of the bacterial suspension to be tested (10^8 cells mL^{-1}) were injected into the agar in the middle of the agar plate. The agar plates were then incubated for 48 h at 36°C . Swarming positive isolates had a turbid zone around the inoculation point.

Twitching motility was assessed in plates containing LB-Agar. Each plate contained 15 mL of agar which resulted in agar depths of about 3 mm. 5 μL of the bacterial suspension to be tested (from same solution as the one used for swimming and swarming tests), were carefully injected into the bottom of the Petri dish, with the help of a pipette. The plates were incubated for 24 h at 36°C initially and then until 48 h at room temperature. Twitching motility positives had a turbid zone around the injection place. Additionally,

it is possible to observe in the edges of the colonies, typical "twitching motility" fimbriae-like structures when observed at 100 times magnification. Compiled in Table 2.2 are volumes of the solutions used in the swimming and swarming agar tests.

2.5.3 Preparation of bacterial suspensions

The organisms were pre-grown on PIA. Working liquid cultures were obtained by transferring colonies from agar plates (24h, 36°C) into Tryptic soy broth (TSB) and incubating in a water bath at 36°C overnight. According to conventional growth curves, the organisms were harvested during or at the end of the logarithmic phase for use in the biofilm formation or transport experiments, respectively. The harvesting at the end of the logarithmic phase was done to minimize the potential for increase in cell numbers during the transport experiments. For further biofilm growth (i.e., inside sediment columns), the defined salts medium, APM50 was used (for details see Table 2.2). For the transport experiments, the organisms were concentrated in reaction tubes by centrifugation and then washed with 6.25×10^{-4} M NaCl to remove traces of nutrient medium by centrifuging at least 2 times at $3000 \times g$ for 5 min at 5°C. The cells were washed with low NaCl concentrations, i.e., 6.25×10^{-4} M NaCl, in order to facilitate cell re-suspension by vortexing. Salt concentration in the cell suspensions was finally adjusted to 1.25×10^{-3} M, 1.00×10^{-2} M, 1.40×10^{-1} M and 1 M NaCl. Cell suspensions prepared in this way typically had cell concentrations of around 10^9 cells mL⁻¹, as determined by total cell counts (TCC) using a standard Thoma cell counting chamber in combination with phase contrast microscopy. Calibration curves were constructed to determine numbers of bacteria in suspension at a given absorbance by plotting TCC against absorbance. On some occasions, colony forming units (CFU) were determined to evaluate the effectiveness of the acid/base treatment for the sand columns.

For sand-packed microscopy flow cell experiments, cells were stained with the nucleic acid-specific fluorochrome SYTO® 9 (Molecular Probes). The staining procedure for bacterial suspensions varied depending on the type of experiment. In case of cell suspensions, 1.5 µL of the SYTO® 9 staining solution was added per milliliter of bacterial suspension. In the case in which bacteria were growing inside the sand-packed microscopy flow cells, two to three pore volumes of the 1.5 µL mL⁻¹ SYTO® 9 solution were pumped through the biofilm-growing microscopy flow cell using a peristaltic pump.

2.5.4 Biofilm growth inside the porous medium

The sand columns were pre-conditioned by pumping growth medium for several pore volumes for at least 5 hours prior to inoculation. The columns were then inoculated with the logarithmic phase growing microorganism and left stagnant for one day. For the inoculation, sterile plastic syringes which contained approximately 1 column pore volume of the inoculum were used. The inoculum was carefully injected through ports located close to the column bottom. After the stagnation period the growth medium flow was re-established at low flow rate. The flow was gradually increased up to the flow rate used for the colloid transport experiments. Biofilm growing periods were from 1 to 3 weeks.

2.5.5 Effluent cell concentrations and bacterial mass determination

Bacterial cell detection in the columns effluents was done either online by measuring optical density at 240 nm or offline by determination of TCC using Thoma cell chambers in collected fractions. For the optical measurements bacterial numbers were calibrated from known bacterial numbers suspended in the same buffer or nutrient media as the one being injected to the column. Optical density was measured using a UV-VIS spectrophotometer (Cary 50, Varian Inc.). For CLSM, bacterial cells were determined by measuring the fluorescence emitted by the SYTO[®] 9 stain when bound to bacterial DNA (as described in the sand-packed microscopy flow cell experiments part). Column effluent fractions were obtained using a fraction collector (Pharmacia FRAC-100). Dry cell mass determination was carried out in accordance with DIN EN 12880. The pellet dry weight was divided by the total number of cells, obtaining the single bacterial dry weight used for the calculations.

2.6 Biochemical and chemical analytical methods

Biofilm content in sand columns was characterized by determining dry weight, cell numbers and EPS contents. EPS were represented by total extracellular carbohydrates and total extracellular proteins. Biofilm quantification was done before and after the colloid transport experiments. Biofilm content from the slow sand filter material was determined by EPS content only.

2.6.1 Determination of dry weight

The determination of the dry weight of sand-biofilm material was done according to the German norm DIN EN 12880. For this determination a porcelain evaporating dish was initially rendered free of any organic traces at 550°C for 30 min and left to cool down inside a vacuum desiccator. The dish was then weighted with 1 mg precision (w_1). The sample was then put on the evaporating dish, weighted (w_2) and let to dry at 105°C (± 2 °C) until apparently dry. After cooling down in the desiccator, the sample together with the evaporating dish were weighted (w_3). The dry mass ($w_3 - w_1$) was only obtained when w_3 remained constant.

2.6.2 Determination of ash content / loss on ignition

The determination of ash content was done according to the German norm DIN EN 12879. After obtaining the dry mass, w_3 , the porcelain dish containing the sample was burned at 550°C for 60 min. After cooling down, the weight of the dish, w_4 , was used for the determination of material lost on ignition ($w_4 - w_1$). Similarly as for the dry weight determination, the ash content was only considered when w_4 remained constant (no more than 2 mg change) after ignition.

2.6.3 Biofilm separation from the sand matrix

Biofilms were separated from the sand matrices by mechanical shear stress (stomacher® 400 circulator) in the presence of a cation exchange resin, CER (DOWEX 50x8, Fluka ref.nr. 44445) in a modified version of the procedure described by (Frølund et al., 1996). The difference in this study was the use of the circulator-digestor and the absence of the initial sediment settling step. This step was not necessary because the material was transferred without excess of fluid directly from the columns to plastic bags used in the circulator. 20-30 g of extruded sand was transferred, together with 90-100 mL of DOWEX extraction buffer and 70g CER per g VS. The CER was washed in extraction buffer for 1 h prior to use. The digestor bags were then put in the circulator-digestor for 15 min. The supernatant was collected in sterile beakers and used for further analysis.

2.6.4 EPS isolation

TCCs were obtained from the extracted supernatant material using a Thoma-counting chamber. EPS isolation was done as recommended in Frølund et al. (1996) and Wingen-der et al. (2001). All analyzes were carried out with analytical grade chemicals. The

bacterial cells were separated from the EPS by centrifugation (12000 x g, 2x15 min, 4°C) and filtration through cellulose acetate membrane filters (0.2 μm pore size). Low molecular weight components were removed from this filtrate by dialysis against deionized water for 1 h and after changing the deionized water, for 24 h (Visking dialysis tubing, Serva, Heidelberg, Germany; with a molecular weight cut of 12000 - 14000). The dialyzate containing the EPS was immediately analyzed or if needed concentrated by freeze drying.

2.6.5 Determination of carbohydrates

This biochemical EPS analysis was conducted in accordance to the protocol described in Wingender et al. (2001). The determination of carbohydrates was done according to the phenol-sulfuric acid-test (Dubois et al., 1956). 0.5 mL of sample are well mixed (vortex) with 0.5 mL of 5 % (w/v) phenol. Immediately, concentrated sulfuric acid is added to this mixture (2.5 mL, 95-97 %) and again very well mixed. After 10 min incubation at room temperature, the reagent tubes with the samples are incubated in a water bath at 30°C for 15 min. Finally the tubes are left at room temperature for 5 min. Acidic polysaccharides were determined by measuring absorption at 480 nm. All samples were done in triplicate. Deionized water or buffer containing the sample were used as blanks. The calibration was done with freshly prepared known concentrations of alginate (from 0 $\mu\text{g mL}^{-1}$ to 200 $\mu\text{g mL}^{-1}$).

2.6.6 Determination of proteins

The determination of proteins was done according to a modified Lowry-method (Lowry et al., 1951; Frølund et al., 1996). For this method, a commercially available protein-test-kit was used (Sigma, Deisenhofen, Germany). The following solutions were used: the modified lowry reagent (alkaline copper tartrate with 78.8 mM sodiumdodecylsulphate) and the Folin-Ciocalteu-phenol reagent (sigma, F-9252). The modified lowry reagent comes in a ready-to-use flask (Sigma, L-1013) which only need to be dissolved in 40 mL deionized water. The working Folin-Ciocalteu reagent solution is prepared by mixing 4.5 mL of the reagent with 22.5 mL of deionized water. This solution is protected from light by placing it in a dark glass flask. 0.5 mL of the sample were carefully mixed with 0.5 mL of Lowry reagent. After 20 min of incubation at room temperature, 0.25 mL of the phenol reagent are added. The mixture is incubated additionally for 30 min at room temperature. Proteins are determined by measuring the absorption at 750 nm. All samples were done in triplicate. Deionized water or buffer containing the sample

were used as blanks. The calibration was done with freshly prepared bovine serum albumin (Bovine serum albumin (BSA), Fraction V, Sigma, Deisenhofen, Germany) at a concentration range from 0 $\mu\text{g mL}^{-1}$ to 60 $\mu\text{g mL}^{-1}$.

2.7 Transport methods

2.7.1 Column packing material

As model porous medium, quartz sand of the type F₃₄ with an average grain size of 0.2 mm was used as column and microscopy flow cells packing material. The sand was washed previous to every experiment several times with deionized water followed by an acid-base treatment (0.2 M NaOH and 0.2 M HCl). Between the acid and base steps, deionized water was applied until neutral pH. Additionally the sand was treated at 550°C for 2 h and washed again, in order to eliminate traces of organic material. Sand filter material (SFM), was taken from an active slow sand filter at a drinking water purification plant. This material consisted on gravel, sand and native mixed biofilm population and natural colloids.

2.7.2 Sand columns

Borosilicate glass columns with an inner diameter of 1.4 cm and 10 cm length were used for most of the transport and remobilization experiments. Bigger columns (2.5 cm and 40 cm length) were used for some remobilization experiments and for experiments with slow sand filter material. To standardize the chemical homogeneity of the columns, remove mineral and organic colloidal residues, and minimize contamination by microorganisms, 10 pore volumes of 0.2 M NaOH and 10 pore volumes of 0.2 M HCl, each followed by the introduction of sterile deionized water were applied to the columns. The acid/base treatment was not done to the SFM columns.

Each column was packed minimizing air introduction as described in Deshpande and Shonnard (1999). For the packing procedure, constant water saturation was maintained during packing by filling the column with water and then step-wise introducing wet sand through a funnel. For the SFM columns, water from the same slow sand filter, was used for this purpose. SFM was homogenized with a spatula previous to packing. The SFM columns were left to stabilize at high ionic strength without flow for 1 day. The flow rate was confirmed before each experiment by measuring precise effluent volumes over time. The column influent was always introduced in an up-stream mode in an

effort to minimize non-fickian types of fluid movement. UV-VIS spectrophotometry was performed online using quartz flow-through cuvettes (Starna, Germany).

2.7.3 Sand-packed microscopy flow cells

Stainless steel flow cells normally used for growing biofilms on the surfaces of glass slides were adapted for porous medium experiments by packing with quartz sand F₃₄. The flow cells consisted of two independent parallel chambers with individual channel dimensions of 8 x 3 x 54 mm corresponding to a volume of 1.32 mL. Microscope glass cover slips (dimensions 60mm x 24mm x 0.17mm) were fixed onto both sides of the flow cell, using additive-free silicone rubber. The inoculation of the flow cells was performed with sterile syringes through ports located close to the flow cell inlet (see diagram in Figure 2.2).

2.7.4 Column hydraulic parameters

For all calculations a sand density of 2.65 g mL⁻¹ and water density of 1 g mL⁻¹ were assumed. Column parameters such as pore volumes, porosity, column volume and density were obtained from column dimensions and the following parameters: weight of dry (treated) sand, wds ; weight of empty, dry glass column, wec ; weight of packed column, wpc . The procedures are indicated in Table 2.6.

Table 2.6: Calculated column hydraulic parameters

Parameter	Quantity	Equal to / how was obtained	Terms in equation
Total pore volume, pv	L ³	$wpc - (wec + wds)$	-
Column volume, V	L ³	$\pi \times r^2 \times h$	r : column radius; h : column length
Porosity, ε	-	$\frac{pv}{V}$	-
Bulk density	M/L ³	$\frac{wds}{V}$	-
Dispersivity, d	L	$0.0169 \times h^{1.53}$	-
Volumetric discharge, Q	L ³ /T	Obtained by dividing volume of collected effluent by the time taken to reach that volume	-

... continued on next page

... continued from previous page

Parameter	Quantity	Equal to / how was obtained	Terms in equation
Darcy flux, q	L/T	$\frac{Q}{A}$	A : cross-sectional area
Average linear velocity, v_x	L/T	$\frac{mL/h}{\pi r^2 \times \varepsilon}$	ε : porosity
Number of pore volumes at given time, U	-	$\frac{v_x t}{L}$	-
Hydrodynamic dispersion coefficient, D_L	L ² /T	$d \times v_x$	D^* (diffusion coefficient) is ignored in these type of systems
Peclet number, Pe	-	$\frac{v_x h}{D_L}$	h : the flow distance, which is chosen as the reference length (length of the sand column)

2.7.4.1 Hydraulic conductivity measurements

The saturated hydraulic conductivity of sterile and biofilm containing columns was measured using a constant head permeameter (Figure 2.3). The permeameter consisted of a constant head reservoir connected to the bottom of a sand column from which the discharge was measured by quantifying the volume of liquid flowing over a period of time. Depending on the magnitude of the discharge, the change in hydraulic head, Δh , could be altered simply by changing the height of the influent reservoir above the discharge point. The permeameter was based on a simple application of Darcy's law (see Section 1.2.1). The hydraulic conductivity was calculated with the formula: $K = (Q \times L) / (A \times \Delta h)$.

2.7.5 Calculation of colloid and biocolloid transport parameters

Breakthrough patterns, evidenced as Breakthrough curves (BTC), as well as attachment or collision efficiencies were the basic colloid transport parameters used for assessing colloid mobility in this study. In sand column experiments, these parameters can be obtained with relative ease if the detection system is able to discriminate well between

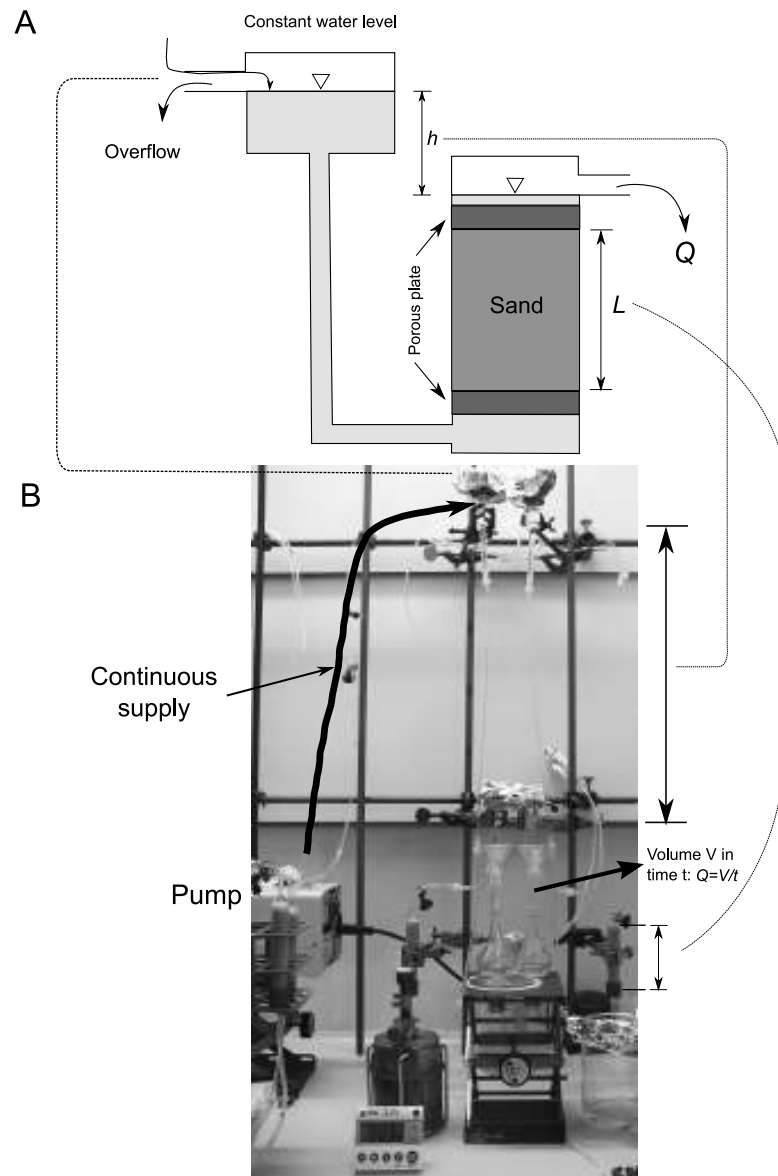


Figure 2.3: A: schematics of a constant head permeameter. B: Constant head permeameter used in this study.

colloidal particles and other material potentially present in the column effluent. This is especially true in complex experimental settings, such as those with high organic matter content or as in the case of this study, the presence of biofilms.

The pulse technique (Grolimund et al., 2001) was used to determine the deposition kinetics of the mobile colloidal particles. BTCs were obtained by following the concentration of particles in the effluent of sand columns immediately after the injection of the colloidal pulse. The colloidal pulse was less than 10 % of a pore volume in all experiments. The deposition rate constant, k_d , was calculated from these breakthrough curves using the normalized suspended particle concentration C/C_0 as:

$$k_d = -\frac{U}{\varepsilon L} \ln \left(\frac{C}{C_0} \right) \quad (2.2)$$

where U is the superficial or Darcy velocity (flow rate divided by area normal to flow), ε is the column porosity and L is the length of the porous medium over which the colloid has been transported (Redman et al., 2003). C/C_0 was obtained by calculating the ratio of the areas under the breakthrough curves through the column and in a by pass experiment in which the column is replaced by normal tubing (C_0). The integration routines were done with the program Origin. The first two moments from the integration were used: μ_0 , which is the area beneath the BTC, was used to obtain C/C_0 as just said, and μ_1 , which is the mean position or center of mass of the BTC, was used to obtain the average travel time of the particles, t_p . High salt concentrations produce fast or favorable deposition conditions. Deposition rates measured at these conditions, were used to obtain the collision or attachment efficiency, α , simply by (Kretzschmar et al., 1999):

$$\alpha = \frac{k_d}{k_{d,fav}} \quad (2.3)$$

where $k_{d,fav}$ is the deposition rate constant for favorable deposition conditions.

2.7.5.1 Colloid and biocolloid transport parameters obtained by CLSM

For transport experiments in sand-packed microscopy flow cells, colloidal suspensions were stained with SYTO[®] 9 ($\lambda_{ex,max}$. 480 nm, $\lambda_{emm,max}$. 500 nm) in the case of bacteria, or with R6G in the case of LRD (see section 2.7). The pulses were introduced at a constant flow of 0.3 mL min⁻¹ into flow cells which were pre-conditioned with the appropriate NaCl solution. Flow cells were placed horizontally on the microscope stage. Observation sites were located at inlet, middle and outlet positions. Breakthrough data were recorded at fixed positions near the microscopy flow cell outlet (still within the porous medium). BTCs were obtained from image analysis data of CLSM cross sectional images recorded

at 10 s intervals. Stained areas were equated to the entire observation area ($230.30 \mu\text{m} \times 230.30 \mu\text{m}$) minus grain areas as measured from a R6G-stained LRD suspension run previously through the same observational spot at extremely low ionic strength (0 M NaCl). R6G-LRD suspensions at very low ionic strength were shown to be very efficiently transported (almost no retention at inlet, middle and outlet positions) through the sand-packed microscopy flow cells. Prior to the experiments the intensities of both the low ionic strength tracer R6G-LRD suspension and the colloidal suspension to be assessed were calibrated to match very closely. This was achieved by using microscope settings (excitation wavelength of 488 nm and a 505 nm long pass filter) that allowed for the simultaneous detection of both types of dyes at a single detection channel and by modifying the microscope detector gain.

Both in the case of LRD and bacterial transport experiments the maximum covered area achieved by the R6G-LRD suspension was taken as 100 % coverage (C_0) and the elution of subsequent colloidal dispersions was taken as a fraction of this measure (C). The method also allowed for the quantification of retained cells at the different observation sites in a non-destructive manner. Transport parameters were obtained from the BTCs generated in this way.

Image analyzes from time series CLSM micrographs were done using ImageJ, a Java program for image processing and analysis (Abramoff et al., 2004). Customized macros were used in order to digitally subtract retained and non-retained particles from the images (see Figure 3.33 for an example). The macros are available here: <http://lamaquina.de/thesis/scripts/ImageJ>. In short, RGB (Red, Green, Blue) CLSM micrographs were converted to gray scale and the mean gray value for each picture was calculated as the sum of the gray values of all the pixels in the image divided by the number of pixels. The process was automatically done for all images belonging to a time series. If no elution of fluorescent material occurred, the image appeared as a black background without or with few gray pixels. As elution of fluorescent material increased or decreased, the amount of gray pixels did so as well and this is what was quantified. The custom macros were able to subtract gray pixels which did not change from one image to another (retained particles) or subtracted only “moving” gray pixels (non-retained particles) creating two new groups of images: one with retained particles information and the other with non-retained particles information. These images were then quantified as explained before and because they belonged to a time series, this data could be plotted against time of elution (See Figures 3.24 or 3.34 for an example).

2.7.6 Colloid transport experiments in the presence of biofilms

In the case of biofilms growing within the porous medium, the electrochemical conditions of the influent had to be modified in a consistent way. The initial ionic strength of the nutrient media (approximately 35 mM) was increased to 70 mM until a low and constant plateau (UV-VIS) was achieved in the column effluent. Two types of electrochemical conditions were set: dominance of monovalent cations (Na^+) or dominance of divalent cations (Ca^{2+}). Colloidal mobility is highly retarded at high ionic strength conditions. It is therefore required, to lower ionic strength to a point where colloid transport occurs. This was achieved by halving the ionic strength in the column influent for 3 pore volumes followed by deionized water influent for an extra 2 pore volumes. This treatment was reproduced for all columns. Transport of an injected colloidal pulse (0.6 mL) after the deionized water influent was quantified through sterile columns (see Section 3.3).

2.7.7 Remobilization experiments

2.7.7.1 Remobilization of LRD from clean quartz sand columns

Clean quartz sand columns were saturated with 70 mM NaCl or 70 mM CaCl_2 as specified in the previous section. 200 mL of R6G-stained LRD (200 mg L^{-1} , $5 \times 10^{-6} \text{ M}$ R6G) were injected to the columns. The LRD-R6G was suspended in exactly the same solution used to saturate the columns. The influent salt concentration was then step-wise decreased as described previously. The effluent was monitored constantly (UV-VIS).

2.7.7.2 Colloid-facilitated remobilization of R6G from sand-packed microscopy flow cells as evidenced by CLSM

The remobilization of R6G was assessed in sand-packed microscopy flow cells as an extra indication of the interaction between the model inorganic clay and this cationic organic dye. The procedure was the following:

- R6G pulse was prepared at a concentration of $5 \times 10^{-6} \text{ M}$.
- 100 μL of the R6G pulse were injected to the flow cell at the same flow rate of the influent solution.
- A colloidal pulse of unstained LRD (2000 mg L^{-1}) was injected to the same flow cell, after 10, 100 and 1000 seconds of the R6G pulse.

- Breakthrough data were recorded at outlet positions (still within porous medium) by CLSM.

2.7.7.3 Natural colloids remobilization from SFM

Laboratory columns were filled with SFM as described in Section 2.7.2. After the stagnation period, SFM columns were saturated either with 70 mM NaCl or 70 mM CaCl₂ for up to 50 hours at a constant flow rate of 0.3 mL min⁻¹. After this period the effluent was relatively clear. A low and stable plateau (UV-VIS) was observed which indicated low colloidal mobilization. The influent salt concentration was then step-wise decreased at constant intervals of approx. 22 - 24 h. The salt concentration steps were: 70 mM → 35 mM → 10 mM → 2.5 mM → 0.625 mM → 0 mM. The effluent was monitored constantly (UV-VIS).

2.8 Statistical methods

All sand columns described experiments were done at least in duplicate and mean values are presented. All CLSM described experiments were done at least in triplicate and mean values are presented. Error bars represent the standard deviation around these mean values. Pearson correlation coefficients, r , were calculated with the open source spreadsheet Gnumeric and considered only significant for $p < 0.05$ (t -test distributions).

Chapter 3

Results

3.1 Introduction

The influence of biofilms on the mobility of colloids should be investigated using a model system which resembles conditions of high permeability and changing ionic conditions. These conditions are typical of many subsurface environments. As also specified in section 1.8, before studying the influence of biofilms on the transport of colloids, the transport characteristics of both LRD and the bacterial particles had to be studied alone. The aim was to obtain data on the transport and initial deposition of bacteria in comparison to the clay colloid. Bacterial transport and remobilization, provided additional data on the first stages of *P. aeruginosa* SG81 biofilm formation in porous media. This was important since the growth of this strain in this type of environments was not studied before. On the other hand, obtaining deposition characteristics of the model colloid in clean, biofilm-free columns was fundamental for judging the influence exerted by biofilms. Most results of colloid transport studies have been obtained from column experiments investigating suspended particle concentrations from influents and effluents only. The decrease in suspended particle concentration in most cases has been believed to follow CFT. By studying retention patterns of colloids inside the porous matrix, researchers were able to demonstrate inconsistencies with the classical CFT even at well defined and controlled physicochemical conditions (Tufenkji and Elimelech, 2005). In certain circumstances (see Introduction and further on this discussion) biofilm growth might contribute to these observed inconsistencies. To study the mobility of colloids within a porous matrix, a microscope flow chamber model of a sand column for CLSM was developed. The transport of LRD labeled with the fluorochrome R6G within a sterile sand matrix was visualized at various ionic strengths. The use of both, sand columns and the CLSM technique using microscopy flow cells, provided a more comprehensive

overview of colloid and biocolloid transport processes in porous media. The CLSM approach allowed for the visualization and quantification of transport processes inside the porous matrix. This is not possible with conventional sand column experiments alone. The results of the initial transport characterization, i.e., without biofilms are presented in sections 3.3 and 3.4. Most of these data were included in Leon Morales et al. (2004). The results of the transport as influenced by biofilm growth is presented in subsequent sections and are greatly based on Leon Morales et al. (2007).

3.2 LRD physicochemical characteristics

3.2.1 Interaction between the colloid and R6G

LRD suspensions were stained with R6G (Fluka, Switzerland), a cationic dye, as a detection aid for CLSM and for UV-VIS or fluorescence spectrophotometry. The concentrations ranged from 5×10^{-6} M to 5×10^{-7} M R6G depending on LRD concentration. The staining procedure was done as described in Tapia Estévez et al. (1993). For less than 200 mg L^{-1} LRD, 5×10^{-7} M R6G was used and for 200 mg L^{-1} and higher concentrations, 5×10^{-6} M R6G was used. The adsorption of the R6G monomer onto LRD resulted in a shift in the absorption maximum of the dye from 527 nm to 535 nm when adsorbed to 200 mg L^{-1} LRD in absence of salt (Figures 3.1 and 3.2). Although the shift on the maximum absorption of the dye was constant at the described conditions, increasing concentrations of salt and increasing concentrations of LRD influenced the extent of the maximum absorbance shift (Figures 3.2 and 3.3). In absence of LRD, salt concentration had little effect on the maximum absorption of the dye (Figure 3.1).

LRD physicochemical properties such as aggregation and settling at high salt concentrations were not altered by the R6G staining. The spectra from Figure 3.4 show that in the clear upper phase (red line), no R6G is present in solution. The spectrum from clean deionized water (black line) is given as reference. In contrast, R6G is present apparently in great concentrations in the LRD sediment phase.

Pulse experiments through the porous medium (as described in 2.7.7.2) were also performed both in sand columns and in sand-packed microscopy flow cells. Pulses of unstained LRD were injected at different times after the R6G injection. R6G-stained LRD was then measured in the column effluents at increasing time intervals. Results from the sand columns and from the sand-packed microscopy flow cells are in good agreement (see quantification in Figures 3.8 and 3.9). They are therefore shown as complementary. For the CLSM approach, observation points were chosen inside the porous medium in

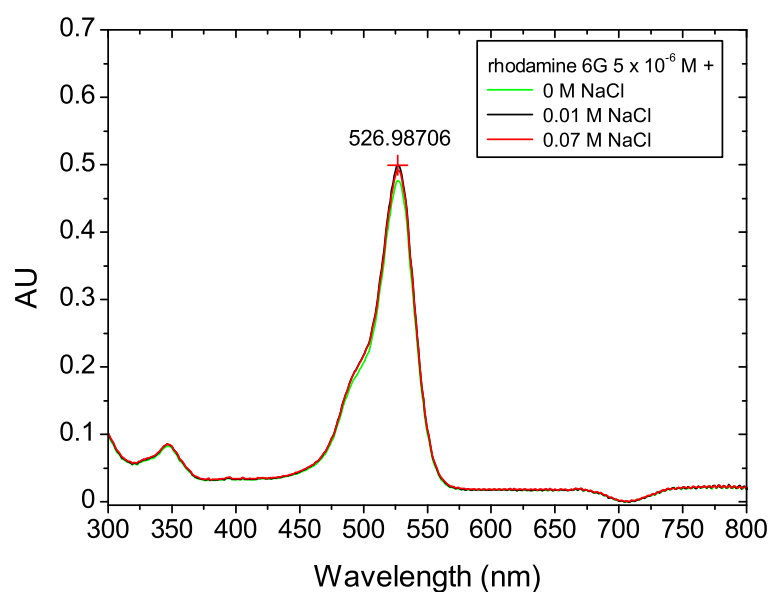


Figure 3.1: Absorbance spectra from rhodamine 6G without laponite RD at different salt concentrations. Each plot represents means of at least duplicates.

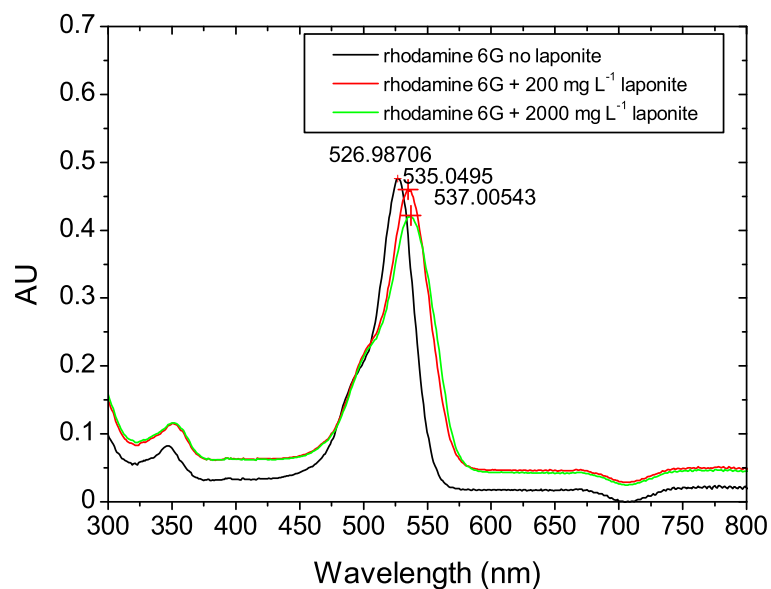


Figure 3.2: Absorbance spectra of rhodamine 6G in interaction with laponite in absence of salt. Each plot represents means of at least duplicates.

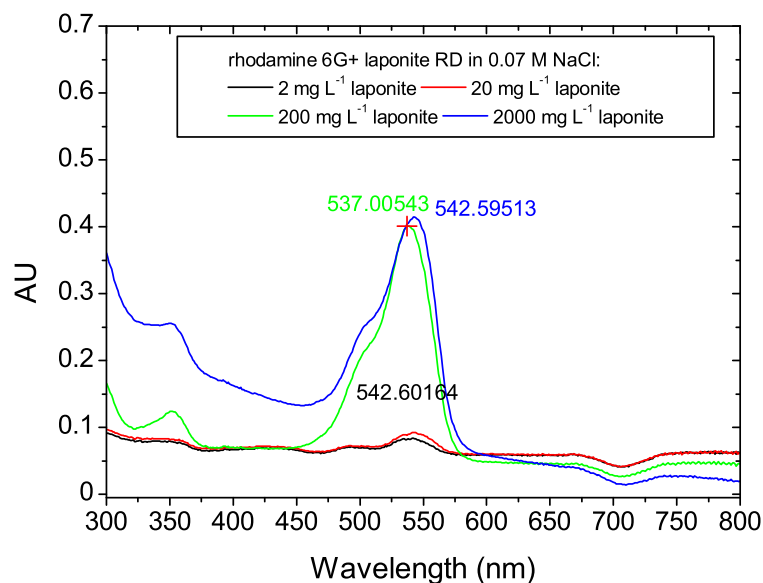


Figure 3.3: Absorbance spectra from rhodamine 6G in interaction with laponite RD at a salt concentration of 0.07 M. The plots represent different laponite RD concentrations. Each plot represents means of at least duplicates.

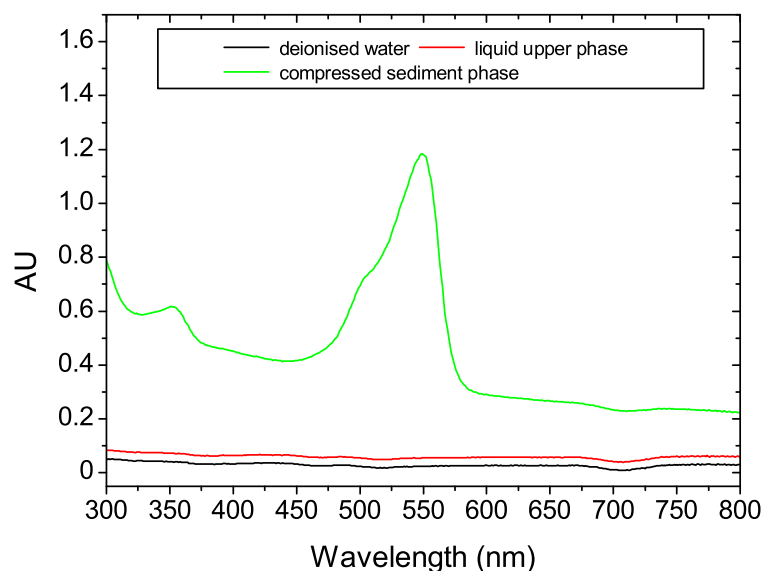


Figure 3.4: The spectra represent samples taken from a sedimented rhodamine 6G-stained laponite RD suspension (sedimentation time was 24 h). Laponite RD concentration was 2000 mg L⁻¹ and the salt concentration was 0.07 M. Each plot represents means of at least duplicates.

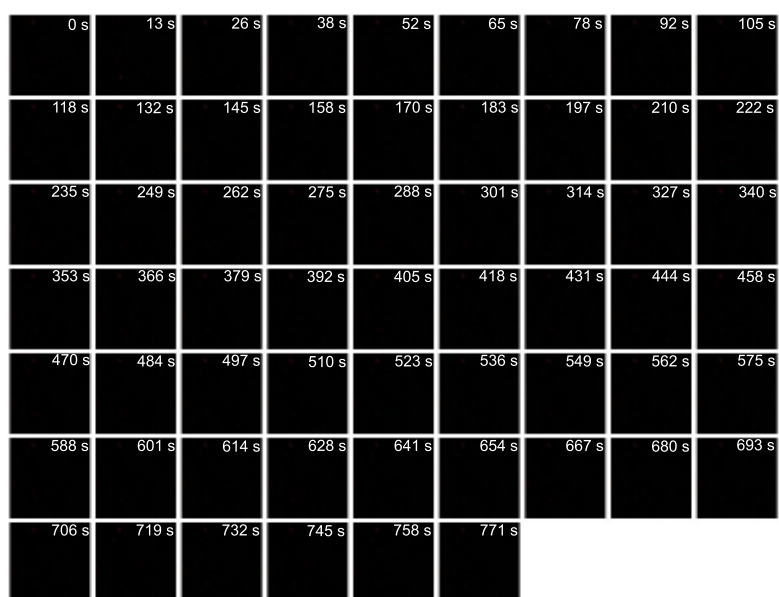


Figure 3.5: CLSM micrographs taken from a fixed position near the sand-packed microscopy flow cell outlet, after the injection of $100\mu\text{l}$ of 5×10^{-6} M rhodamine 6G. Each micrograph represents $460.7 \times 460.7 \mu\text{m}$ and it is part of a time series (time in seconds is specified in each micrograph). No rhodamine 6G elution can be observed.

order to detect both retention to the sand grains surfaces and mobilization through the pores. Observation points were set at inlet, middle and outlet positions. Images were taken before and after pulse injections. Time series images were taken additionally at the same outlet positions in order to obtain elution profiles of R6G or LRD-R6G complexes.

R6G elution did not occur when injected in absence of the colloidal clay (see time series images in Figure 3.5). Images from inlet positions, taken before and after pulse injection, show complete R6G retention at these positions (Figure 3.6). Unstained LRD pulses were injected subsequently after 10 s, 100 s and 1000 s. Figure 3.7 shows time series micrographs, after 10 s of R6G injection. Remobilization of R6G was observed up to the longest time of 1000 s (around 17 min) after R6G injection. Quantification of R6G remobilization at the specified times can be observed in Figure 3.8.

The results obtained from column experiments in which the effluent was analyzed by UV-VIS can be seen in Figure 3.9. As it can be observed, these results are consistent with the ones obtained with the CLSM approach.

3.2.2 Colloid aggregation and stability

Colloid aggregation of LRD was confirmed visually (Figures 3.10 and 3.11), photometrically, and microscopically. At constant pH conditions, aggregation was generally favored

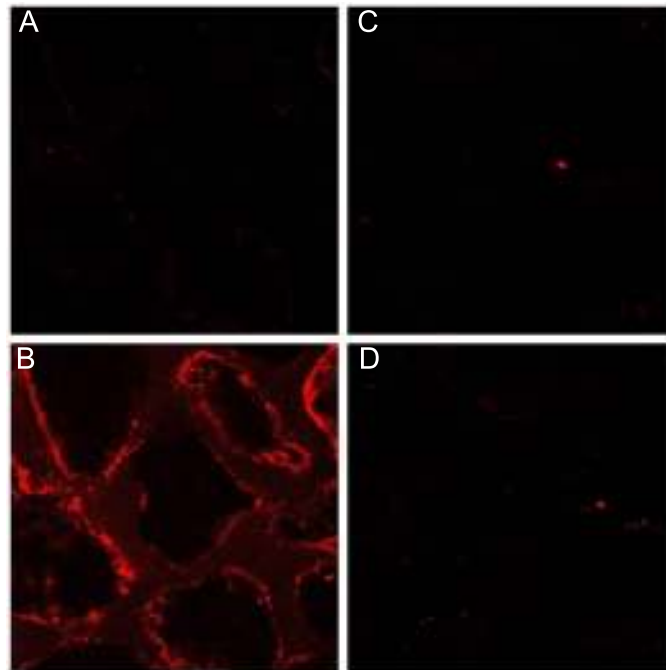


Figure 3.6: Detection of rhodamine 6G in sand grains before (A) and after (B) pulse injection at inlet positions. C and D are before and after images at middle positions. Each picture represents $460.7 \times 460.7 \mu\text{m}$.

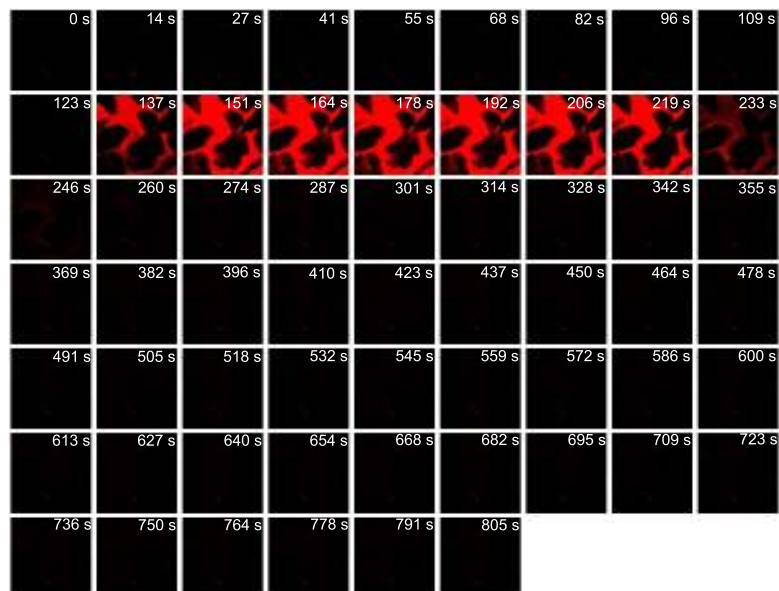


Figure 3.7: Remobilization of rhodamine 6G previously retained to sand grains caused by the injection of an unstained laponite RD pulse. This is after 10 s of rhodamine injection. The same was done after 100 s and after 1000 s. Pictures represent $460.7 \times 460.7 \mu\text{m}$ and are part of a time series taken from a fixed position near the sand-packed microscopy flow cell outlet.

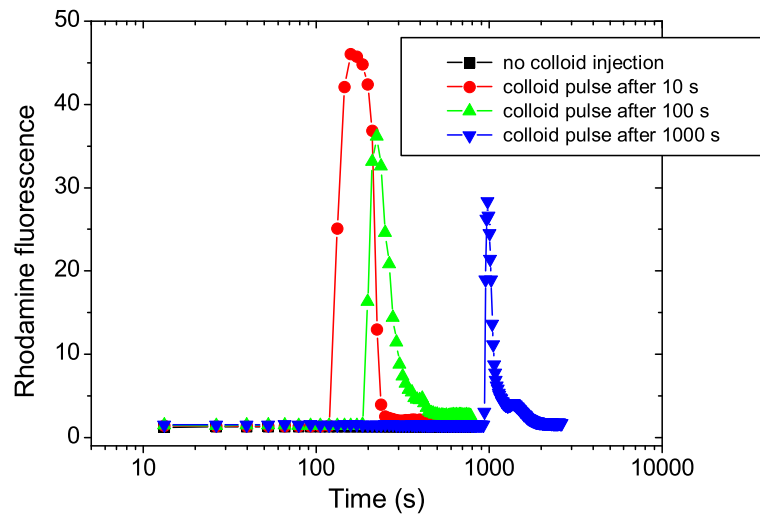


Figure 3.8: Remobilization of rhodamine 6G previously retained in quartz sand by laponite RD colloidal pulses. Image analysis of time series micrographs obtained by CLSM.

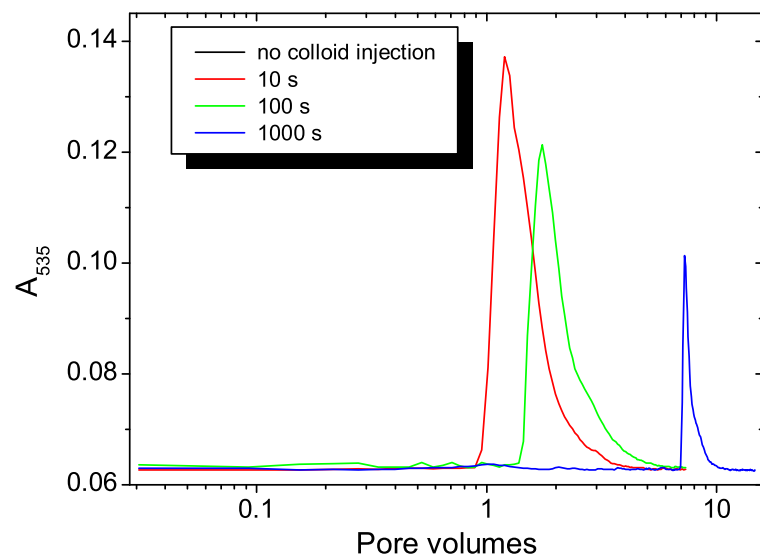


Figure 3.9: Remobilization of rhodamine 6G previously retained in quartz sand by laponite RD colloidal pulses. These were obtained from sand columns by UV-VIS analysis.



Figure 3.10: Aggregation process of rhodamine 6G-stained laponite RD. Left: 2000 mg L⁻¹ stained laponite RD suspended in deionized water. Right: same suspension in 70 mM NaCl.



Figure 3.11: Right: 2000 mg L⁻¹ LRD+R6G suspended in 70 mM NaCl before dialysis. Left: same suspension after dialysis. No rhodamine outside the dialysis tube, no decrease in rhodamine 6G spectrophotometric signal were found.

by high ionic strengths but was dependent on LRD concentration. For instance, 2000 mg L⁻¹ LRD at 7×10^{-2} M NaCl was highly aggregated with aggregates sizes of several micrometers (see Figure 3.10 right and Figure 3.13), but 20 mg L⁻¹ LRD at 7×10^{-2} M NaCl was less aggregated and contained smaller-sized aggregates (as evidenced by epifluorescence microscopy of R6G-stained LRD preparations). When dispersed in deionized water, LRD suspensions were clear and apparently non-aggregated after approximately 40 minutes of stirring (Figure 3.10 left). The pH of the suspensions was dependent on the LRD concentrations and ranged from pH 10 for the highest LRD concentration used in this study (2000 mg L⁻¹) to pH 6.6 for less concentrated suspensions (20 mg L⁻¹). The pH of the working LRD suspensions was adjusted when necessary to 7 where indicated by using 0.2 M HCl or 0.2 M NaOH. Varying the pH of the colloidal suspension resulted in changes of the aggregation state. A pH of 5.5 promoted aggregation of the colloidal suspension (Figure 3.12) which indicates that the colloid is not longer stable at low pHs. Absorbance measurements to detect LRD were done at 535 nm in all sand column experiments and fluorescence detection of the LRD-R6G complex was used for the same purpose in the sand-packed microscopy flow cell experiments.

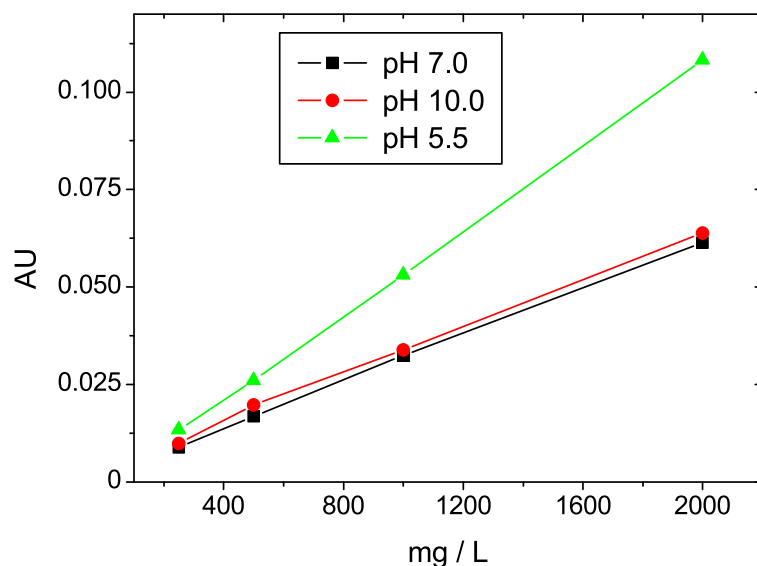


Figure 3.12: Changes on laponite RD aggregation states at different pH values as determined by UV-VIS detection signal.

3.2.3 LRD retention mechanisms in the porous medium

In this series of experiments, suspensions of LRD at different concentrations and at high ionic strength were introduced to sand-packed microscopy flow cells, in order to assess mechanisms of retention and the effects of retention on local hydrodynamic conditions. LRD suspensions were prepared at 2000 mg L^{-1} , 200 mg L^{-1} and 20 mg L^{-1} . The ionic strength was kept constant at 70 mM . In the case of 2000 mg L^{-1} LRD concentration, aggregation was evident after several seconds of LRD contact with the electrolyte. The LRD aggregates under this conditions were around $10 \mu\text{m}$ (Figure 3.13).

LRD suspensions at 2000 mg L^{-1} were completely retained, as revealed by CLSM time series images, when injected into quartz sand-packed microscopy flow cells. No R6G-stained LRD was detected in the flow cells outlets. Additionally in bacterial inoculated flow cells, remobilization of retained bacterial cells was also observed (Figure 3.15). The color pixel intensity of the complete stack of CLSM images obtained for this experiment (180 images, including the ones in Figure 3.15) is plotted against time in Figure 3.16. A peak of bacterial remobilization before the LRD clogging event is evident. Scanning electron micrographs show LRD retention and gelation processes as well (Figure 3.14).

At a LRD concentration of 200 mg L^{-1} , retention also occurred, however, less bacterial remobilization occurred. CLSM time series images revealed that many LRD aggregates were still small enough to pass through the porous medium pores; they were retained, however, onto the surface of sand grains (Figure 3.17). When LRD concentration was 20 mg L^{-1} , LRD aggregates were absent and clogging did not occur. Despite of absence of clogging, retention occurred at inlet positions of sand-packed microscopy flow cells

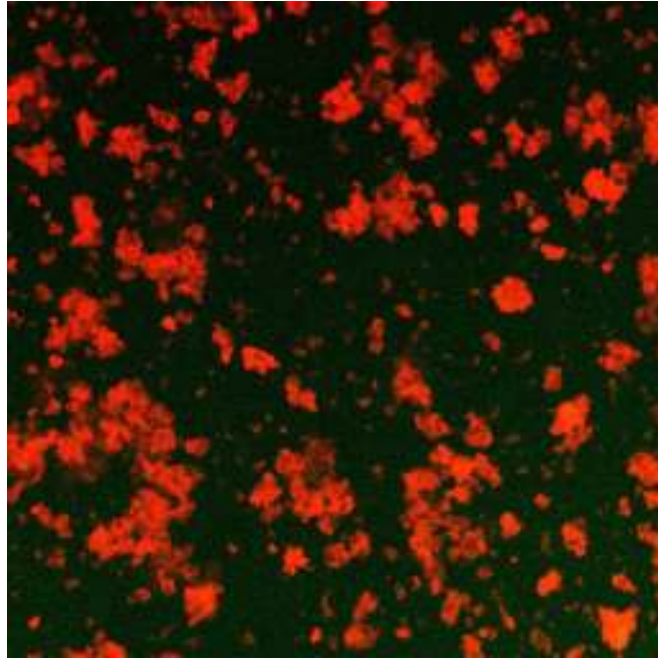


Figure 3.13: Laponite RD aggregates at a concentration of 2000 mg L^{-1} and 70 mM NaCl . This suspension was injected to sand-packed microscopy flow cells. The epifluorescence micrograph represents $230.3 \mu\text{m} \times 230.3 \mu\text{m}$.

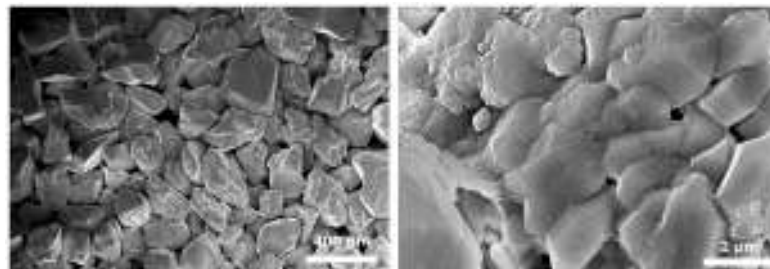


Figure 3.14: Scanning electron micrographs of clean F_{34} quartz sand (left) and sand coated with laponite RD (2000 mg L^{-1}). The laponite was retained as a gel-like substance at elevated ionic strength ($7 \times 10^{-2} \text{ M}$).

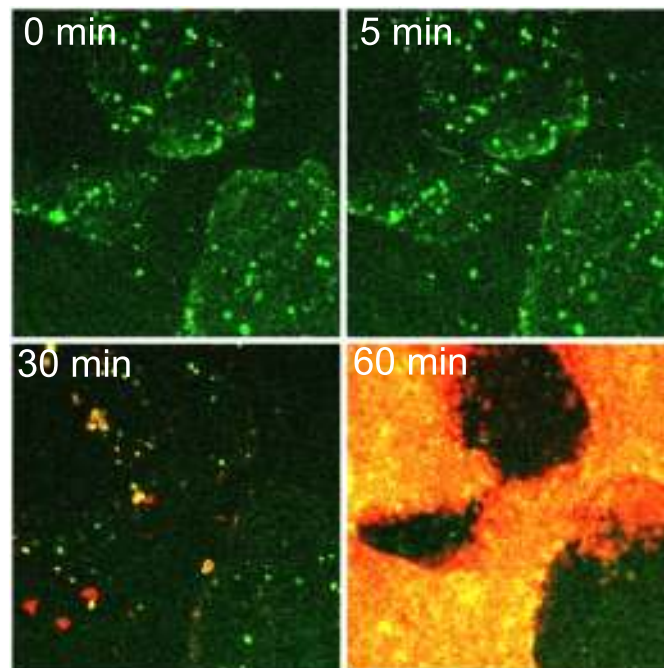


Figure 3.15: CLSM micrographs showing the retention of 2000 mg L^{-1} laponite RD + $5 \times 10^{-6} \text{ M}$ rhodamine 6G at 70 mM NaCl . The images are taken from a time series of approx. 1 h. The flow rate was maintained constant at 0.1 mL min^{-1} . Images represent $230.3 \mu\text{m} \times 230.3 \mu\text{m}$. Remobilization of retained bacteria is evident in the 5 min image.

(Figure 3.18).

As can be seen in Figure 3.19, LRD complete remobilization was achieved after approximately 30 min of deionized water influent. Remobilization can be observed by the disappearance of fluorescence coming from R6G-stained LRD (see 30 min image in Figure 3.19). By quantifying the mean pixel intensity in each of the micrographs obtained in this experiment (some of them shown in Figures 3.18 and 3.19), it was possible to obtain a graphical representation of the LRD retention and removal from the porous medium (Figure 3.20). Plotted data includes the period of retention at high ionic strength (such as the one in Figure 3.18) delimited by the green square and a subsequent period of remobilization (blue square). The period of remobilization, was stimulated by changing the LRD influent to LRD-free deionized water. All other parameters, including the flow rate, were maintained constant. It can be seen that at these conditions the remobilization process mostly occurs within 8 seconds after changing the influent.

3.3 Quantification of LRD transport parameters

The mobility of the model colloid LRD through sand columns at different pore fluid ionic strengths was studied systematically. BTCs were obtained by plotting the ratio of

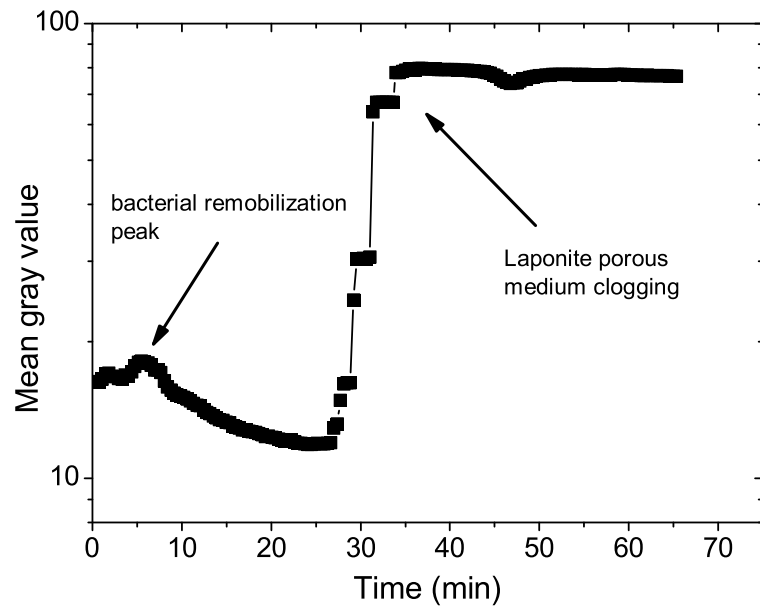


Figure 3.16: Image analysis of the complete times series set for the 2000 mg L^{-1} laponite RD suspension as it is retained in the porous medium by straining (see previous Figure).

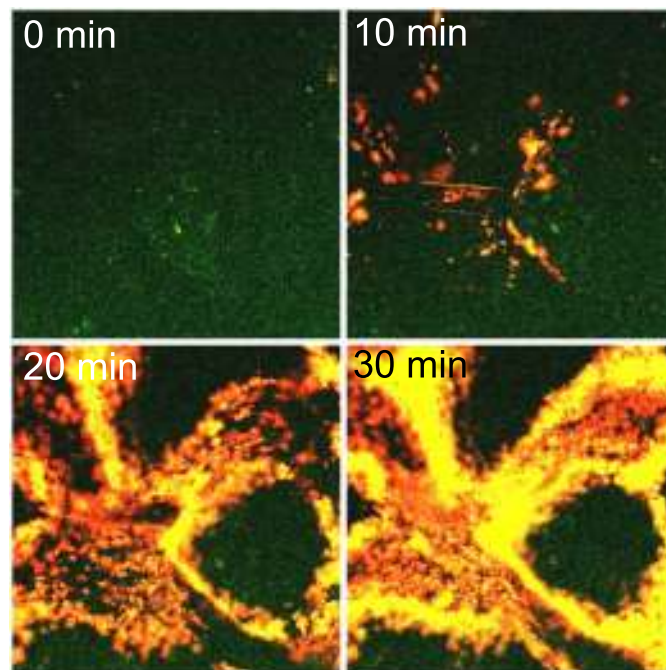


Figure 3.17: CLSM micrographs, showing 200 mg L^{-1} laponite RD + $5 \times 10^{-6} \text{ M}$ rhodamine 6G at 70 mM NaCl retention in sand-packed microscopy flow cells. The images are taken from a time series of approx. 1 h. The flow rate was maintained constant at 0.5 mL min^{-1} . Images represent $230.3 \mu\text{m} \times 230.3 \mu\text{m}$.

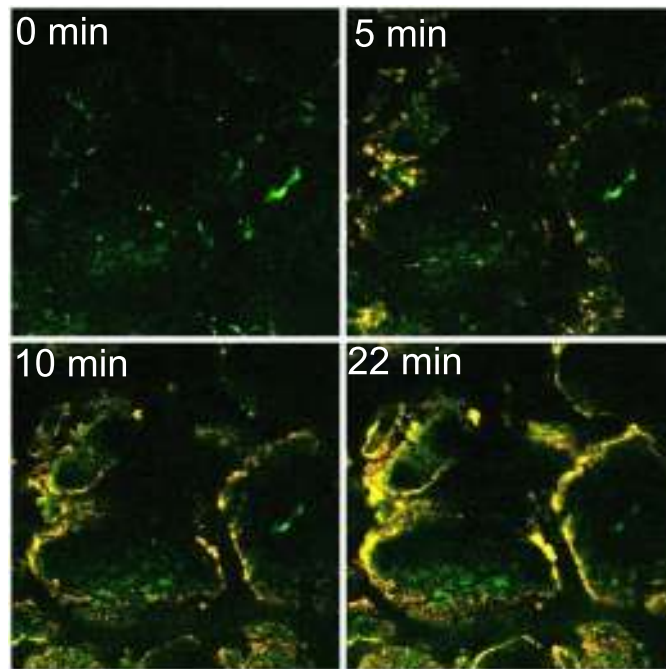


Figure 3.18: CLSM micrographs showing 20 mg L⁻¹ laponite RD + 5 × 10⁻⁷ M rhodamine 6G at 70 mM NaCl retention in sand-packed microscopy flow cells. The images are taken from a time series of approx. 1 h. The flow rate was maintained constant at 0.5 mL min⁻¹. Images represent 460.7 μm × 460.7 μm.

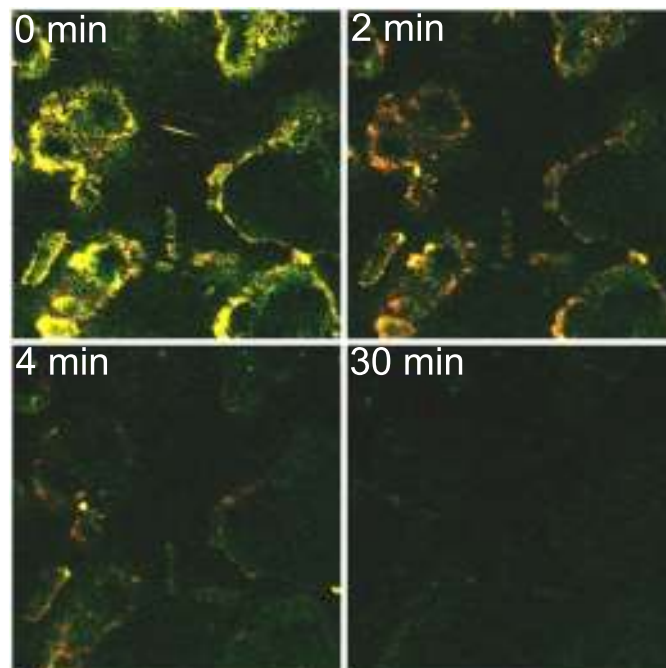


Figure 3.19: Complete remobilization of laponite RD (20 mg L⁻¹) from sand matrices caused by deionized water influent. Images represent 460.7 μm × 460.7 μm.

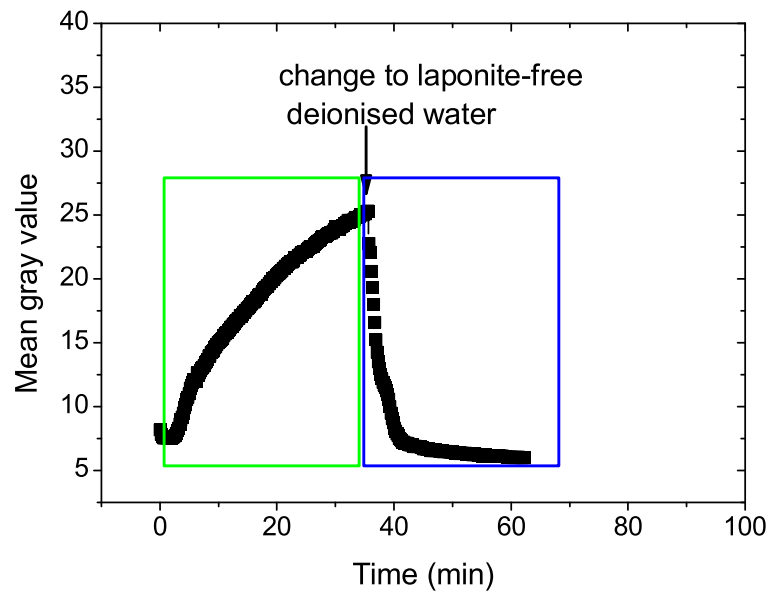


Figure 3.20: Image analysis quantification of laponite RD retention and remobilization observed in Figures 3.18 and 3.19.

injected particles to eluted particles with time. For the sand column method, UV-VIS was used as detection system. For the CLSM method, quantification of the fluorescence signal was used to obtain BTCs. Transport parameters, including collision efficiencies and deposition rate coefficients were obtained from these BTCs. The results from both methods follow a similar trend, for this reason, the information obtained from both methods, is presented in a combined manner. Sand column and sand-packed microscopy flow cell relevant hydraulic parameters are shown in Table 3.1.

Table 3.1: Sand column and sand-packed microscopy flow cell packed characteristics

Type of column	Flow rate (mL h ⁻¹)	Approach velocity (m s ⁻¹)	Pore volume (mL)	Porosity	Bulk density (g cm ³)	Pe
Sand columns 1.4 cm diameter	50 ^a	9.02 x 10 ^{-5a}	7.50 ^a	0.47 ^a	1.36 ^a	152 ^a
Sand columns 1 cm diameter	50 ^a	1.77 x 10 ^{-4a}	3.34 ^a	0.42 ^a	1.40 ^a	152 ^a
Sand-packed microscopy flow cells	18 ^a	2.08 x 10 ^{-4a}	0.54 ^a	0.42 ^a	n.d	210 ^a

^aerror equal or less than 1 %, n = 6, n.d: not determined

In the absence of electrolyte or at low salt concentrations i.e., 6 x 10⁻⁴ M NaCl, LRD was highly mobile (See Table 3.2). It was found that the mobility of LRD decreases with increasing ionic strength. BTCs obtained with the sand column method at different ionic strengths for LRD can be observed in Figure 3.21. It can be seen in Figure 3.21 that in

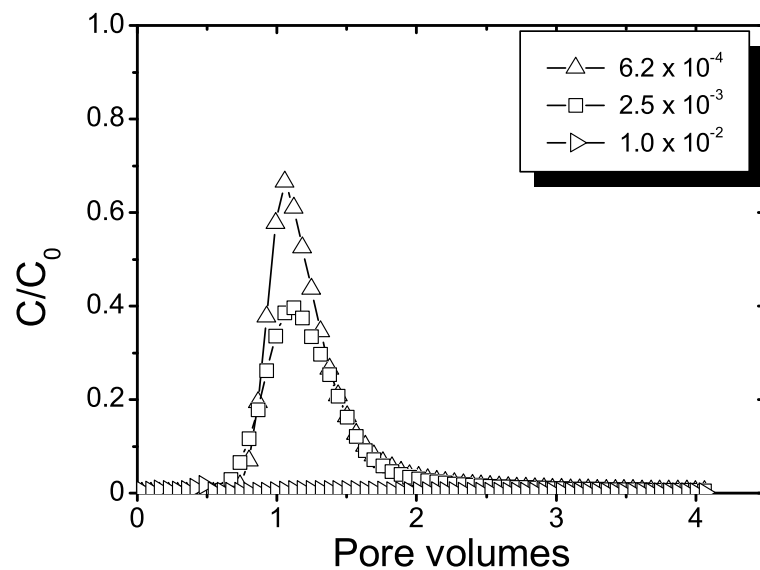


Figure 3.21: Laponite RD transport profiles through non-inoculated sand columns as a function of salt concentration (Moles per Liter NaCl).

the case of sand columns, almost complete LRD retention is observed when the pore fluid ionic strength was set to 10 mM NaCl.

Direct observation and quantification of LRD elution profiles (used later to obtain BTCs) was possible by using the CLSM method. CLSM micrographs representing LRD transport time series, can be seen in Figure 3.22. It can be seen that when the colloid is dispersed in deionized water, transport occurs without retention through the sand matrix, this is in accordance to results from classical sand column experiments. At high LRD (2000 mg L^{-1}) and electrolyte concentrations ($7 \times 10^{-2} \text{ M NaCl}$), the clay is highly aggregated and gelation occur on the surface of sand grains (Figure 3.14). The advantage of the CLSM method described is that these observations can be done online and in a non-destructive manner.

When salt concentration in the LRD dispersing solution is increased to 2.5 mM, increasing aggregation occurs and LRD starts to get retained onto sand grains surfaces (Figure 3.22). As it will be expanded later, image analyzes allowed the digital separation of particles retained on sand grains surfaces and those being transported through the interstitial pores.

When the ionic strength of the LRD dispersing solution was 5 mM, the size of the aggregates as well as LRD retention on top of sand grains is increased. This is not only qualitative information but image analysis allowed for colloid transport quantification (Figures 3.23 and 3.24).

At an ionic strength of 10 mM or higher, the aggregates start to be retained at the flow cell inlet and the transport of LRD with the pore fluid is decreased. LRD aggregates are

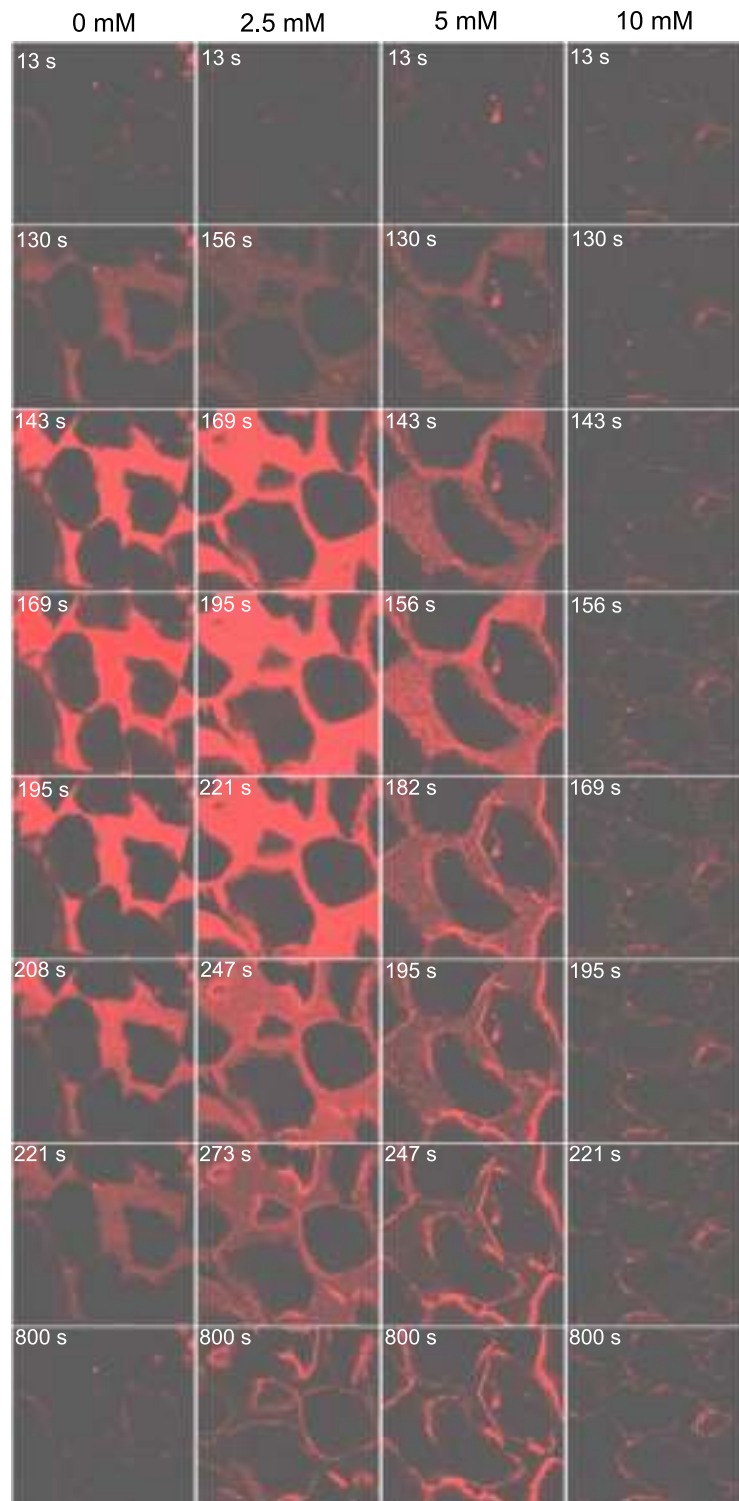


Figure 3.22: CLSM micrographs ($460.7 \mu\text{m} \times 460.7 \mu\text{m}$) showing the elution of a pulse of laponite RD dispersed in deionized water, at 2.5, 5 and 10 mM NaCl. Sand grains appear dark while pore space appears red during elution of laponite-rhodamine 6G complexes.

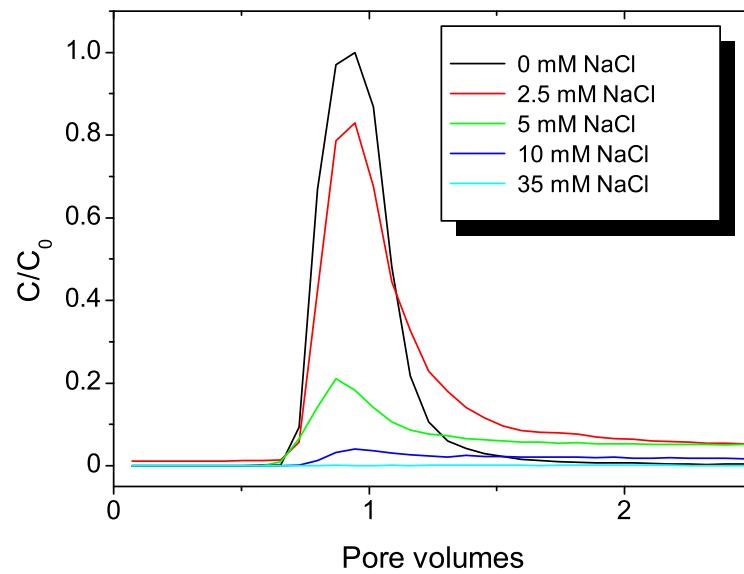


Figure 3.23: Laponite RD BTCs obtained from image analysis CLSM method

clearly retained on the sand grains.

The quantification of fluorescence from the CLSM images is used in combination with image analysis to construct the BTCs shown in Figure 3.24. Separation between eluted particles and retained particles from these images gives information on the kinetics of retention inside the porous medium (see third column of Figure 3.24).

The images shown in Figure 3.24 are one replicate examples of the CLSM analyzes. The same type of analyzes were done for minimum triplicates at each ionic strength; the combined results can be seen in Figure 3.25 and in Table 3.2. From Figure 3.25, it is evident especially from the sand columns, that the main change in collision efficiency, α , happens between 0 mM and 10 mM salt concentration. Above 10 mM salt concentration there was a lesser collision efficiency change and the retention in the porous medium, was almost complete.

Table 3.2: Laponite RD combined transport parameters at different ionic strengths

mM NaCl	Sand columns				CLSM method			
	C/C_0	kd (s^{-1}) ($\times 10^{-3}$)	η ($\times 10^{-4}$)	α	C/C_0	kd (s^{-1}) ($\times 10^{-3}$)	η ($\times 10^{-4}$)	α
0	0.82 ^a	1.23 ^c	4.63 ^b	0.03 ^b	0.99 ^a	0.05 ^d	0.4 ^c	0.001 ^c
0.6	0.71 ^a	2.04 ^c	8.23 ^b	0.05 ^b	0.83 ^a	0.70 ^b	8.47 ^b	0.02 ^b
2.5	0.51 ^b	4.06 ^c	16.6 ^b	0.09 ^b	0.88 ^a	0.72 ^c	5.87 ^b	0.02 ^b
5	0.38 ^a	5.41 ^b	23 ^a	0.12 ^a	0.59 ^a	3.07 ^b	22.6 ^a	0.08 ^a
10	0.003 ^c	55.8 ^c	144 ^a	1.00 ^c	0.09 ^b	15.8 ^a	110 ^a	0.39 ^a
35	0.03 ^a	36.4 ^c	83.1 ^a	0.81 ^c	0.003 ^a	38.2 ^a	254 ^a	0.94 ^a

Standard error equal or less than ^a10 %, ^b20 %, ^c40 %, ^d69 %

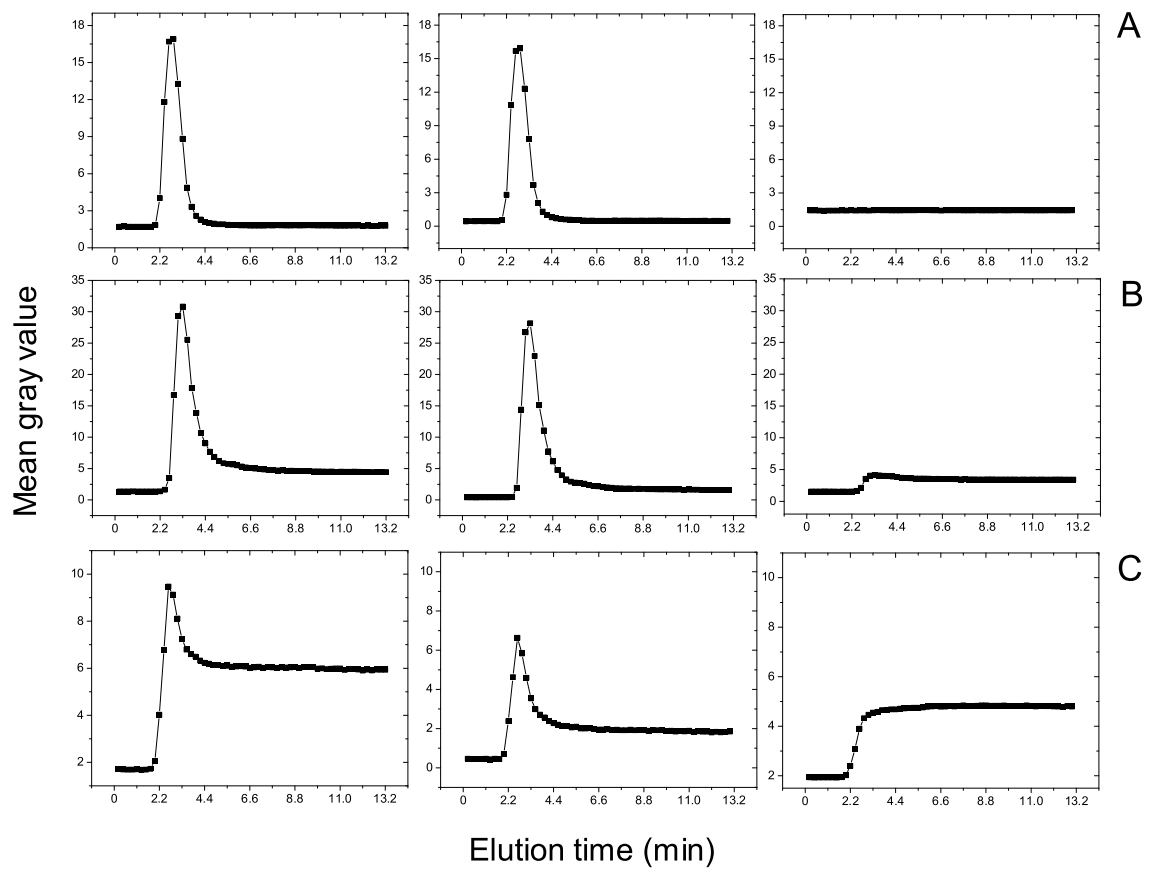


Figure 3.24: Image analysis from CLSM micrographs. First column of images represent the total elution profile, including both retained and non-retained particles. Second column, non-retained particles and the third column represent the kinetics of particle retention. Row of columns A: 0 mM NaCl, B: 2.5 mM NaCl, C: 5 mM NaCl.

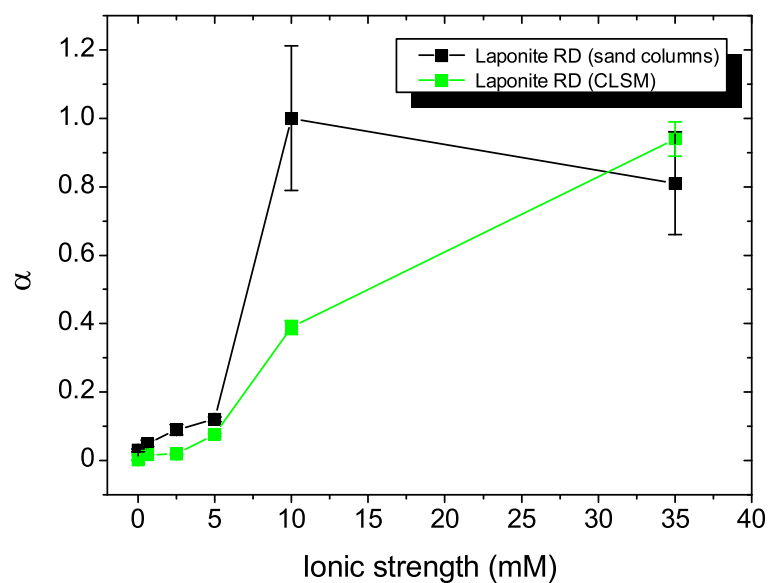


Figure 3.25: Collision efficiencies for laponite RD as a function of ionic strength

3.3.1 Influence of ionic concentration and type on LRD remobilization from water saturated sand

The remobilization of both LRD and bacteria from sand columns and sand-packed microscopy flow cells was assessed at different pore fluid ionic concentrations and ionic species. Ca^{2+} and Na^{+} were chosen to represent these differences in ionic composition due to the reason that they are common in many subsurface environments. In the case of LRD, a remarkable effect on the remobilization of the colloid was observed (Figure 3.26) for columns exposed to either type of cation.

In the case of Na^{+} saturated columns, colloid remobilization was evident as UV-VIS signal increments, after decreasing ionic concentration to around 28 % of the starting value of 35 mM. This trend followed after each ionic strength decreasing step. At a concentration of 0.6 mM NaCl, the colloid was completely remobilized.

In contrast, columns exposed to Ca^{2+} presence, did not show LRD remobilization up to several pore volumes of deionized water influent. As seen in Figure 3.26, LRD remained in the first centimeters of the sand column even after all ionic strength decreasing steps. Visual observation of R6G-stained LRD (pictures in Figure 3.26) was confirmed by constant optical (UV-VIS) measurements. Although these experiments were done in duplicate, the UV-VIS data presented comes from single columns. The reason for this was the difficulty to simultaneously measure two columns for such long periods of time. The qualitative behavior, however, of the R6G-stained LRD, evident in the pictures, was almost identical in each of the two columns.

3.4 Transport of *P. aeruginosa*

For these experiments, bacterial cells were grown and washed as explained in the Materials and Methods (Section 2.5.3). The cells were not fixed in order to alter as less as possible their chemical and physiological conditions. The non-logarithmic growing bacterial cells were suspended in deionized water or in various salt concentrations. The bacterial cells were used in their stationary phase of growth, in order to minimize the possibility of increments in cell numbers during the experiments. In all cases, bacterial pulses had average concentrations (Thoma cell counts) of 1.7×10^9 cells mL^{-1} .

The mobility of *P. aeruginosa* SG81 through saturated porous media was assessed at various ionic strengths. This experiments also combined the use of the classical sand column approach, with the newly introduced sand-packed microscopy flow cells and CLSM method (for details see the materials and methods section). The information obtained

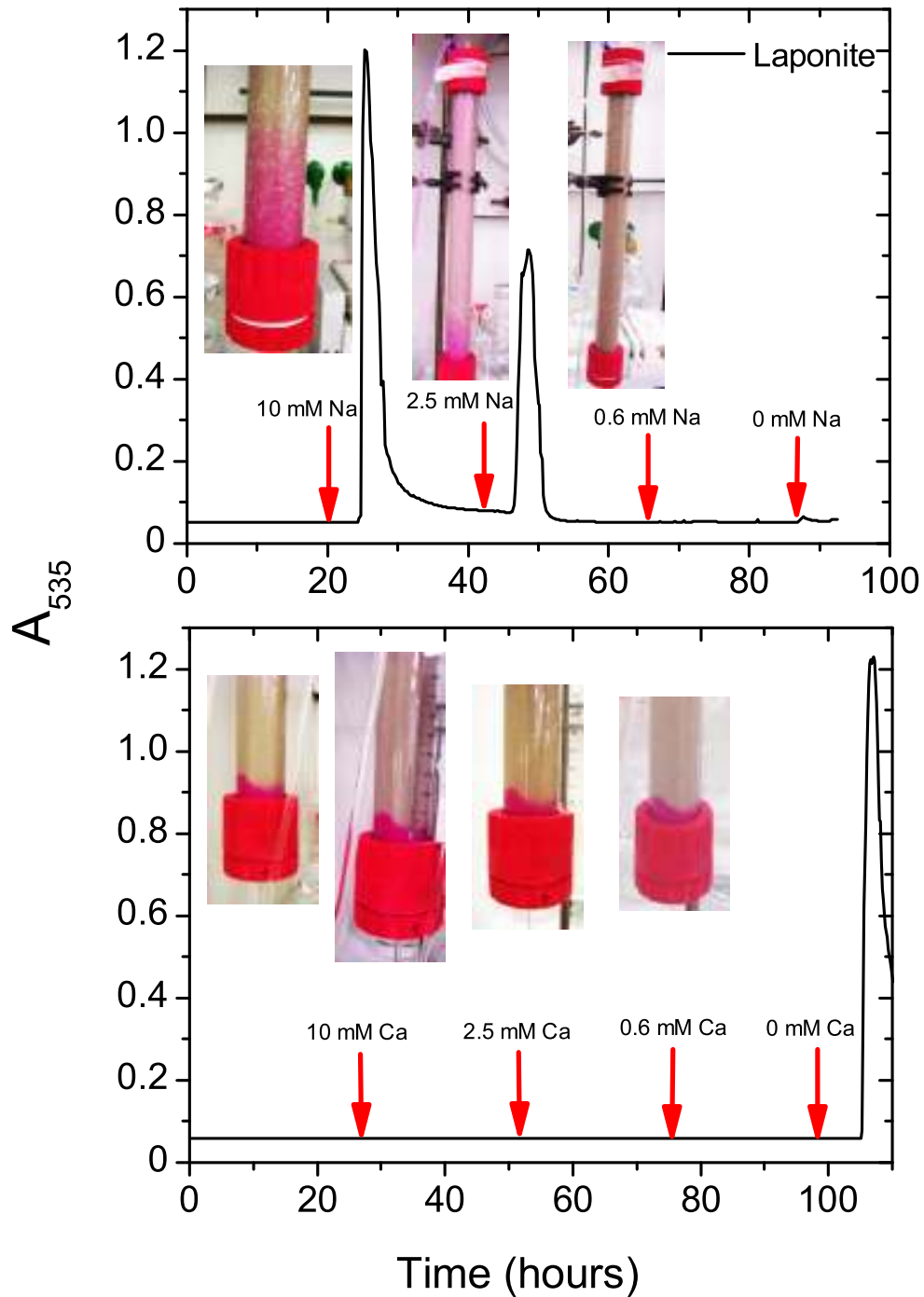


Figure 3.26: Influence of fluid phase cation type and concentration on colloid remobilization. Upper figure: when the dominant cation in solution was Na^+ . Lower figure: dominant cation was Ca^{2+} . Experiment done in duplicate columns.

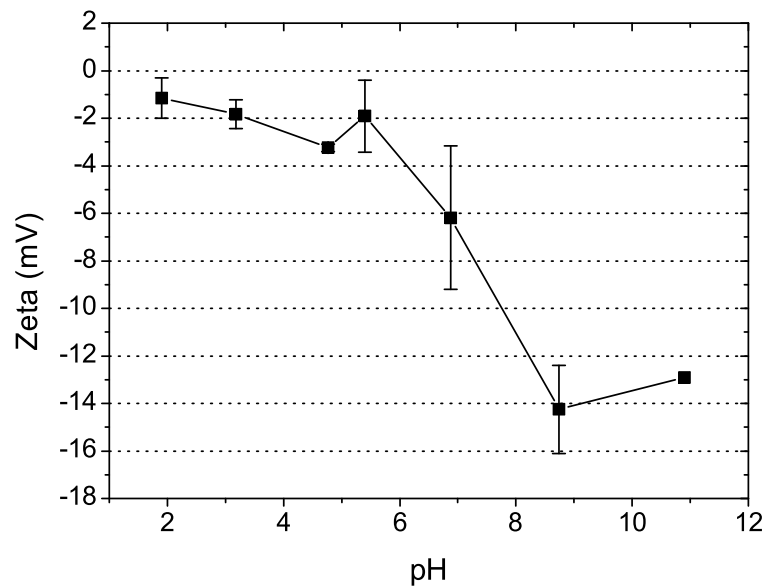


Figure 3.27: Zeta potentials from *P. aeruginosa* SG81 cells at different pH values

with the CLSM method, allowed the direct quantification of both eluted bacterial cells and attached cells. These data did not rely on the quantification of influent/effluent bacterial concentrations only, which is the inherent limitation of the commonly used sand column, UV-VIS method.

3.4.1 Bacterial zeta potential measurements

Zeta potentials or electrokinetic potential represents an indication of the electrical potential at the cell surface which is important in the likelihood of attachment. Figure 3.27 shows zeta potential from duplicate samples of *P. aeruginosa* SG81 suspended in 0.14 M NaCl. The results show that at the pH range measured, the bacterial cells do not show an isoelectric point. At pH ranges of interest for this study, i.e., 7-8, bacterial cell surfaces remain negatively charged. The zeta potential at physiological pH ranges was between -7 mV and -11 mV.

3.4.2 Quantification of bacterial transport parameters

Bacterial transport parameters were obtained from sand columns and the CLSM method in the same way as for LRD. The transport of both *P. aeruginosa* SG81 and its non-mucoid mutant SG81R1 was assessed in sand columns. CLSM was used only for the mucoid strain. BTCs obtained for both types of bacteria are shown in Figure 3.28. Further transport parameters for these bacteria can be seen in Figure 3.36 and Tables 3.3 and 3.4.

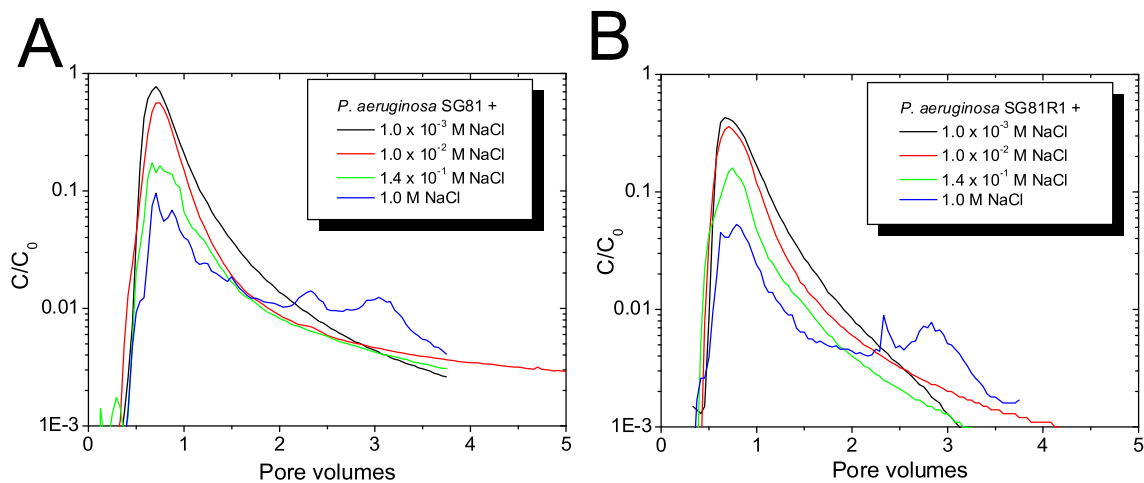


Figure 3.28: BTCs obtained from sand-packed columns and injection of a pulse of *P. aeruginosa* SG81 (A) and *P. aeruginosa* SG81R1 (B).

The results show the same trend of decreased particle transport with increasing ionic strength as observed for LRD. The results also show that the non-mucoid strain was generally more mobile than the mucoid strain, especially at high ionic strengths. In both cases, BTCs obtained at high ionic strengths, i.e., 140 mM or higher, are not smooth but rather irregular and with several regions of sudden increased elution.

Contrary to the case of LRD particles, individual bacterial cells were clearly visible in the CLSM micrographs at all ionic strengths tested. As evident from Figure 3.29 through Figure 3.32, bacterial cells showed different velocity profiles which were, however, not quantified. At 0 mM, some bacterial retention is already evident (yellow arrows). The quantification of bacterial retention by image analysis of CLSM micrographs was done to all replicates, an example of this quantification can be seen in Figure 3.34.

At an influent salt concentration of 1 mM (Figure 3.30) there was still high bacterial mobility, with a peak of bacterial elution at approximately 156 s. This mobility is confirmed by looking at the quantified α values from both the CLSM and sand column methods (see Table 3.4). Also from Figure 3.30 it is evident that bacterial retention increased at this influent salt concentration (yellow arrows).

At 10 mM influent salt concentration, bacterial aggregates were already evident. Quantification from both sand columns and CLSM image data, showed bacterial decreased mobility (Figure 3.31, Table 3.4). Retention in the porous medium is evident at these conditions (see image at 13 s compared with image at 800 s in Figure 3.31).

At concentrations above 140 mM, it is clear from the CLSM micrographs in Figure 3.32, that most traveling particles are retained in the porous medium. Retention also happened in the sand columns, additionally, the BTCs obtained by measuring column effluent particle concentration showed tailing and irregularities consistent with processes of

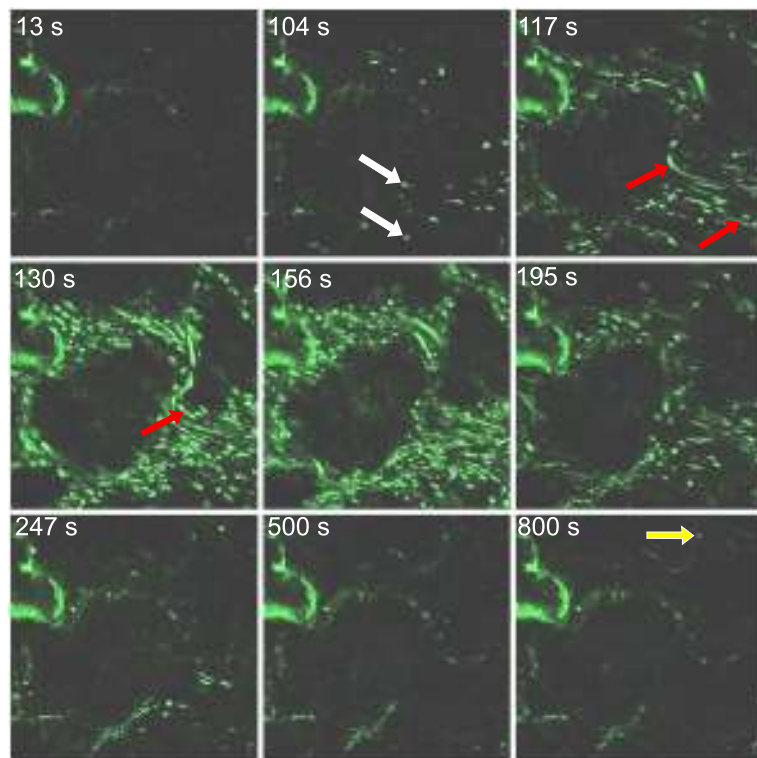


Figure 3.29: CLSM micrographs showing the elution of a bacterial pulse at an ionic strength of 0 mM. Arrows show different states of bacterial mobilization: white arrows show slow moving particles, red arrows show fast moving bacterial particles and yellow arrows, static or retained bacterial cells.

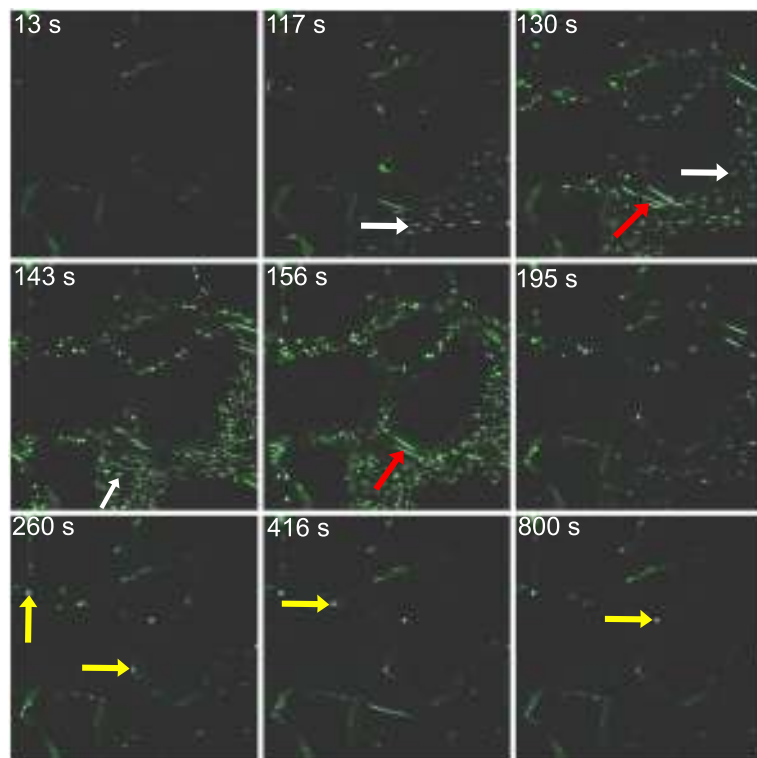


Figure 3.30: CLSM micrographs showing elution profiles of a bacterial pulse at 1 mM salt concentration

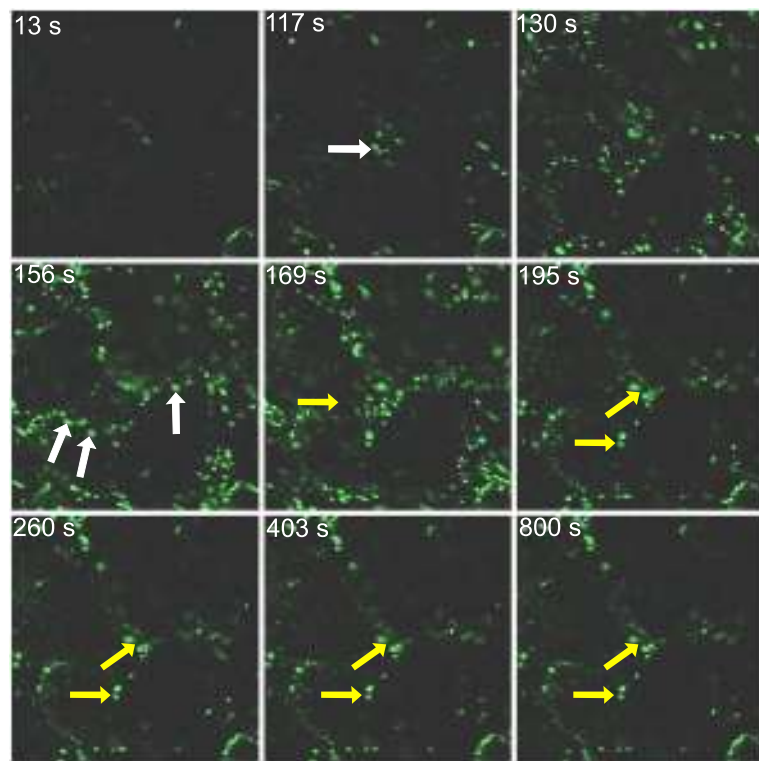


Figure 3.31: CLSM micrographs, showing bacterial elution and retention at an influent salt concentration of 10 mM

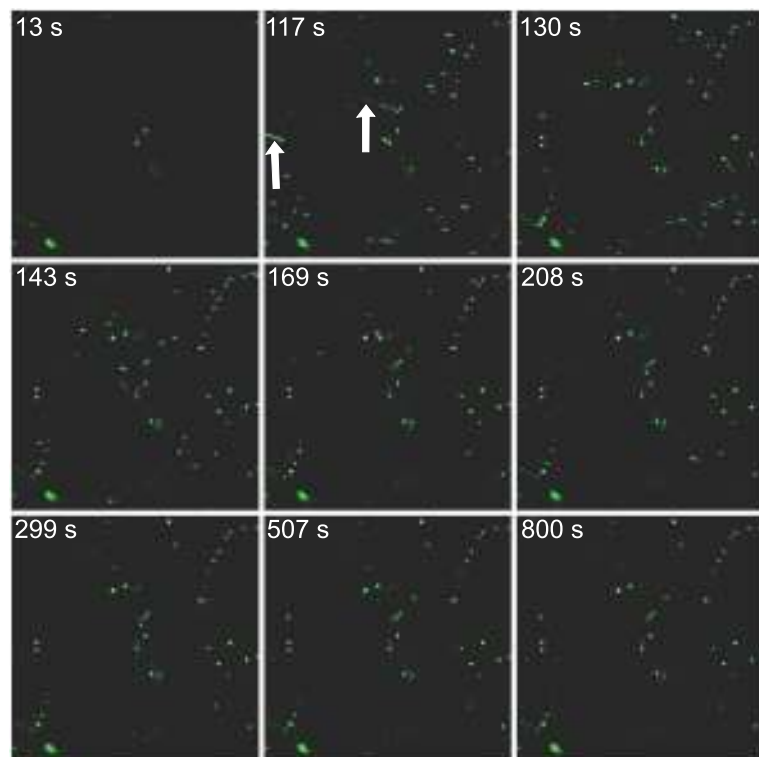


Figure 3.32: CLSM micrographs showing bacterial retention profiles when influent salt concentration was 140 mM

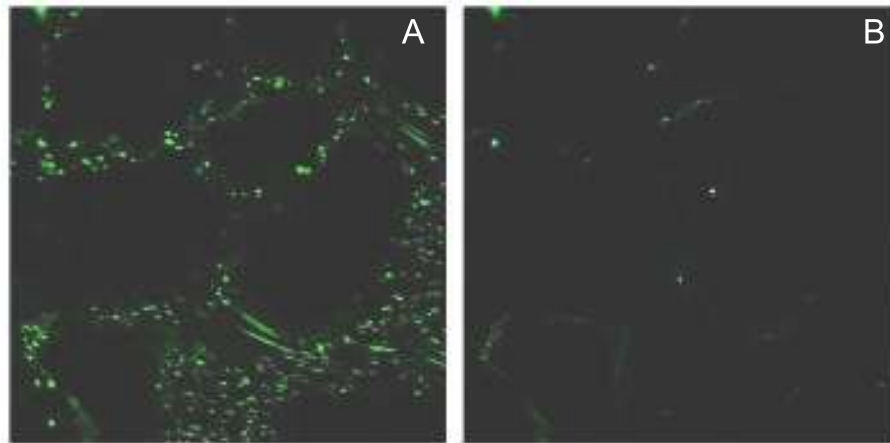


Figure 3.33: Subtraction of non-attached bacteria from a CLSM micrograph. Left image: both attached and non-attached bacteria during pulse elution. Right image: only attached bacteria from the same image are evident.

reversible attachment (Figure 3.28).

The left image (A) in Figure 3.33 is taken from the time series shown in Figure 3.30 at approximately 160 s after bacterial pulse injection. The right image (B) is the same image in which non-attached bacteria are digitally subtracted (see Section 2.7.5.1). The same procedure was done for all time series taken, up to 5 replicates for each salt concentration. By doing this to every image in the time series, it is possible to quantify the kinetics of bacterial retention inside the porous medium (see last column in Figure 3.34).

From the first row in Figure 3.34 it is possible to see that there was some bacterial retention even at an influent salt concentration of 0 mM (upper right corner image). Each point of the plots in this figure represent the mean gray pixel value (see Section 2.7.5.1) of each CLSM micrograph and the resulting subtracted images. In agreement also with data from the sand packed columns, it is possible to see that retention increases with increasing salt concentration. Compared with LRD, however, bacterial cells remain mobile over a wider range of ionic strengths (see Figure 3.25 compared to Figure 3.36).

Tables 3.3 and 3.4 combine all replicates retention information (collision efficiencies) including additional transport parameters such as deposition rate coefficients and C/C_0 values (See Section 2.7.5). As said before, CLSM reported data is taken as means of at least triplicates and standard errors are given as percentages of variation around the mean.

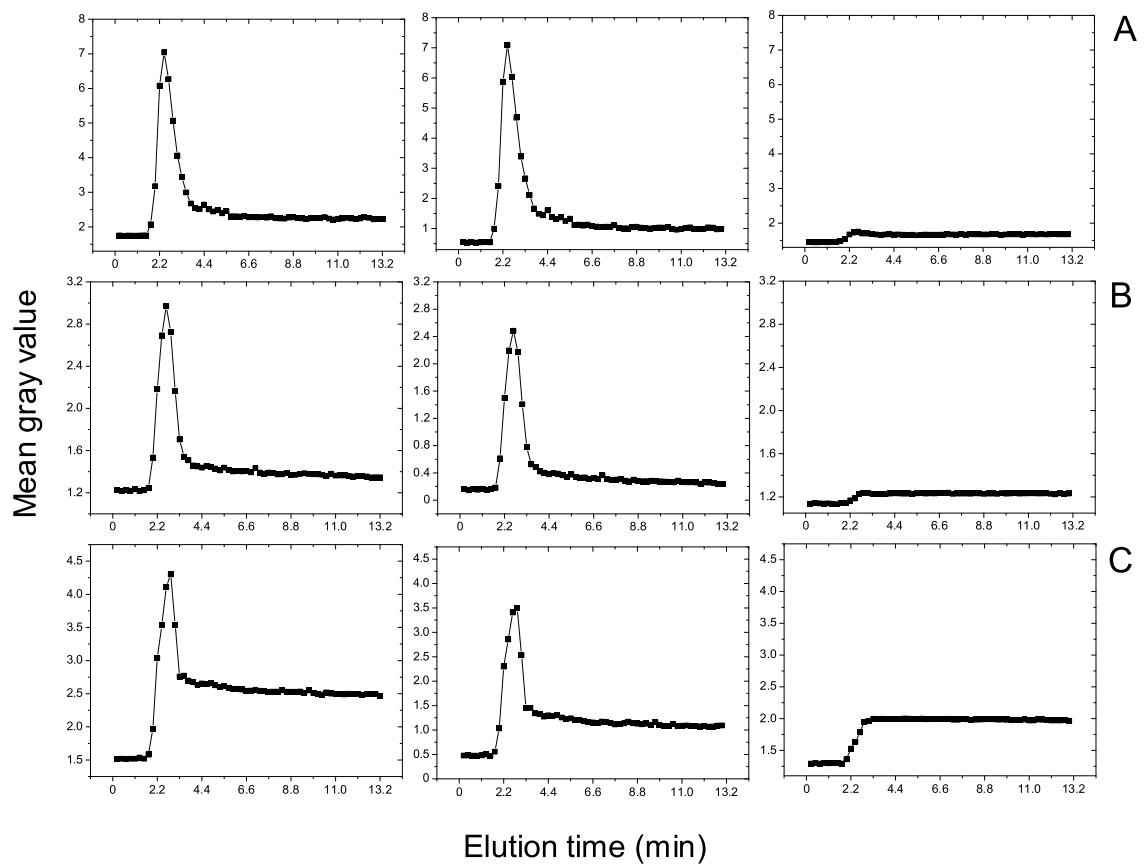


Figure 3.34: Image analysis from CLSM micrographs. First column images represent the total elution profile, including both retained and non-retained bacterial particles. Second column, non-retained bacteria and the third column represent the kinetics of bacterial retention. Row A: 0 mM NaCl, B: 10 mM NaCl, C: 140 mM NaCl.

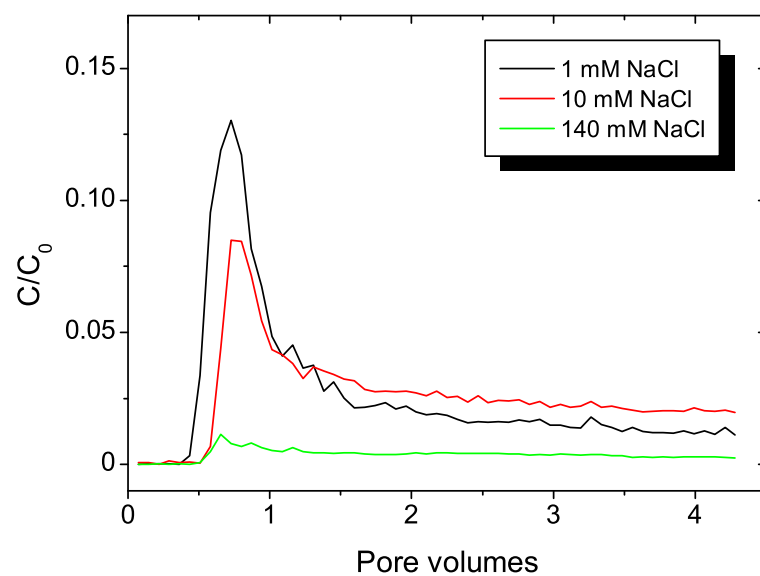


Figure 3.35: BTCs of *P. aeruginosa* SG81 obtained from image analysis information, CLSM method

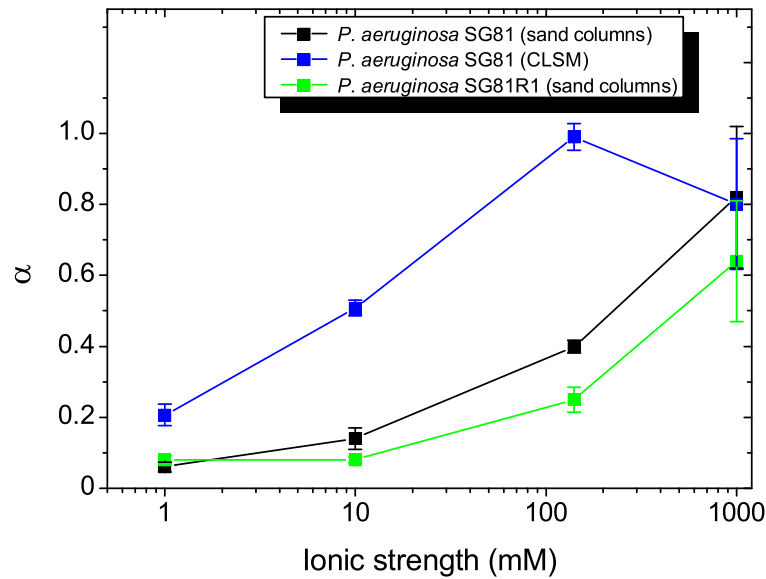


Figure 3.36: Collision efficiencies (α) for *P. aeruginosa* SG81 and SG81R1 as a function of ionic strength. Results represent averages of at least duplicate experiments.

Table 3.3: *P. aeruginosa* SG81R1 combined transport parameters at different ionic strengths

mM NaCl	C/C_0	$kd(s^{-1} (x10^{-3}))$	$\eta (x10^{-3})$	α
0	0.80 ^a	1.35 ^c	0.53 ^b	0.09 ^b
1	0.90 ^a	1.21 ^c	0.24 ^b	0.08 ^b
10	0.82 ^a	1.14 ^b	0.45 ^a	0.08 ^a
140	0.53 ^a	3.65 ^c	1.49 ^b	0.25 ^b
1000	0.24 ^c	9.19 ^c	3.44 ^b	0.64 ^c

Standard error equal or less than ^a10 %, ^b20 %, ^c40 %

3.4.3 Retention at different columns depths as evidenced by CLSM

Another advantage of the CLSM was the possibility of quantify the retention of bacterial cells at different column (sand-packed microscopy flow cell) depths. After injecting a pulse of bacteria as specified before and at different influent salt concentrations, before/after CLSM micrographs were recorded for each concentration. It is clear from Figure 3.37, that most of the retained bacterial cells are located at inlet positions, this is more evident at higher salt concentrations.

3.4.4 Remobilization of bacterial cells from sand matrices

Bacteria were remobilized from sand matrices by applying electrochemical disturbances, i.e., decrements on ionic concentration or by physical disturbances, i.e., increments in flow rate. Again, this was performed in both sand columns and in sand-packed microscopy flow cells. As it can be seen in Figure 3.38, bacterial elution coincided with the

Table 3.4: *P. aeruginosa* SG81 combined transport parameters at different ionic strengths

mM NaCl	Sand columns				CLSM method			
	C/C_0	kd (s^{-1}) ($\times 10^{-3}$)	η ($\times 10^{-4}$)	α	C/C_0	kd (s^{-1}) ($\times 10^{-3}$)	η ($\times 10^{-4}$)	α
0	0.77 ^a	1.09 ^d	6.05 ^c	0.09 ^c	0.96 ^a	0.41 ^a	1.90 ^a	0.12 ^a
1	0.85 ^a	0.7 ^c	3.87 ^c	0.06 ^c	0.92 ^a	0.76 ^c	3.54 ^b	0.21 ^b
10	0.67 ^b	1.73 ^c	9.64 ^b	0.14 ^c	0.81 ^a	1.93 ^a	8.93 ^a	0.51 ^a
140	0.29 ^a	5.10 ^a	28.4 ^a	0.40 ^a	0.59 ^a	4.85 ^b	22.5 ^a	0.99 ^a
1000	0.09 ^c	8.72 ^c	48.6 ^a	0.82 ^c	0.62 ^b	4.84 ^c	22.4 ^c	0.80 ^c

Standard error equal or less than ^a10 %, ^b20 %, ^c40 %, ^d47 %

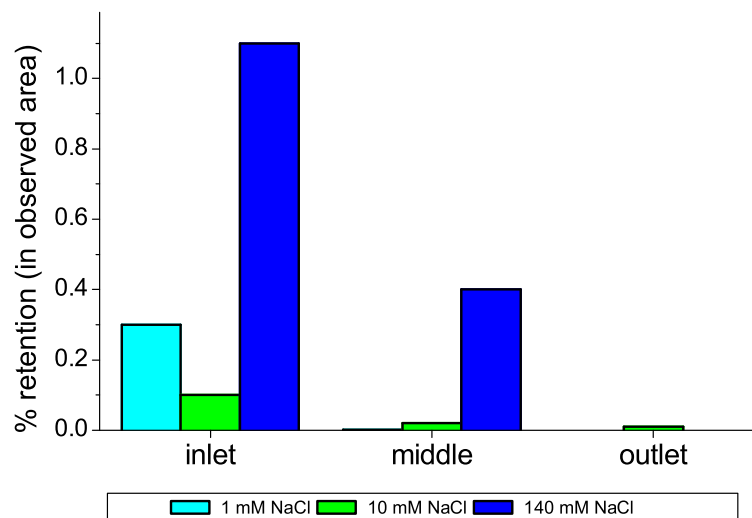


Figure 3.37: Bacterial retention at different microscopy flow cell distances

measured UV-VIS signal. In the case of the mentioned Figure, the disturbance applied was the reduction of ionic strength.

Massive bacterial detachment was evident after increasing influent flow rate by a factor of 5 (Figure 3.39). Previously, the sand-packed microscopy flow cells had been inoculated and grown with the mucoid strain for 4 days. A peak of remobilized bacteria is observed at around 162 s after flow rate increase. A similar effect on bacterial remobilization was observed when decreasing the ionic strength in the column influent from 70 mM to deionized water (Figure 3.40). In this case a peak of remobilized bacteria can be observed at around 480 s after ionic strength change in the flow cell influent.

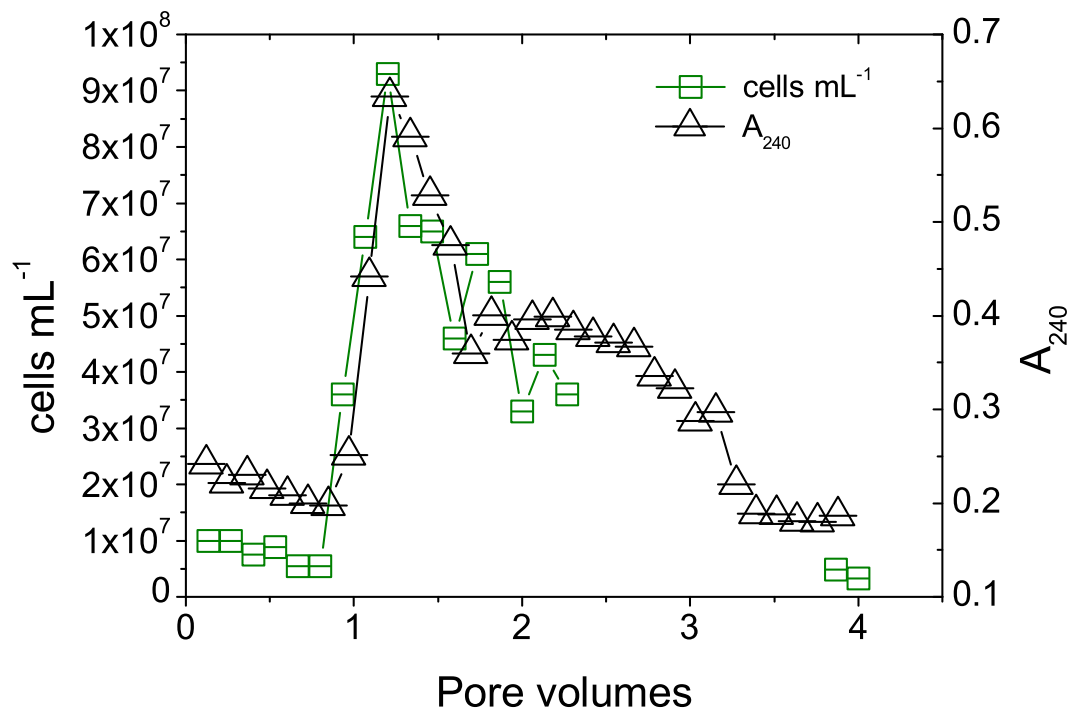


Figure 3.38: Release of biofilm cells after a sudden change in ionic strength from 70 mM NaCl to deionized water

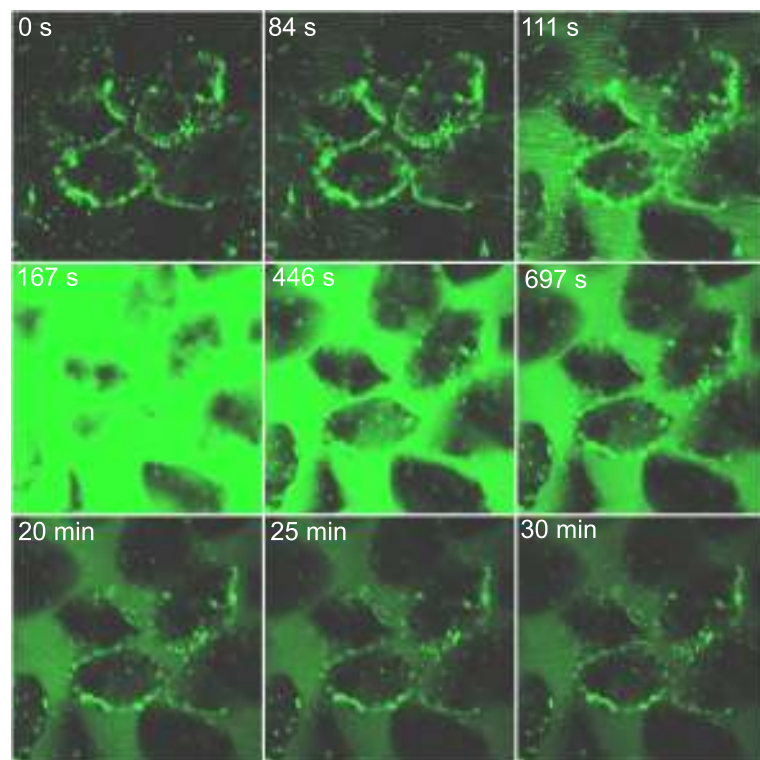


Figure 3.39: Remobilization of bacterial cells from biofilm grown microscopy flow cells stimulated by increasing flow rate 5 times

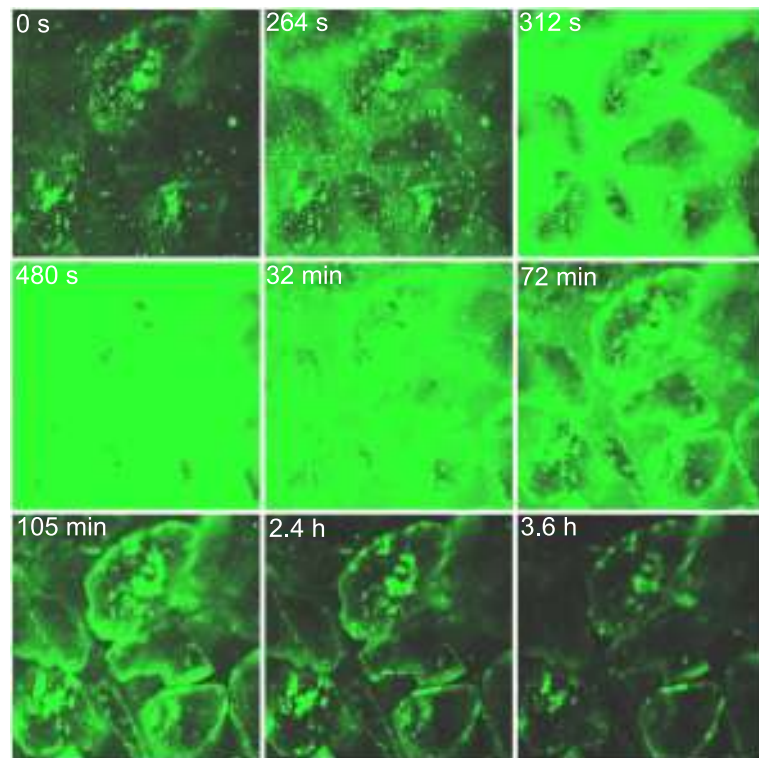


Figure 3.40: Remobilization of bacterial cells from biofilm grown microscopy flow cells stimulated by decreasing the ionic strength of the influent

3.4.5 Bacterial physiological states and transport

3.4.5.1 Bacterial survival

Bacterial cells are not inert particles, they are living microorganisms which are affected by physical chemical and physiological factors. For this reason, it was important to have information on the effect of bacterial preparation on their physiology. As described in the Materials and Methods section, for the transport experiments, bacterial cells were washed (centrifuged) and re-suspended in very low ionic strength solutions or in de-ionized water. The physiological state of the bacterial cells, previously to transport experiments represents therefore valuable information. In Figure 3.41, it can be seen that bacteria remain largely viable even after 72 hours after preparation.

3.4.5.2 Impact of attachment on bacterial transport after remobilization

These experiments were done to assess whether there was a difference in the transport patterns of bacteria recently detached from the porous medium and their planktonic counterparts. In order to achieve this, two subpopulations were obtained from the same strain. In one case, the bacteria were grown in absence of a surface, i.e., planktonic.

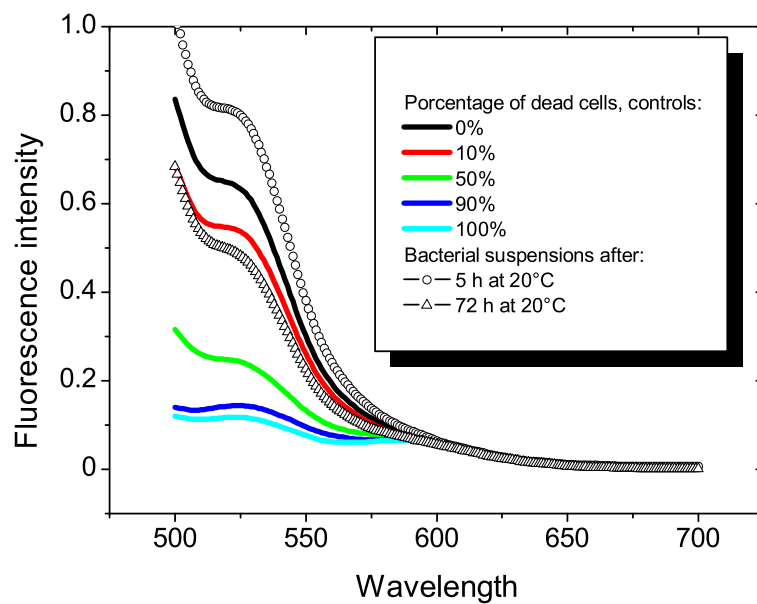


Figure 3.41: Survival of bacteria after bacterial pulse preparation. Results are from duplicates. Standard deviations were always less than 5 %, not plotted for clarity.

In the second case, previously attached bacteria were remobilized by physicochemical perturbations.

The effluent UV-VIS signal at the wavelength used for bacterial detection during the collection of detached bacteria is shown in Figure 3.42. The numbers indicate the different periods of bacterial concentration in the effluent during the bacterial collection process. During the first period, nutrients are replaced by a 70 mM NaCl buffer solution. The concentration of suspended bacteria decreases drastically during the first period and remains low (plateau during period 2) for several hours. When the salt influent is replaced by deionized water and the flow rate is increased 10 fold, a peak of remobilized bacteria is obtained (period 3). The population of detached bacteria used in the transport experiments described below, is collected during this last period.

Microscopically, the cells obtained from the planktonic culture (Population 1) showed increased motility as compared to their recently detached counterparts (Population 2). Sample videos showing Population 1 (planktonicSG81.swf) and Population 2 (detachedSG81.swf) can be found on <http://lamaquina.de/thesis/movies>. Both populations were calibrated to be equally concentrated and the same volume of bacteria was applied for each experimental run.

Elution patterns for the two types of bacterial populations are shown in Figure 3.43. The breakthrough patterns are shown individually in order to show the variability in detached bacteria transport patterns. BTCs from planktonic bacteria show typical elution profiles as obtained (see Section 3.4.2) previously for this bacterial strain. Detached bac-

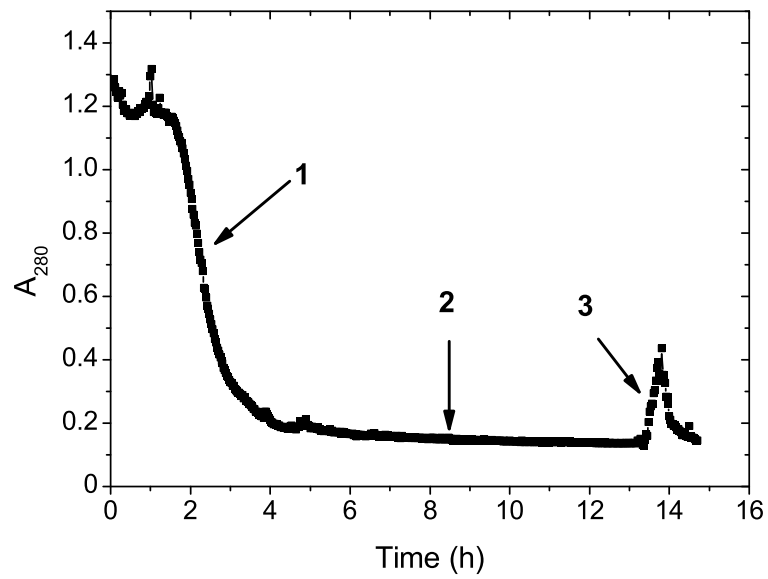


Figure 3.42: UV-VIS detection signal in the column effluent resulting from suspended bacterial concentrations during the collection of the detached bacteria populations. The numbers indicate the different periods of bacterial concentration in the effluent.

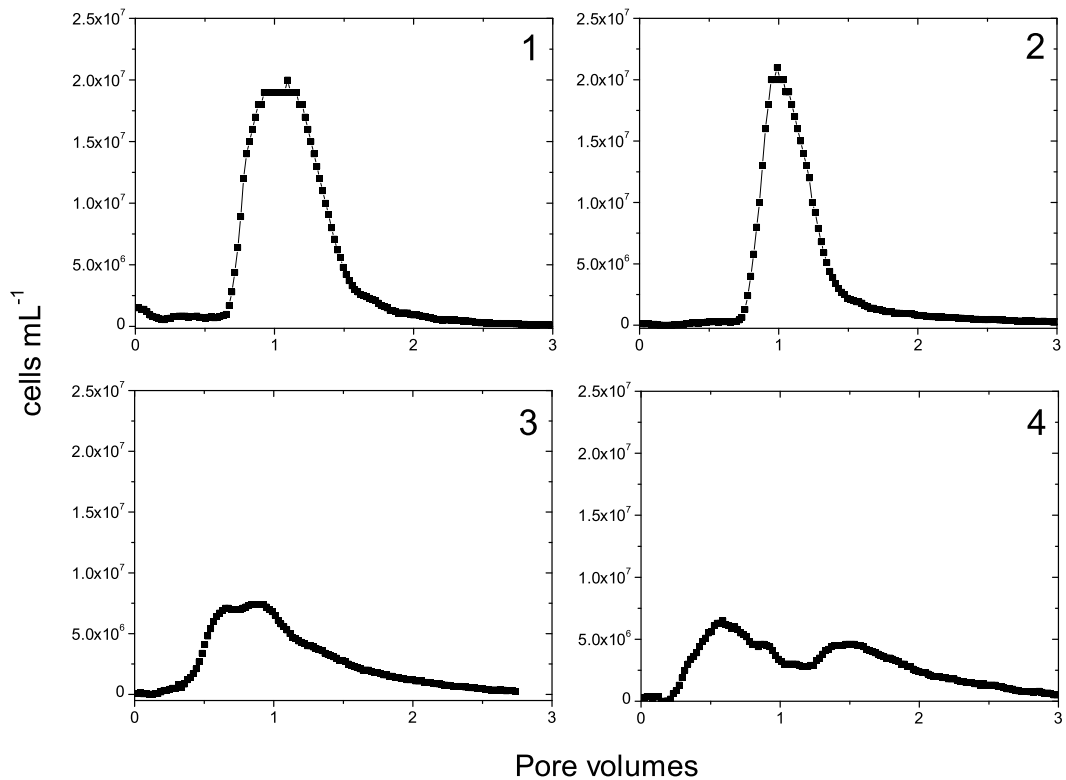


Figure 3.43: BTCs of planktonic bacteria (1 and 2) as compared with those of biofilm detached bacteria (3 and 4). The pulses contained the same amount of cells and were prepared at the same conditions.

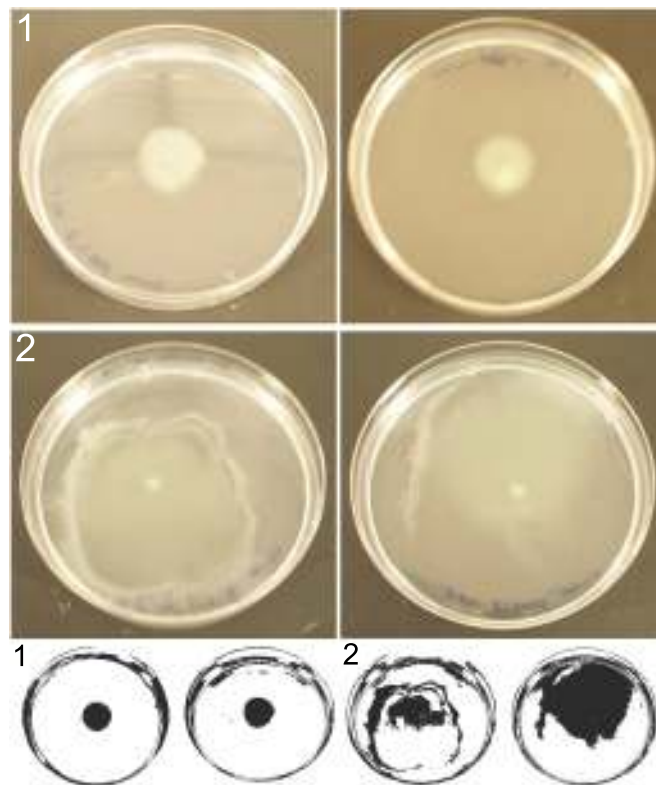


Figure 3.44: Examples of agar test swimming results for planktonic cells (1) and sand detached cells (2) of *P. aeruginosa* SG81. The turbid zone is clearly bigger in the case of the latter. None presented typical dendritic type of growth. Smaller pictures are 8-bit thresholded copies of the same images for enhanced contrast.

teria in contrast, show altered elution patterns consistent with reversible attachment events and significantly less transport. Planktonic cells had an α of 0.26 ± 0.09 and detached bacteria an α of 0.49 ± 0.11 ($n=5$) at a constant ionic strength of 1×10^{-3} M.

In addition to the transport experiments, the two types of *P. aeruginosa* SG81 populations were assessed in motility agar for swimming, swarming and twitching motility. As it can be seen in Figure 3.44, recently detached cells were able to form a wider turbid zone when inoculated in the middle of an agar test dish as compared with their planktonic counterparts. In terms of swarming and twitching motility, no significant differences were found. In non of the tests there was the typical dendritic type of formation as evidenced for other non-mucoid strains (Rashid and Kornberg, 2000). Results are in Table 3.5. Degree of mobility was assessed as follows: (-) no movement, (+/-) weak movement, (+) moderate movement, (++) strong movement, (+++) very strong movement.

As seen from Figure 3.43 and from the collision efficiencies, bacteria were more mobile when not detached (planktonic) from the porous medium even at the same ionic strength. It is evident from Figure 3.44 that detached cells formed wider turbid zones in the agar dishes after the incubation period as compared to the non detached coun-

Table 3.5: Assessment of swimming, swarming and twitching motility in agar media

	Swimming	Swarming	Twitching motility
<i>Planktonic cells</i>			
A	-	-	+/-
B	-	-	+/-
C	+/-	+/-	+/-
D	+/-	+/-	+/-
E	+/-	-	+/-
F	+/-	-	+/-
<i>Detached cells</i>			
A	++	+	-
B	++	+/-	-
C	+	-	+/-
D	++	-	+/-
E	+	-	+/-
F	+/-	-	-

A-F represent replicates

terparts. In Table 3.5 it can be seen that planktonic cells had less swimming capacity as compared with their detached counterparts.

3.5 Remobilization patterns from natural colloids at different ionic conditions

To prove the relevance of laboratory columns results for the transport of colloids in natural environments, columns packed with slow sand filter material, SFM, were used. The remobilization patterns of natural colloids from these systems were obtained using UV-VIS detection. Ca^{2+} and Na^{+} -exposed columns were subjected to a step-wise decrease in ionic strength as done with model laboratory columns (Section 3.3.1). Figure 3.45 shows the remobilization patterns of natural colloids after Na^{+} and Ca^{2+} influence respectively from SFM-packed columns. After a period of stabilization, the columns influent was changed as described in the Materials and Methods (Section 2.7.7.3). In the case of Na^{+} columns colloid remobilization occurred after every step-decrease in ionic strength (upper images in Figure 3.45). DAPI (4'-6-Diamidino-2-phenylindole - a DNA binding fluorochrome) stained particles seen in the micrographs (Figure 3.46) show different morphologies and cell sizes consistent with both bacteria and microalgae (diatoms). Increments in particle concentrations in the effluents of these columns coincided with the UV-VIS peaks observed (Figure 3.45).

In the case of Ca^{2+} columns no remobilization of microorganisms and other particles can be observed during the treatment as compared with Na^{+} columns. UV-VIS peaks

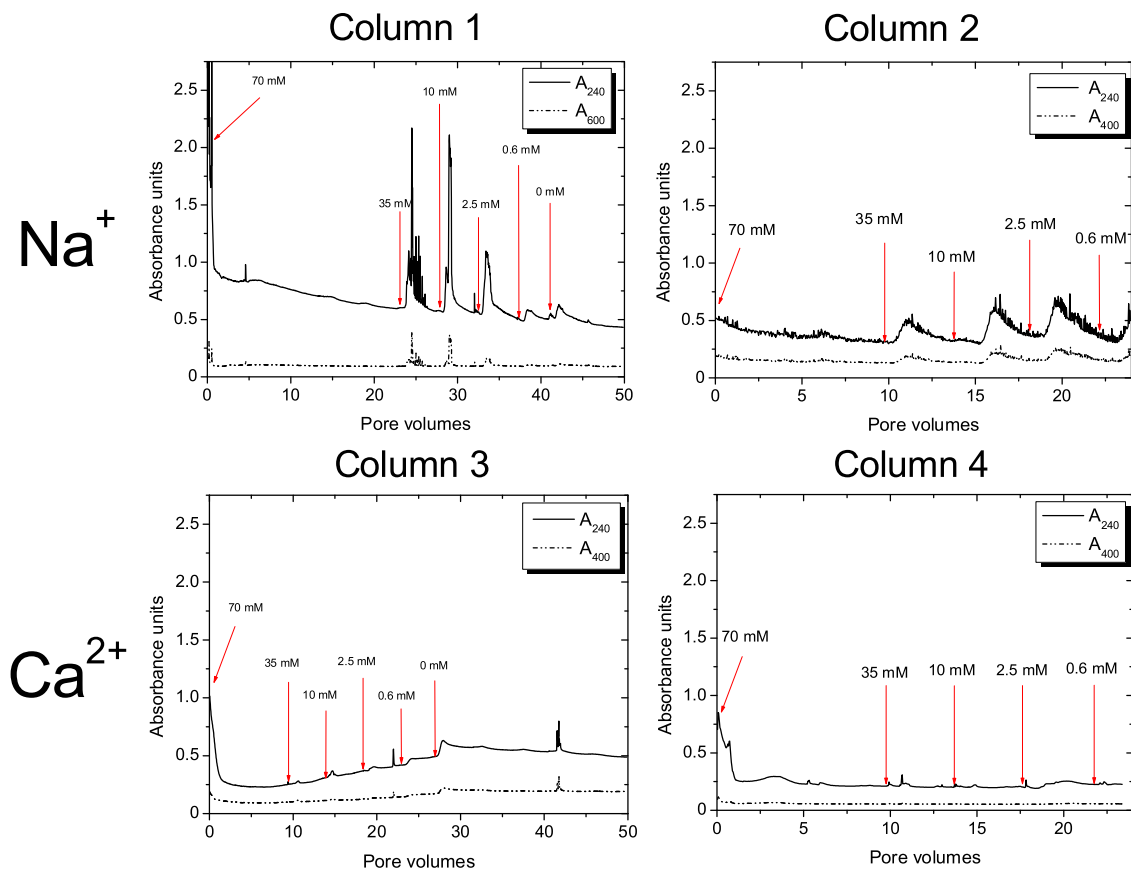


Figure 3.45: Remobilization of natural colloids from slow sand filter material packed in chromatography columns. Upper plots represent columns with Na^+ ions dominance in the influent. Lower plots correspond to the dominance of Ca^{2+} ions in the influent. Each plot represent a different column.

were absent in these columns and no increase in DAPI-stained particles was observed during the ionic strength decreasing steps. Remobilization begins only after several pore volumes of deionized water influent (lower images in Figure 3.45). Distributions shown in Figure 3.47 indicate a wide range of particle size distributions with outstanding peaks at sizes of around $1 \mu\text{m}$ and around $20 \mu\text{m}$ which is again consistent with typical bacterial and diatoms sizes.

3.6 Porous media biofilms

3.6.1 Growth of biofilms inside sand columns

Biofilms of *P. aeruginosa* SG81 were grown in sand columns as model biofilms. The formation of biofilms in sand columns was not evident macroscopically even at the longest experimental period of 3 weeks of biofilm growth. Direct observation was possible only by using CLSM in sand-packed flow cells in combination with SYTO 9 staining

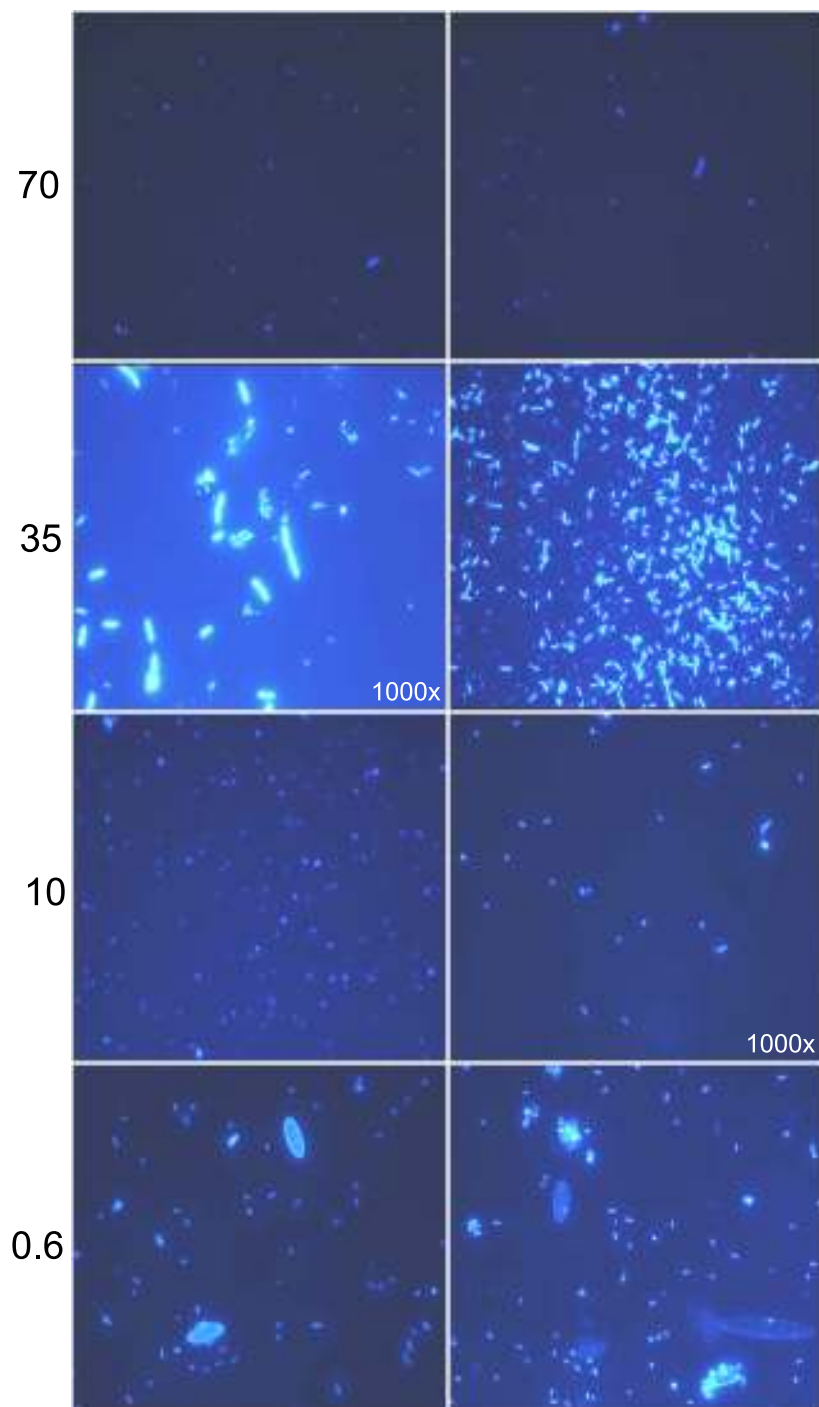


Figure 3.46: Effluent samples at different influent salt concentrations: 70 mM, 35 mM, 10 mM and 0.6 mM. There was a stable and low plateau in the detected particles (UV-VIS) when the salt concentration was 70 mM. DAPI staining, magnification: 400x except where indicated otherwise.

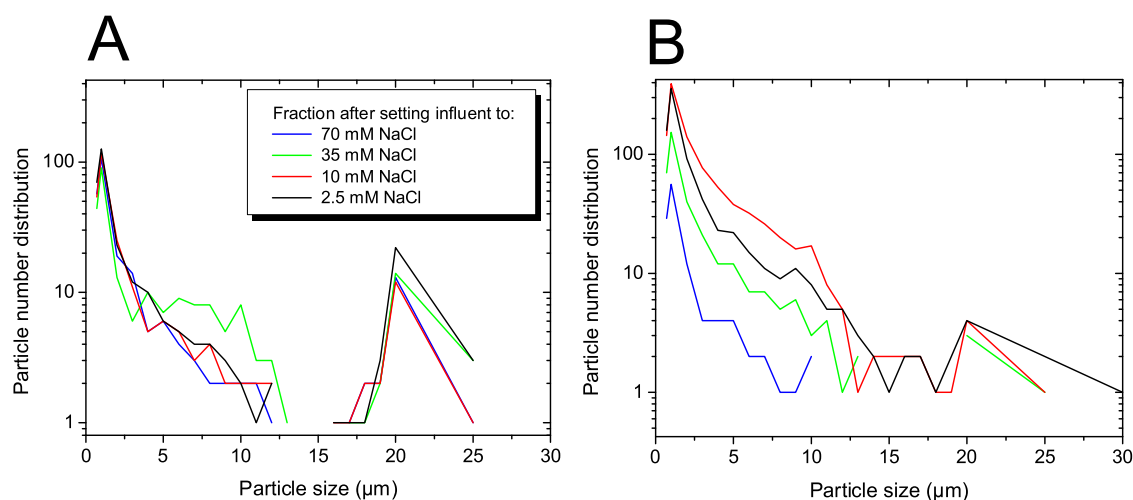


Figure 3.47: Particle size distributions for two example columns

as described in the Materials and Methods section (an example in Figure 3.48). SEM provided qualitative information on the extent of biofilm growth (confluent or patchy) in the porous medium (Figure 3.49). Quantification of biofilm growth in sand columns was done indirectly by measuring changes in the saturated hydraulic conductivity of sand columns (as in Figure 3.50), by quantifying remobilization of attached cells (see Figure 3.38) and by quantification of EPS components (Figure 3.51).

Calcium was expected to have an important role on biofilm stability (resilience to detach) at decreasing ionic strength conditions. A clear effect of calcium on remobilization kinetics of both LRD particles and natural colloids had been already observed (Figure 3.26 and 3.45 respectively). Since the initial steps on biofilm formation and biofilm cohesion rely to a great extent on the same electrochemical principles, a similar type of effect on biofilm stability was hypothesized when divalent cations were dominant.

The patchy nature of biofilms grown in our sand columns was also evident when using electron microscopy (Figure 3.49). Sand grains appeared largely uncovered, especially in regions exposed to higher pore fluid velocities (protuberances, smooth surfaces). As seen in Figure 3.49 non-confluent biofilms were formed in more abrupt and hidden regions which were probably less affected by high flow rates.

3.6.1.1 Influence of biofilm growth on the saturated hydraulic conductivity of sand columns

Changes in sand column hydraulic conditions are indirect evidence of both biofilm formation and its possible influence on colloid transport. Darcy's law was used to obtain the saturated hydraulic conductivity of sand columns at different times after inocu-

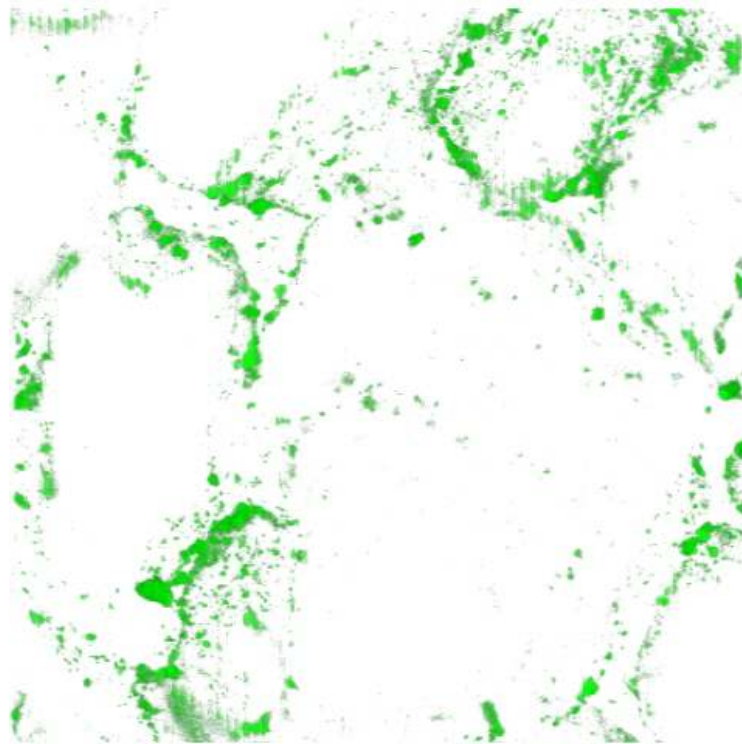


Figure 3.48: Three-dimensional image of SYTO® 9-stained biofilms growing on the surface of sand grains. CLSM image reconstruction, stack size: $x = 460.7 \mu\text{m}$, $y = 460.7 \mu\text{m}$, $z = 110 \mu\text{m}$.

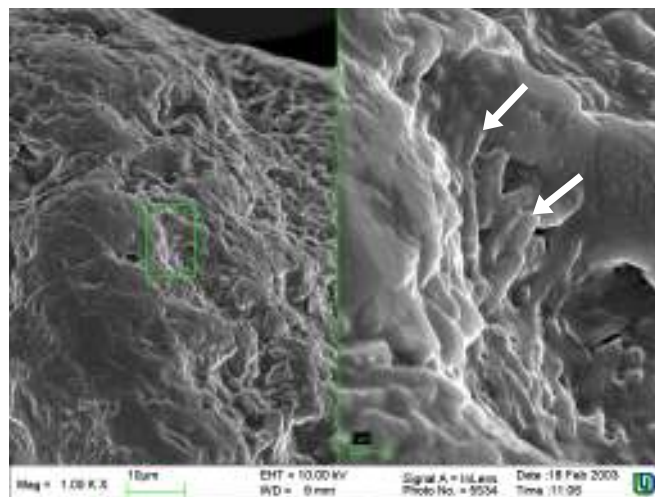


Figure 3.49: Left: scanning electron micrograph showing the surface of a sand grain ($200 \mu\text{m}$ approx. diameter) with generally sparse bacterial colonization as suggested by EDX analysis. Right: Region of enlargement showing bacterial colonization on quartz sand. A bacterial microcolony composed of several cells and their extracellular polymer matrix is evident.

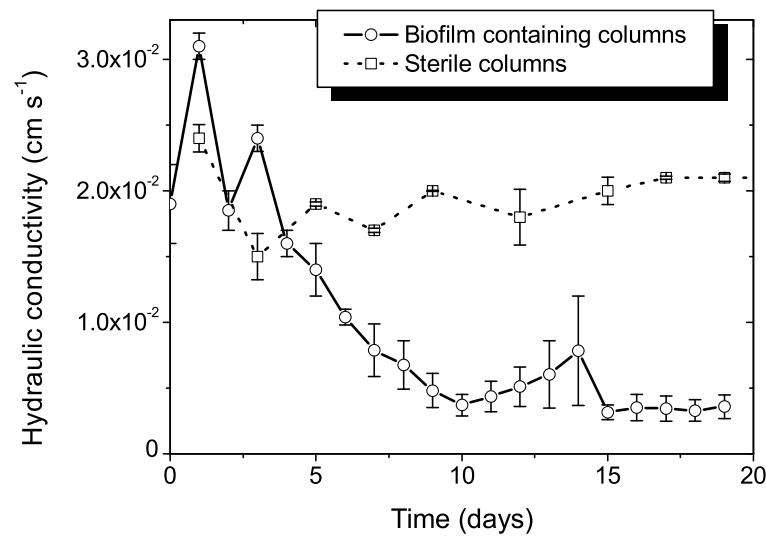


Figure 3.50: Changes in porous matrix hydraulic conductivity induced by biofilm growth. Hydraulic conductivity was measured using a constant head permeameter.

lation with *P. aeruginosa* SG81. This parameter was measured constantly during the biofilm growth period. Results indicate that after an equilibration period, the measured hydraulic conductivity decreased steadily until a more or less constant lower plateau was reached for the rest of the observation period. This plateau was observed after approximately 7-10 days of constant high nutrient load influent (Figure 3.50).

In non-inoculated columns a reduction in saturated hydraulic conductivity, K , was observed after the first hours of column packing. The determined K values remained more or less stable and higher than those obtained with the biofilm growing columns (Figure 3.50). K averages for the first 3 and the last 3 days of measurements were compared for both non-inoculated and inoculated columns. Taking these averaged K from the non-inoculated columns as 100 %, no difference in K was found during the first 3 days of treatment. In contrast, during the last 3 days of observation, K decreased 83 % in the inoculated columns.

3.6.1.2 Quantification of biofilm components in sand columns before the colloid transport experiments

As described in the Materials and Methods (Section 2.5.4), biofilm growth was stimulated for 1, 2 and 3 weeks. To monitor the extent of biofilm formation the biofilm was extracted and biofilm cells counts as well as concentration of EPS were determined. Depicted in Figure 3.51 are the concentrations of the three chosen biofilm indicators, proteins in EPS, carbohydrates in EPS, and cells; found in the sand columns before the colloid transport experiments were performed.

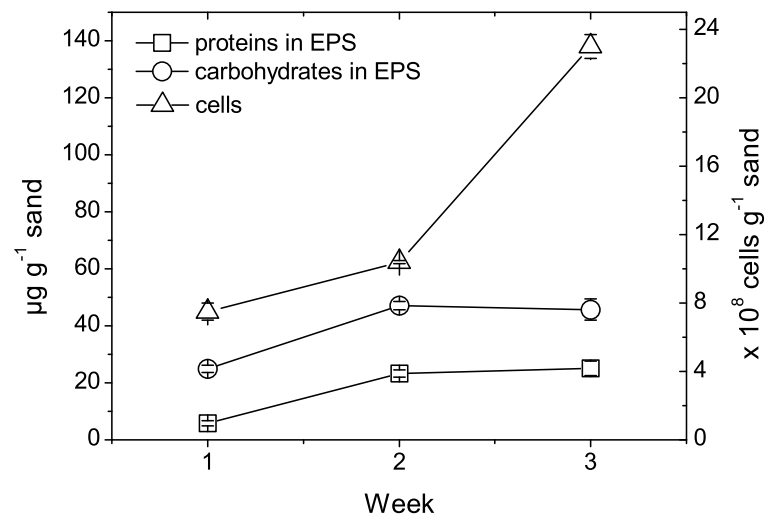


Figure 3.51: Biofilm components (cells and EPS) in sand columns before colloid transport experiments. Cell numbers are represented in the right y-axis.

The cell/carbohydrate ratio (single cell mass in μg was obtained as described in Section 2.5.5) increased with time, from a value of 5 after 1 week of biofilm growth to a value of 8 after 3 weeks of biofilm growth. Although the cell/protein ratio was relatively high for all weeks, it decreased with time, from approximately 19 in the first week, to around 14 in the third week of biofilm growth. The carbohydrate/protein ratio decreased from around 4 in the first week to a value of 2 in the third week of biofilm growth.

3.7 Influence of biofilms on the transport of LRD through permeable sand

The transport of LRD in sterile and non-sterile (with biofilm growth) columns was investigated in the presence of either Na^+ or Ca^{2+} as dominant pore fluid ionic species. Collision coefficients, deposition rate coefficients, particle fraction in column effluent (C/C_0) and colloid travel times were calculated from the recorded BTCs and are shown in Table 3.6. Cell counts and EPS analysis were performed as described previously in the Materials and Methods (Section 2.6).

In sterile columns, the LRD colloid was transported through both Na^+ and Ca^{2+} treated columns using deionized water as the background solution. However, a significant increase in collision efficiency, calculated from the BTCs obtained (Figure 3.54 and Figure 3.57), was observed in the Ca^{2+} columns (Table 3.6) compared with the Na^+ columns. For each of the treatments, Ca^{2+} and Na^+ , there was incomplete colloid re-

tention in the sterile columns. In non-sterile columns, biofilms developed increasingly with time after constant nutrient influent. Two types of effects on colloid transport, which are described in Sections 3.7.1 and 3.7.2, were observed depending on the dominant ionic species present during the ionic strength reduction steps.

3.7.1 Influence of biofilms on LRD transport in the presence of monovalent cations

In the presence of Na^+ ions, changes in the ionic concentration of the influent resulted in more drastic remobilization of bacterial cells and an alteration of LRD transport patterns as seen in Figures 3.52 and 3.54. In Figure 3.52, where UV-VIS detection is used exclusively, it can be seen that bacteria are apparently remobilized in two fronts the first of which was not sufficient to allow for bacterial detection by absorbance at 535 nm. As R6G-LRD complex maximum absorption is at 535 nm probably, the first peak of the second image (B) in Figure 3.52 is due to the elution of LRD. There is an apparent early elution and altered transport pattern due to hydrodynamic changes in the porous medium caused by biofilm growth and to LRD/bacterial co-elution.

At constantly high ionic strength conditions, the elution of LRD through biofilm-colonized sand columns resulted in the enhancement of bacterial cells detachment (Figure 3.53). Normally, as seen on the same figure for the sterile control, there would not be any particle mobilization. This detachment event was proportional to LRD concentration and therefore to LRD aggregation state. This effect was similar to effects observed with other types of disturbances, such as the ones described in Section 3.4.4.

By using fluorescence as detection system, it was possible to discriminate LRD-R6G complexes from other co-eluting particles. This improvement on the detection system was important for the obtention of colloid collision efficiencies and other transport parameters under conditions in which co-eluting particles might interfere with UV-VIS detection only systems. The breakthrough curves obtained in this way from Na^+ treated columns (Figure 3.54) showed no retention of the R6G-stained LRD. When compared with BTCs obtained in the sterile counterparts, there is a significant increase in the area under the curves after two and three weeks of biofilm growth. Different degrees of tailing were also evident.

A pulse of LRD as described earlier was also injected into columns packed with slow sand filter material. These sand columns were treated in exactly the same way as the model systems, except that they were not supplied with nutrient media but directly with the buffers at the different ionic conditions. The BTCs obtained during colloid transport,

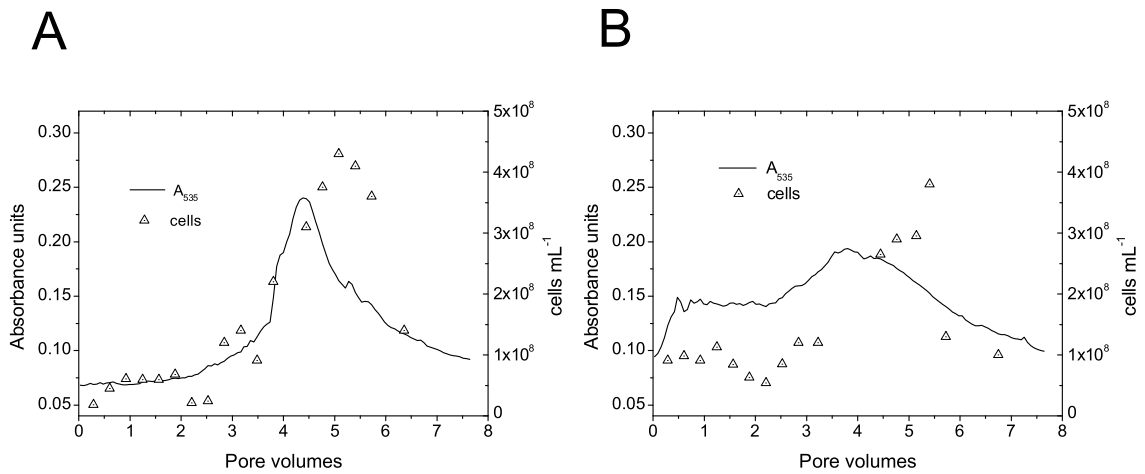


Figure 3.52: Absorbance measurements and total cell counts of the effluents from inoculated sand columns after injection of a colloidal pulse at low ionic strength. A: Unstained laponite RD, B: rhodamine 6G-stained laponite RD. Graphs are means of duplicate experiments.

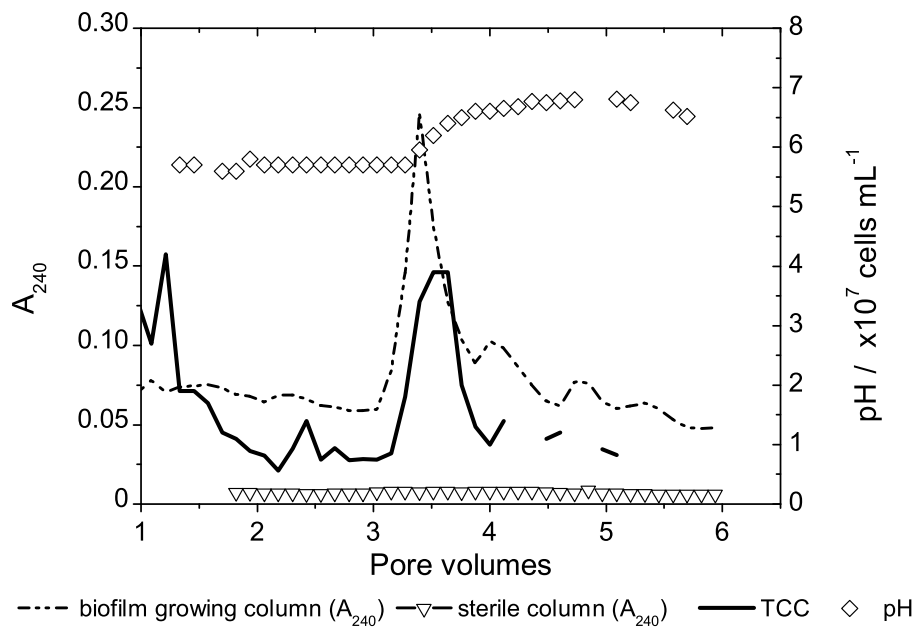


Figure 3.53: Column effluent after the introduction of 2000 mg L^{-1} laponite RD dispersed in $7 \times 10^{-2} \text{ M NaCl}$. Note the retention of a similar laponite suspension in control (biofilm-free) columns (empty triangles). Results were obtained from duplicate experiments.

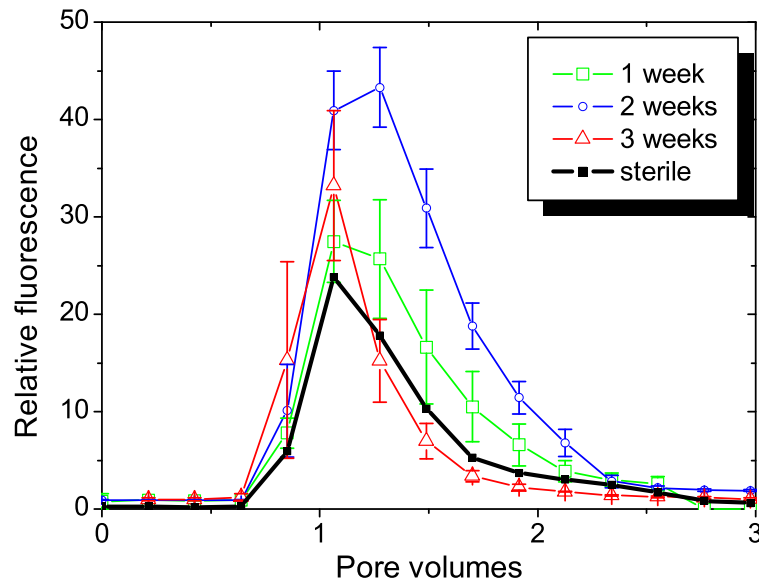


Figure 3.54: Laponite RD breakthrough in columns in which Na^+ ions were predominant before the establishment of low ionic strength conditions by replacing the salt influent with deionized water after 1, 2 or 3 weeks of biofilm growth (means SE; $n = 3$). Also plotted, are sterile controls at the same electrochemical conditions (means SE; $n = 9$).

as well as, total cell numbers, are plotted in Figure 3.55. Cells and EPS remaining in the columns after colloid transport are shown in Figure 3.56. It can be seen that in the case of Na^+ treated columns the elution of LRD occurs comparable to the model systems.

3.7.1.1 Biofilm quantification from Na^+ treated sand columns after colloid pulse injection

The quantification of biofilm indicators shown in Figure 3.56, allowed their correlation with colloid transport patterns. In terms of the ratio of EPS components remaining in sand columns after the colloid transport experiments, in the Na^+ treated columns, cell/carbohydrate, cell/protein and carbohydrate/protein ratios remained constant even after a growing period of 3 weeks (Figure 3.56).

3.7.2 Influence of biofilms on LRD transport in the presence of divalent cations

Contrary to what happened with Na^+ treated columns, in Ca^{2+} treated columns it was found that colloid retention (measured as collection of breakthrough patterns and collision efficiencies) was proportional to biofilm age (Table 3.6, Figure 3.57). EPS analyzes indicate that colloid retention also increased with an increase of the EPS content, es-

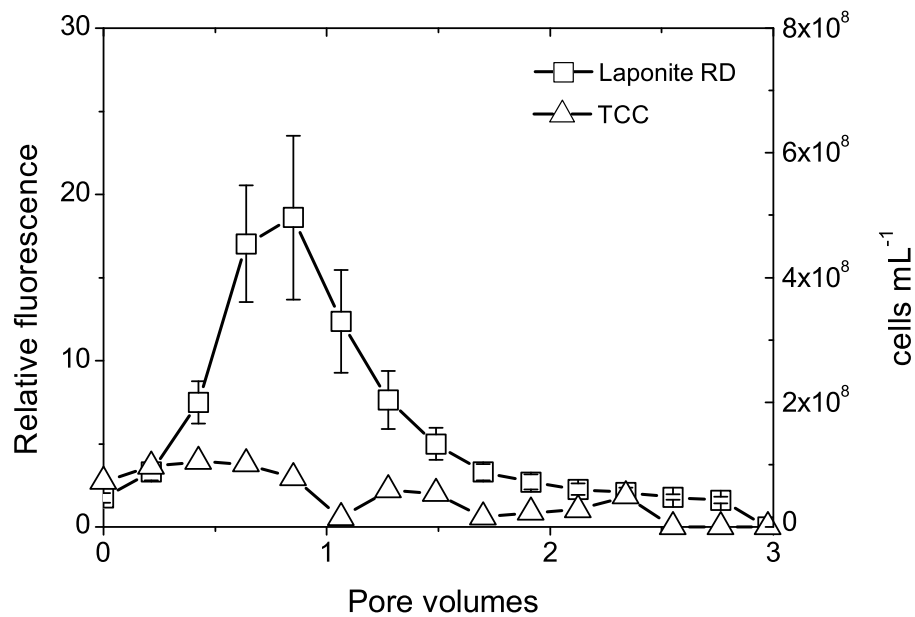


Figure 3.55: Breakthrough patterns of laponite RD when injected in columns packed with slow sand filter material at the same conditions as established for the quartz sand systems (Na^+ saturated columns).

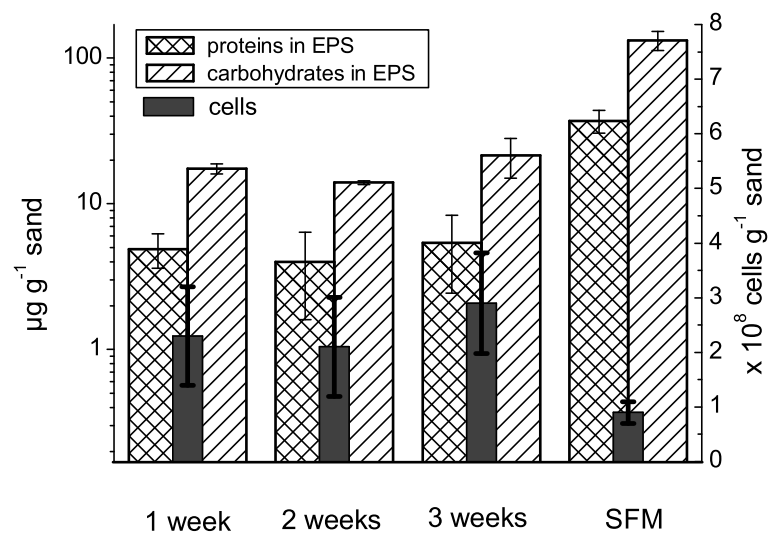


Figure 3.56: Biofilm components (cells and EPS) remaining in sand columns after colloid transport experiments and Na^+ exposure. Cells numbers are represented in the right y axis.

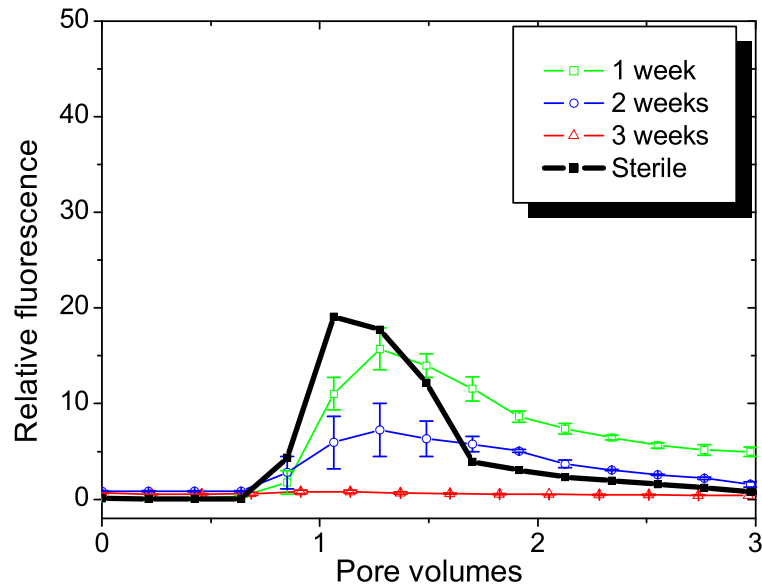


Figure 3.57: Laponite RD breakthrough through columns in which Ca^{2+} ions were predominant before the establishment of low ionic strength conditions by replacing the salt influent with deionized water after 1, 2 or 3 weeks of biofilm growth (means SE; $n = 3$). Also plotted, are sterile controls, at the same electrochemical conditions (means SE; $n = 9$).

pecially proteins remaining in the sand columns after the colloidal pulse transport (Figure 3.59 compared to Figure 3.56). At the established confidence level (Section 2.8), the correlation between carbohydrates and colloid retention (0.917) was not significant. The correlation between proteins and colloid retention was significant (0.999) as was the correlation between cell concentration and colloid retention (0.998).

In SFM-packed columns, colloid retention was evident in Ca^{2+} treated columns (Figure 3.58) in contrast to what happened with Na^{+} treated columns. Cells and EPS data obtained after the colloid transport in these columns can be seen in Figure 3.59.

3.7.2.1 Biofilm quantification from Ca^{2+} treated sand columns after colloid pulse injection

When looking at the ratios of EPS components remaining in Ca^{2+} exposed columns, it is possible to see that the cell/carbohydrate ratio increased from 2 to 3, the cell/protein ratio decreased from 16 to 3 and the carbohydrate/protein ratio decreased from 7 to 1 (Figure 3.59). The ratio of total EPS plus cells remaining in Ca^{2+} treated columns divided by total EPS plus cells remaining in Na^{+} treated columns was 1.5 for the first week, 1.9 for the second week and 2.2 for the third week.

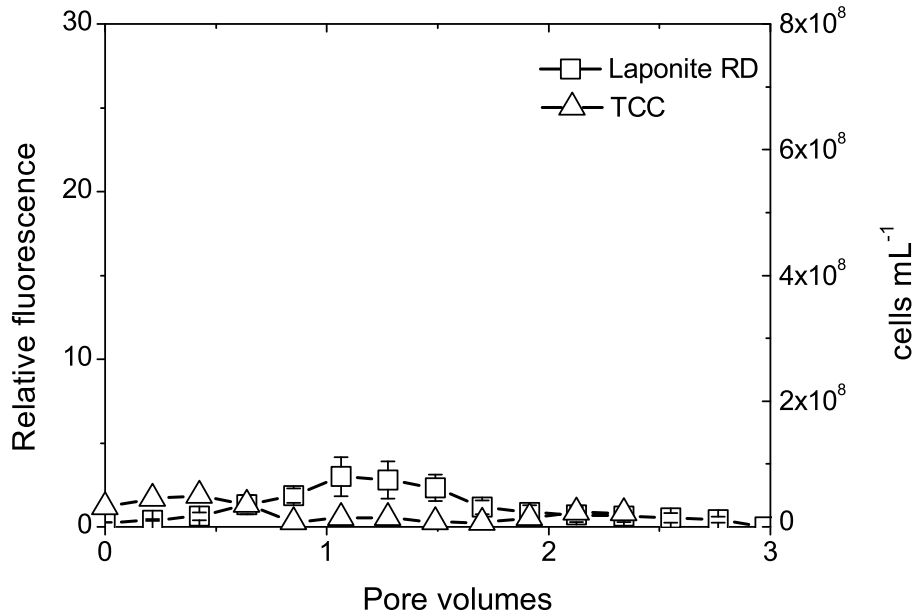


Figure 3.58: Breakthrough patterns of laponite RD when injected in columns packed with slow sand filter material at the same conditions as established for the quartz sand systems (Ca²⁺ saturated columns).

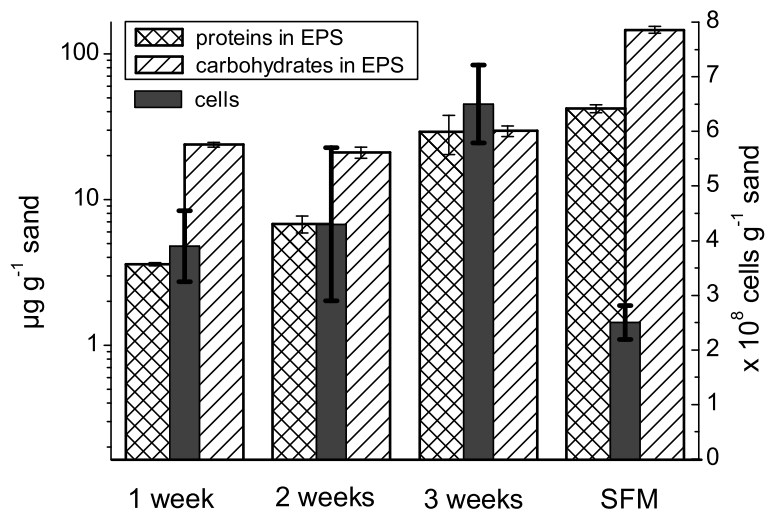


Figure 3.59: Biofilm components (cells and EPS) remaining in sand columns after colloid transport experiments and Ca²⁺ exposure. Note the steady increase on EPS protein content with time. Cells numbers are represented in the right y-axis.

Table 3.6: Transport parameters obtained from the colloid transport experiments

Week	Cation	C/C_0	k_d (s^{-1}) ($\times 10^{-3}$)	Colloid travel time (s)	Collision efficiency
1	Ca ²⁺	0.57 ^a	0.82 ^a	688 ^a	0.1 ^a
	Na ⁺	0.79 ^a	0.46 ^a	516 ^a	0.06 ^a
2	Ca ²⁺	0.29 ^a	1.8 ^a	689 ^a	0.22 ^a
	Na ⁺	0.99 ^a	0.013 ^a	516 ^a	0.002 ^a
3	Ca ²⁺	0.02 ^a	7.5 ^b	532 ^b	0.9 ^b
	Na ⁺	0.90 ^a	0.21 ^a	492 ^a	0.03 ^a
Sterile columns	Ca ²⁺	0.65 ^a	0.68 ^b	654 ^a	0.08 ^b
	Na ⁺	0.79 ^a	0.44 ^b	547 ^a	0.05 ^b

Standard error less or equal to ^a10 %, ^b20 %

Chapter 4

Discussion

4.1 Introduction

The most general goal of the research presented in this thesis can be summarized as: “to investigate the influence of biofilms on colloid retention-remobilization processes in model sediment columns, at changing fluid ionic conditions”. The experimental conditions used, resembled highly saturated and highly permeable subsurface porous environments. Colloid transport and biofilm formation under these circumstances have a huge impact in natural pristine and contaminated environments (see Sections 1.1 and 1.8 for further clarification on this). For this reason, the results obtained, are discussed mainly in terms of their significance to natural subsurface environments. One part of the discussion explains decisions made in terms of colloids used, analytical methods used and on the general experimental setting used. The other part of the discussion deals with the interpretation and analysis of the obtained results and how close are these findings to accomplish the proposed goals.

4.2 Field scale vs. laboratory scale approach

Field scale colloid transport studies have been commonly used when investigating transport processes in the subsurface, including the transport of natural colloids (Bunn et al., 2002; Hess, 2002). While nothing done entirely in the laboratory will come close to reality as field studies do, they do not necessarily reflect exactly the transport behavior of the colloidal particles. At present, technology does not offer a completely “non intrusive” alternative yet. The determination of colloid transport patterns always involves intrusive and destructive activities such as sampling (which most of the times has to

be done from man made sampling wells). The addition of special tracers which can be easily measured by using standard laboratory methods has been also a common practice for many years (Flury and Wai, 2003). In some cases, even bacteria are used as tracers (as described in Harvey, 1997). This practice implies an alteration of the natural environment which is difficult to suppress. Even in idealized experimental conditions, natural environments are extremely complex and it would be impossible to predict or account for every possible source of interaction. These so-called “black boxes” are some of the biggest problems when doing transport experiments at field scale. When the underlying principles are well known, however, field scale studies are invaluable for the refinement of models and for predictions at scales which can be translated into direct practical actions and solutions to environmental problems.

The influence exerted by biofilms on the transport of colloidal particles in the subsurface is still considered on many respects a “black box” as discussed above. It is clear that biofilms colonize subsurface environments (see Section 1.6 for more information) and that they participate on many environmental processes. It is less clear, however, (and the main motivation for this research) which will be their role on colloid transport. It was necessary then to isolate as much as possible the conditions in which biofilms would exert an impact on colloid transport. This was achieved by using sand columns and the quartz sand/LRD/*P. aeruginosa* SG81 system. This system was appropriate to minimize and control as much as possible factors such as influent water chemistry and type of colloid present. In a field scale study this would have been difficult to achieve.

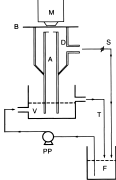
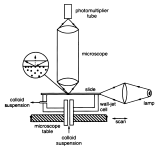
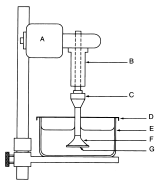
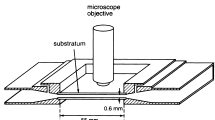
Findings from laboratory scale studies using model systems need however to be tested in the field. The present work does not go as far as this but it includes laboratory experiments which use natural porous material including natural, heterogeneous colloidal particles. Transport patterns under similar conditions as for the model systems were obtained for these “natural” systems as well. It is considered a first step towards studying biofilm influence on natural colloid transport at field scale.

4.3 Discussion on the laboratory methods used

There are several alternatives when doing colloid deposition experiments in the laboratory (see Table 4.1). Basically, a colloid carrying system is needed which will allow the contact between colloids and collectors. The carrying systems are electrolyte solutions which have a controlled chemistry and which are being forced through the collecting system by using some sort of pumping device or by gravity. 1-1 inorganic electrolytes such as NaCl (the electrolyte used in our experiments) were used because they do not

specifically interact with the surfaces of particles and collectors (Elimelech et al., 1995). Collectors can be planar continuous surfaces, or -as in our case- granular materials.

Table 4.1: Common techniques in particle deposition kinetics (greatly based on Elimelech et al., 1995)

Technique	Diagram	Description	Example references
Stagnation-point flow		After colloidal suspension forced through small circular hole in tube (A) towards a transparent flat collector (B), a stagnation-point flow is formed. Deposition of colloidal particles on B can be observed with a microscope (M)	Redman et al. (2003); Elimelech et al. (2003); Yang et al. (1999)
Evanescent wave scattering technique		Stagnation-point flow method based on the measurement of the light scattered by deposited particles from the evanescent wave. With this technique it is possible to monitor deposition of smaller particles than with a light microscope based technique.	Holmqvist et al. (2007); Clapp et al. (1999)
Rotating disc		A constant-speed motor (A) promotes the rotation of a shaft (B) that holds a disc with a collector cover-glass (C). The particle suspension is contained in a glass beaker (D) supported by an adjustable lab jack. After the experiment, the suspension is removed, the disc rinsed, and the particles deposited on the cover glass are enumerated.	Neville et al. (1999); Bondoc and Fitzpatrick (1998); Martin et al. (1991)
Parallel-plate channel		In this system a colloidal suspension is forced to flow in between two parallel plates. Deposition will take place on these parallel plates. Deposition can be observed by using a microscope. The colloidal suspension is recirculated by using a peristaltic pump. Hydrodynamics of the channel can be controlled by adjusting the flow rate of the pump.	Bos et al. (1996); Busscher et al. (1997); Habash et al. (1997); Hendricks et al. (2000); van der Mei et al. (1997)

... continued on next page

... continued from previous page

Technique	Diagram	Description	Example references
Packed-bed technique		See Section 2.7	Most of the literature available on colloid transport through porous materials

Based on the information presented in Table 4.1, it is probably clear why the packed-bed technique was used for our experiments. Not only for resembling closely our target conditions (high permeability, relatively high approach velocities) but also for being a widely accepted technique among people studying colloid transport.

Both direct and indirect methods can be used to obtain key transport parameters such as collector efficiencies and deposition rates in these type of systems. Direct methods imply counting the amount of retained particles directly from the collector's surface. Normally, especially crafted columns are set, so they can be disassembled at any given time and divided in "slices" from which colloids can be counted using different methods (Elimelech et al., 1995). In the case of this study, this type of columns were not used due to the challenge that would represent to keep such systems in sterile conditions when the inoculation of bacteria or the growth of biofilms was required. Also, less intrusive and destructive methods were preferred. The determination of transport parameters (see Section 2.7.5) when using sand columns relied therefore, on indirect particle quantification. This was done as explained before, by measuring bulk particle concentration changes before and after contact with the collector surface, i.e., particles concentration in column influent and in column effluent.

When using the packed-bed technique, there are two possibilities for the injection of colloidal suspensions: the step-input technique, and the short-pulse technique. In general, both techniques produce very similar results when properly applied (Kretzschmar et al., 1997). In the case of the step-input technique, the volume of the colloid suspension injected to the column is generally bigger than one column pore volume. In this case, the BTCs obtained are not symmetric (see Figure 4.1A) and transport parameters must be obtained in the early stages of colloid breakthrough, i.e., before the plateau of eluting particles. In the case of the short pulse technique, a small volume of the colloidal suspension is injected to the column, typically the size of the pulse is less than 10 % of the column pore volume. BTCs obtained from this method are generally

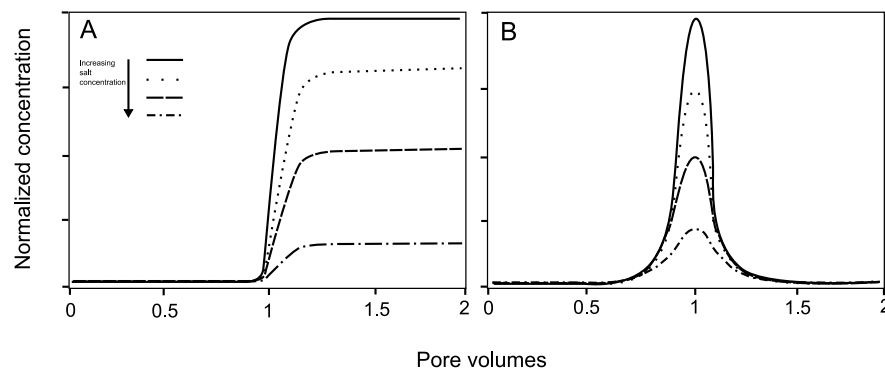


Figure 4.1: Two common colloid injection techniques used in particle deposition experiments. A: step-input technique in which one column pore volume or more equivalent of colloid suspension is injected. B: short-pulse technique in which the size of the injected particle suspension is generally less than 10 % of the column pore volume.

symmetric (Figure 4.1B) and the whole BTC can be used to obtain colloid transport parameters. All important transport experiments presented in this thesis were done using the short-pulse method. The reasons for choosing the short-pulse technique over the more traditional step-input technique, include:

- Small volume size of injected colloids which minimize the possibilities of retained colloids influencing deposition (blocking effects).
- Minimize the time of colloid contact with electrolyte or R6G before entering to the column. As discussed later, time can be an important factor in the colloidal behavior of suspensions in presence of electrolytes or cationic dyes.
- Baseline corrections in the case of BTCs produced by short-pulse experiments can be easier because baselines can be obtained on both sides of the breakthrough peak.
- Short pulses can resemble more closely natural events in which intermittent mobilization of colloids is observed.
- Less amount of colloids, electrolytes and time are needed per experiment. Besides being an economic advantage, this represents less disturbances in the case of experiments involving biofilm formation (see Section 4.9).

4.3.1 The use of CLSM sand-packed microscopy flow cells for transport experiments

Due to the limitation of determining influent/effluent particle concentrations in sand columns, a method, that was not entirely new in terms of the experimental setting (see

Figure 1.10), was adapted to our experimental conditions (see Section 2.7.3) and used in parallel with the more established sand column experiments.

Transport parameters obtained using the CLSM method were equivalent to those obtained using sand columns. This demonstrates that the method, even though still under active development in the laboratory, can be adequate for colloid transport studies. Although the information provided by 2D image stacks was sufficient to semi-quantitatively determine transport parameters under carefully controlled conditions, the method is expected to provide more detailed information when more complete 3D image stacks are available. The impediments to obtain these types of images at the moment are the impossibility to penetrate through an opaque substratum such as sand grains and the higher processing speed needed. This limits the observation to the first layer of sand grains and 100 to 200 micrometers from the interface between sand grains and the flow cell wall to the center of the packed flow cell. One way of addressing these limitations is the use of transparent materials in conjunction with 2-photon microscopy which could offer the possibility to assess both biofilm formation and colloid transport at a higher range of distances and even at several layers of particle substrata. Nevertheless CLSM has provided important insights into the spatial distribution of biofilms growing inside porous materials by allowing the determination of both elution of colloids (outlet BTCs) and the direct observation of colloid retention at different distances from the inlet position. This is not achievable with sand column experiments.

4.4 Interaction between LRD and R6G

The lamellar structure of clay minerals and that of their synthetic counterparts such as LRD, confers these substances huge surface areas which results in their great adsorption capacity. Organic dyes have been used for studying clays for several years. Clays have such a strong affinity for the adsorption of organic dye molecules, that they are commonly used in industrial processes for color removal from special systems (Jaruwong et al., 2005). In order to visualize the LRD colloid by using CLSM and for UV-VIS or fluorescence spectrophotometry, LRD dispersions were stained with rhodamine 6G, a cationic dye (see Sections 2.2 and 3.2.1).

The adsorption capacity of clays is due to a great extent -although not exclusively- to cation exchange processes. The inclusion of amphiphilic molecules improves the hydrophobic character of clay surfaces and facilitates the adsorption of apolar molecules as well (López Arbeloa et al., 1998). Several studies have been devoted to studying the interactions between organic dye molecules and clay surfaces (López Arbeloa et al., 1996;

Jaruwong et al., 2005; Yariv et al., 1989; Yermiyahu et al., 2003) and models have been proposed on the process (Margulies et al., 1988).

Based on literature information and mainly on research published by López Arbeloa et al. (see Literature section) on the use of rhodamines for clay studies, Rhodamine 6G was chosen as the LRD staining agent. Unstained LRD was detectable by UV-VIS spectrometry in sterile, clean sand columns, when no other co-eluting material was present. This was not true in biofilm growing columns due to the great amount of co-eluting material. Since the direct detection of LRD was important, it was necessary to use this procedure (The staining procedure can be found in Section 2.2) for LRD detection. The advantages of using Rhodamine 6G are that it is very photostable and it can be detected both by UV-VIS and fluorescence.

Tapia Estévez et al., used various clay/rhodamine systems which demonstrated the high affinity of this dye for clay surfaces (López Arbeloa et al., 1998; Tapia Estévez et al., 1993; López Arbeloa et al., 1996). They characterized the evolution of rhodamine 6G spectra with time and at different relative clay/dye concentrations, going from 0.1 % to 100 % of the cation exchange capacity of the clay (CEC). They demonstrate that at dye loading ranges < 10 % CEC, the adsorption of the dye to clay (including LRD) surfaces and interlammellar spaces is complete.

In Figure 3.1, it can be observed the absorption spectrum of rhodamine 6G in the absence of LRD and at different NaCl concentrations relevant for this study. It can be seen that NaCl does not influence neither the shape or the absorption maxima of the dye monomers (approx. 527 nm). Secondly, a small shoulder located at a higher energy can be noticed (at around 490 nm). This absorption shoulder is believed to be due to dye aggregation and dimerization. It has been shown that in the case of dye-clay associations, a metachromatic effect occurs as the dye molecules start to aggregate on the surface of the clay or in the interlamellar space. The effect is characterized by a diminution of the absorbance of the main absorption band, which corresponds to the absorption of the R6G monomer, and an increase of the shoulder placed at higher energies. The metachromatic effect increases with time and it is an indirect indicator of the degree of clay dispersion in the aqueous medium (López Arbeloa et al., 1996).

As can be seen in Figure 3.2, there is a slight increase in this absorbance shoulder but the major absorbance is kept at around the absorption maximum for the dye monomeric state. There is an apparent shift in the absorption energy in the presence of the clay though (from around 527 nm in the absence of clay to approximately 535 nm for 200 mg L⁻¹ LRD and to 537 nm for 2000 mg L⁻¹ LRD). According to the results this might be due to clay concentration but since it was kept constant at 200 mg L⁻¹ for most of the transport experiments, this was not investigated further. Important to notice here is

that the clay dispersion state in deionized water is not apparently altered by the addition of R6G.

On the other hand as salt is added to the system (Figure 3.3), the metachromasy effect starts to take place. This is in agreement with visual inspection of the aggregation state of the clay at these salt concentrations. Further confirmation of the strong R6G-LRD association can be seen in Figure 3.4 where no rhodamine is found in the upper phase of a sedimented LRD dispersion.

The objective of this study clearly was not to perform a complete spectroscopic study on R6G absorption in LRD but rather to assure it was used in a suitable form according to literature information and the objectives of this thesis. R6G loading (3.5 % of the clay CEC) was chosen in order to assure the complete adsorption of the dye to the clay surfaces. The uniform dispersion of the dye was assured through the drop-wise-high stirring speed staining technique.

Additional pulse experiments through the porous medium (as described in 2.7.7.2) also confirm the strong interaction between the clay colloid and the cationic dye R6G. Sand grain surfaces are negatively charged. Pulse sizes were always less than 10 % pore volume size. Complete retention of a R6G pulse, was therefore expected. Pulses of unstained LRD were injected at different times after the R6G injection (see Sections 2.7.7.2 and 3.2.1). The level of LRD-induced R6G remobilization was assessed by measuring R6G-stained LRD in the column effluents. As said before, studies about the interaction between clays and organic dyes are abundant in the literature. However, no studies were found comparing the adsorption of R6G to sand grains and to clay surfaces. These experiments were expected to clarify if rhodamine could be irreversibly attached to sand grains and if there would be some sort of preferential interaction with either sand surfaces or LRD surfaces. Ideally, the preferential interaction should be between LRD and R6G. As the results show, this was always the case. R6G retention on the sand grains is evident from both Figures 3.5 and 3.6 in absence of LRD. This is very likely to be due to electrostatic interactions. The process is however reversible and R6G could be remobilized by unstained LRD even after almost 20 min of interaction (see Figures 3.7, 3.8 and 3.9). According to the results of both CLSM and sand columns experiments (Figures 3.8 and 3.9 respectively) the process appears to become irreversible with time. This is concluded from the almost linear decrease in absorbance and fluorescence peak intensity with time of LRD injection. Since most of the transport experiments are within a time framework of less than 30 min and all LRD-R6G suspensions are freshly prepared outside the sand material, the interaction between R6G and sand grains should be irrelevant.

From what was said before, it is evident that rhodamine molecules interact and remain

strongly bound to the clay surface. It is therefore reasonable to assume that all rhodamine fluorescence detected in the colloid transport studies comes from the clay-dye complexes and not from free R6G. Secondly, it can be also said that R6G is probably not interfering with LRD aggregation and dispersion processes. R6G was therefore found to be a good detection aid in our colloid transport studies.

4.5 Factors determining the transport of LRD through porous media

The aggregation of LRD observed in the presence of relatively high NaCl concentrations, i.e., > 2.5 mM (Figures 3.10 and 3.11) was expected to play an important role on the movement of the clay through water saturated sand. Indeed, particle aggregation and deposition in porous materials have been found to be very closely related (Grolimund et al., 2001; Elimelech et al., 1995).

When injected into quartz sand-packed microscopy flow cells, LRD suspensions at 2000 mg L^{-1} as revealed by CLSM time series images, were retained mainly by straining mechanisms (physical hindrance) (Figure 3.15). Sudden remobilization of bacterial cells from previously inoculated flow cells coinciding with LRD retention, suggests a physical alteration of the flow conditions at the pore space. Considering the macroscale size of LRD aggregates under this conditions (Figure 3.13), clogging processes leading to localized increased flow velocities (and therefore shear stress) might be responsible for bacterial remobilization. Gelation observed by SEM might also have contributed to the porous medium clogging process.

The quantification of fluorescence intensity shown in Figure 3.16, shows that the first peak in fluorescence intensity corresponds to the moment of bacterial remobilization caused by hydrodynamic shear stress. After this first peak, a prolonged tailing event is observed which is typical from bacterial transport and remobilization from sand columns (Strauss and Bolster, 2004) and which is probably due to slow and steady bacterial release after the first peak. The second plateau shows the aggregated LRD clogging process of the porous medium.

As pointed out by Davis et al. (2001), straining is only one of the two possible mechanisms by which colloids can be deposited in porous media. The other mechanism is interception and it is due mainly to electrostatic interactions. At the maximum LRD-NaCl concentration used in this study (2000 mg L^{-1} LRD and 70 mM NaCl), it was not possible to determine if electrostatic interactions had also a role on the observed retention. In preliminary sand column experiments, no LRD was detected in column effluents

either at the described concentrations, nor at one (200 mg L^{-1}) or two (20 mg L^{-1}) orders of magnitude less.

Images obtained with the CLSM method (Figures 3.17 and 3.18) showed that LRD retention was occurring clearly in absence of straining, i.e., space between sand grains was sufficient for aggregates to pass through. This is especially evident when LRD concentration is 20 mg L^{-1} .

If electrostatic interactions between the LRD aggregates and the surface of sand grains were mainly responsible for the retention of the colloid in the porous medium, then the colloid should be remobilized simply by eliminating ions in solution. This hypothesis is clearly demonstrated when deionized water is allowed to flow through the sand-packed microscopy flow cells and all other conditions are kept constant. In Figure 3.19 it can be seen, how, in a relatively short period of time all the retained LRD is subsequently remobilized from the porous medium. As discussed in Section 4.4, the possibility of R6G-only remobilization is unlikely. Figure 3.20 shows the quantification (by image analysis) of the complete stack of micrographs comprising this retention/remobilization process.

This demonstrates that LRD retention under the described conditions, was mainly due to electrostatic interactions. At higher LRD concentrations, straining might represent an additional mechanism of retention but is not fundamental in LRD retention in porous media.

4.6 LRD transport quantification

From the previous experiments, it was clear that at relatively high salt concentrations, straining did not represent a fundamental retention mechanism, when LRD concentrations were 200 mg L^{-1} or less. For LRD transport quantification at different ionic strengths, 200 mg L^{-1} was chosen because R6G detection at lower LRD concentrations was a limiting factor. For similar reasons the maximum salt concentration used for the transport experiments was 70 mM . In order to minimize the contact between the electrolyte and the colloidal suspension, all suspensions were freshly prepared and only put in contact with electrolyte right before the deposition experiment.

LRD colloid transport through sand columns at different pore fluid ionic strengths was studied systematically (Section 3.3) using both sand columns and the CLSM method. The CLSM method allowed for the detection of particles still inside the porous medium. The direct quantification of retained particles was then done by image analysis (something not possible with the traditional sand column method).

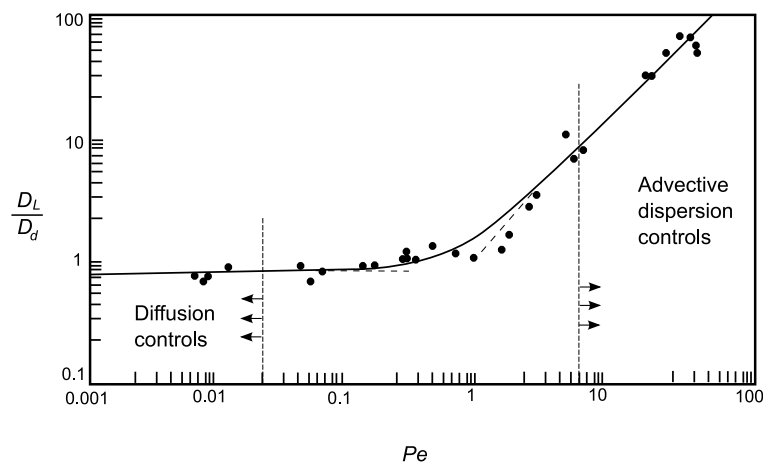


Figure 4.2: Peclet number and advection/diffusion transport mechanisms. Figure modified from Fetter (1998).

Typical hydrological sand column parameters are shown in Table 3.1. The shown hydraulic parameters demonstrate that at the established flow rate and packing conditions, advective/dispersive movement would be dominant. This is an important condition for our experiments because all calculations are based on the assumption that diffusion processes would be minimal and could be ignored. In fact, in most cases relevant for groundwater flow, diffusion is insignificant and is generally neglected (Fetter, 1998).

Peclet numbers, Pe , calculated for the used systems demonstrate dominance of advective conditions. These numbers represent a dimensionless number relating the effectiveness of mass transport by advection to the effectiveness of mass transport by either dispersion or diffusion. In Figure 4.2 the ratio D_L/D_d versus the Peclet number is plotted. D_L represents the longitudinal dispersion coefficient and D_d is the molecular diffusion coefficient. The mentioned Figure compiles experimental results from a variety of sand columns and tracer experiments (as reviewed in Fetter, 1998). It is clear from these data, that above Pe of approximately 10, the mechanism that controls transport in porous media is advection. Peclet numbers compiled in Table 3.1 for our sand columns and sand-packed flow cells are at least one order of magnitude higher than this boundary ($Pe = 10$).

The study of the movement of LRD in isolation shows that transport parameters follow predictable patterns in terms of aggregation and deposition at different ionic strengths. The vast amount of studies available in the literature (see Section 1.3 and Table 1.1) suggest a fundamental influence of ionic strength on both the aggregation and deposition of colloidal particles in a wide variety of environments.

Although the results obtained from sand columns and the CLSM method are equivalent, there are some noticeable differences that will be discussed later. In terms of results

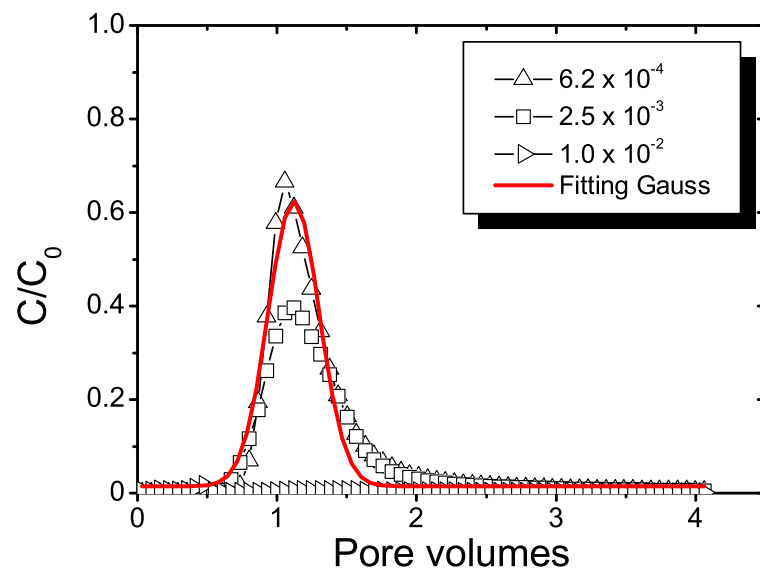


Figure 4.3: Laponite RD BTCs with added Gaussian fit

obtained from the sand columns (Figure 3.21, Table 3.2), several researchers have reported consistently, a decrease of colloid transport with increasing ionic strength. This has been observed for both natural (Grolimund et al., 2001, 1998; Laegdsmand et al., 2003) and artificial (Davis et al., 2001; Grolimund et al., 1998; Kretzschmar and Sticher, 1998; Liu et al., 1995; McCarthy et al., 2002; Saiers and Lenhart, 2003) colloids.

LRD was drastically affected by relatively small changes in ionic strength. From Figures 3.21 and 3.23, it is evident, especially from the sand columns, that the main change in collision efficiency, α , happens between 0 mM and 10 mM salt concentration. Highly aggregated LRD suspensions (at 2000 mg L^{-1}) were retained in the porous medium with the influence of clogging effects as observed by CLSM. Smaller aggregates (at 20 mg L^{-1}) were also retained inside clean bed sand columns at high ionic strengths. These facts and the mobility patterns observed indicate that the transport of LRD is determined almost exclusively by electrostatic interactions.

It is obvious from the BTCs obtained (Figure 3.21) that the value of C/C_0 decreases with the increase on electrolyte concentration. By adding a Gaussian (Figure 4.3) fit to the BTCs, it is possible to see that the curves are highly symmetric and with little tailing. This indicates that reversible colloid retention and release during the deposition process is small. Considering the small size of the colloidal pulse and that the columns were initially free of retained colloids, the influence of previously retained colloids is highly unlikely.

As said before, although the trend on particle deposition is consistent in both the sand columns and CLSM deposition methods there are obvious differences. In the case of BTCs obtained from the CLSM method, when electrolyte concentration is 10 mM, there

is still observable colloid elution (C/C_0 of around 0.2). This apparent discrepancy can be explained by the fact that the observation point used in the CLSM method is still inside the porous medium. As said before, the location had as advantage the simultaneous observation of both eluting colloids and colloid retention.

Even though the CLSM method provided valuable information on LRD deposition it is still considered a semi-quantitative method due to inherent limitations discussed before (See Section 4.3.1). Even if the penetration depth limitation is surpassed, an observation spot of roughly $500 \mu\text{m} \times 500 \mu\text{m}$ can only be representative in limited conditions. First of all, the porous medium should be homogeneous and without preferential paths and there should be clean bed conditions. These conditions were met in the experiments described in this study. We consider that at this stage of development, the CLSM method should be always complemented with methods that are more comprehensive and therefore representative such as sand columns. When used in the right conditions, the method, provides valuable direct information that is otherwise not evident. Furthermore, due to the reason that the CLSM is not an intrusive method, there can be multiple observation spots along the whole length of the porous bed. For highly detailed deposition experiments, non-intrusive deposition information all along the sand-packed microscopy flow cell could be valuable.

A complementary aspect of colloid transport in subsurface environments is the potential for remobilization. Remobilization can have as a consequence increments in the pore fluid concentration of substances (pollutants), which have been accumulated for certain periods of time. The LRD deposition experiments discussed above demonstrated that remobilization or reversible deposition did not occur in the time frame of the experiments. In order to clarify the role of electrolyte type and concentration on the remobilization of previously retained colloids, the experiments described in Section 3.3.1 were performed. As discussed in the introductory part, the chemistry of many natural subsurface environments is dominated by either monovalent or divalent cations. As said before Ca^{2+} and Na^+ were chosen because they dominate many subsurface and highly permeable environments.

It has been widely reported in the literature the drastic influence of Ca^{2+} and other divalent ions on the deposition of a wide variety of colloidal particles as compared to monovalent ions. It was important to know if that was the case for remobilization of previously retained colloidal particles. As it can be seen in Figure 3.26 the effect of divalent cations is drastic. No colloid remobilization can be observed for the columns initially saturated with Ca^{2+} ions. The colloid deposition behavior in the presence of calcium and other divalent cations compared with monovalent cations can be explained by classical DLVO theory of colloidal stability. The well known Schulze-Hardy rule states that diva-

lent counterions reduce colloidal stability in a much more efficient way as monovalent counterions do (for details see Verwey and Overbeek, 1948). Accordingly, agreements have been found on the more effective lowering of particle electrokinetic charge in divalent cation presence as compared with monovalent cations (Grolimund et al., 1998).

4.7 *P. aeruginosa* SG81 transport quantification

Even though in terms of size bacteria fall in the range of colloidal particles, one must take care when considering deposition and remobilization patterns in analogy with inorganic colloids. Bacteria are highly complex microorganisms which respond dynamically to environmental stimuli. Bacterial responses and their extremely active and complex metabolism can result in profound changes in the way these “biocolloids” are transported through porous media. In fact, the study of bacterial and other biological entities such as viruses is a well established research subject. Bacterial transport, including deposition and remobilization represents a fundamental condition for biofilm formation (being not less important as any of the steps presented in Section 1.6).

The quantification of bacterial transport parameters was performed using exactly the same experimental setting as used for LRD deposition experiments in order to make them comparable. Besides the quantification made in both sand columns and CLSM sand-packed microscopy flow cells, other complementary experiments were performed in the case of bacterial transport. Zeta potentials (Section 3.4.1) have been used as an indication of the likelihood of bacterial attachment in soil, or to surfaces such as silicon rubber and stainless steel. The zeta potential of a particle is the electrical potential present at its shear plane. This is at some distance from the surface. The zeta potential is therefore a function of the surface charge of the particle. The zeta potentials for *P. aeruginosa* SG81 plotted in Figure 3.27 were obtained at a wide range of pH values and at similar electrochemical conditions dominant during our deposition experiments. In Table 4.2 a compilation of zeta potentials from several strains at similar conditions than our study, is presented. As can be seen in this Table, a wide variety of bacterial strains remain negatively charged at physiological conditions.

Zeta potentials obtained show that bacterial surfaces remain negatively charged through a wide range of pH values. Considering that sand grains surfaces are also negatively charged, it was expected that at low electrolyte concentration, bacterial deposition would be equally low. Bacterial deposition quantification at low ionic strengths (see Figures 3.28, 3.29, and Table 3.4) showed low deposition at these conditions. Also from the deposition quantification experiments it is obvious that deposition increases with

Table 4.2: Zeta potentials for several bacterial strains

Strain	Electrolyte (M)	pH	Zeta potential (mV)	Reference
<i>P. aeruginosa</i>	0.15	7	-9	Bruinsma et al. (2001)
<i>Escherichia coli</i> JM109	0.1	7.3-7.5	-32	Baikun and Logan (2004)
<i>P. aeruginosa</i> PA01	0.1	7.3-7.5	-21	Baikun and Logan (2004)
<i>Bacillus subtilis</i>	0.1	7.3-7.5	-26	Baikun and Logan (2004)
<i>Enterobacter</i> strain IS2	<0.01	7	-24	Gannon et al. (1991)
<i>Pseudomonas</i> strain KL2	<0.01	7	-21	Gannon et al. (1991)
<i>Pseudomonas</i> strain DF2	<0.01	7	-19	Gannon et al. (1991)
<i>P. aeruginosa</i> AK1	<0.01	7	-19	Gannon et al. (1991)
<i>P. aeruginosa</i> AK1	PBS	7	-7	Gottenbos et al. (1999)
<i>Streptococcus sanguis</i> C7-2	0.06	7	-12.4	Weerkamp et al. (1988)
<i>S. mutans</i> C7-3	0.06	7	-7.1	Weerkamp et al. (1988)
<i>S. salivarius</i> B3-4	0.06	7	-4.8	Weerkamp et al. (1988)
<i>Streptococcus sanguis</i> C7-2	0.06	7	-12.4	Weerkamp et al. (1988)
<i>P. aeruginosa</i> SG81	0.14	6 to 8	-7 to -11	This study

increasing electrolyte concentration. From the point of view of the zeta potential measurements, this was as expected.

Considering the preparation for bacterial zeta potential measurements (see Section 2.3.1.3), a complete EPS separation from the cell surfaces was not achieved. Several studies have investigated the potential role of EPS on cell surface characteristics (including zeta potentials) and finally on cell adhesion to different surfaces. Tsuneda et al. (2003) made a study of correlation between EPS content and zeta potential in relation with bacterial adhesion. They found in carbohydrate dominated EPS, a weak correlation when EPS presence was low as compared to EPS-rich strains. They concluded that EPS decreased the electrostatic interaction (repulsion) between the cells and surfaces facilitating in this way, bacterial adhesion. In similar studies (Tsuneda et al., 2004) a good correlation between bacterial surface potential and cell adhesiveness was found. This suggest that the suppression of electro-repulsive forces promotes bacterial adhesion onto glass beads.

Bacterial deposition decreased with increasing salt concentrations. This indicates an important role of electrostatic interactions which therefore are on qualitative agreement with the general DLVO theory (Verwey and Overbeek, 1948). According to this theory, decreasing ionic strength results in the thickness of the electrical double layer around bacteria and sand grains also increasing. This increase in the thickness of the double layer increases the amount of energy needed for the bacteria to overcome a potential energy barrier and enter into the secondary minimum. For like-charged surfaces, attachment can occur in this secondary minimum. In fact, bacterial attachment at the secondary minimum has been found as an important attachment mechanism at relatively low ionic strength conditions (Redman et al., 2003). For lower ionic strengths,

BTCs were more or less smooth and presented little tailing which suggests lower detachment rates. In the case of higher ionic strengths, i.e., higher than 140 mM, BTCs showed many irregularities and prolonged tailing events. Besides of this behavior it is possible to see sudden peaks during the tailing process (see Figure 3.28) which suggest the importance of reversible attachment processes under these conditions (Strauss and Bolster, 2004).

Detachment of bacteria from our sand columns and sand-packed microscopy flow cells occurred by both sudden increments in the flow rate and decrements in ionic strength. Both effects are widely reported in the literature (Becker et al., 2004; Camesano and Logan, 1998; Jewett et al., 1999; Johnson et al., 1996; Li and Logan, 1999; Powelson and Mills, 2001; Tufenkji and Elimelech, 2004) and are indicative of the high relevance of electrostatic interactions for bacterial attachment. Although not included in our experiments, several researchers have inverted the electrical charge of the collectors (e.g., sand grains) by covering them with metal-oxyhydroxides (Bolster et al., 2001; Becker et al., 2004; Knapp, Herman, Hornberger, and Mills, Knapp et al.). The most commonly used has been Fe(III)-oxyhydroxide. In all cases there was a drastic increase on the amount of retained bacteria, regardless of the ionic strength used.

CFT (see Section 1.3.2) assumes colloid deposition rate coefficients as invariant with transport distance. This means that log linear decreases in mobile and retained colloid concentrations with increasing distance from the source should be observed. Several researchers have found discrepancies with this assumption (Camesano and Logan, 1998; Martin et al., 1996; Tong et al., 2005). In most cases decreasing bacterial deposition rate coefficients have been observed with distance from source (faster than predicted by log linear rate). In the present study, a systematic determination of bacterial or colloidal concentrations at increasing distances from the source of injected colloids was not performed. For most of the deposition experiments instead, the complete fraction of bacteria recovered in column effluents divided by the total injected bacteria was used to obtain deposition parameters. It is not possible, therefore, to determine if there are deviations from CFT at this stage.

The mentioned discrepancies were not measured directly. However, a set of experiments were performed which demonstrate the profound changes in transport patterns that can occur for the same bacterial strain. These quantified changes might have extreme importance in the field and in cases where transport is not appropriately described by CFT.

Most studies of bacterial transport use freshly prepared, cleaned bacterial cells that have been grown in exactly the same conditions, i.e., either in liquid culture or on solid agar. In this study, bacterial deposition experiments in which the same strain was used,

at equal concentrations and suspending solution but originating from distinct environments were performed. A great amount of published literature suggests that these two populations differ in their physiological conditions. It is widely known that physiological changes in bacteria influence the highly dynamic bacterial surfaces. It was hypothesized, that these physiological changes must have an impact on deposition too.

Biofilm forming microorganisms, including various pseudomonads, are known to undergo multiple phenotypical changes throughout the biofilm formation process (Sauer and Camper, 2001; Sauer et al., 2002). Flagella and type IV pilli are related to motility processes in pseudomonads such as swimming, swarming and twitching motility (O'Toole and Kolter, 1998).

A significant difference in collision efficiency (See Section 3.4.5.2) was found for bacteria grown in the absence of a surface i.e., planktonic and those previously attached to the porous medium. Collision efficiencies for recently detached biofilm cells was significantly higher as those from bacteria grown in absence of a surface. Recently detached bacteria had less motility or self propulsion as compared with the other subpopulation (direct microscopic observation). It is very likely that the change in deposition patterns is due to differences in the physiological state of the bacteria and in changes on motility patterns. These motility changes were determined in our experiments by means of agar motility tests (see Figure 3.44 and Table 3.5).

Differences in α values had been already reported for *Pseudomonas fluorescens* at two different physiological conditions (Smets et al., 1999). The fact that these changes were observed in populations with just different ages (stationary phase/decay phase), demonstrates that even slight differences among subpopulations of bacteria can have a pronounced effect on their deposition patterns. More specific bacterial adhesion experiments have demonstrated the influence of bacterial growth stage and the evolution of surface macromolecules. Walker et al. (2005) found for example that cells in stationary phase were more adhesive than those in mid-exponential phase. The phenomenon was attributed to macromolecule-induced bacterial surface charge heterogeneity which diminishes electrostatic repulsion between the cells and the collectors.

An important difference between the subpopulations used for the experiments shown in Section 3.4.5.2, was the strong motility present in the cells grown in planktonic conditions. Recently detached cells in contrast showed little or no motility at all (refer to the mentioned Section for links to video examples on this). In our experiments, low self-propulsion was related with high attachment rates. This is in contrast with other studies (O'Toole and Kolter, 1998) which suggest that motility is necessary for biofilm development in *P. aeruginosa* biofilms. In other experiments, however, motility deficient cells have been found to be highly adherent (Deziel et al., 2001). It is possible that this

is not a discrepancy at all, but just consequence of differences in physicochemical conditions. Camesano and Logan (1998) for example found that the fractional retention of motile cells (*P. aeruginosa* P17) decreased by 65 % and the collision efficiency decreased from 0.37 to 0.003 when the fluid velocity was decreased from 120 to 0.56 m day⁻¹. They did not observed substantial changes for non-motile counterparts for similar flow velocity changes. Although our pore velocities were high enough for advection to be dominant (see Table 3.1), they were relatively low in order to reproduce velocities encountered in natural subsurface environments. These pore velocities were, however, not low enough for self propulsion state to influence cell retention in our sand columns. It is more likely that changes in the chemical make up of the cell surfaces had a higher influence on deposition in this case.

4.8 Laponite RD and bacterial transport

It is evident from the introductory part, that LRD particles and bacterial cells are significantly different. The most obvious differences are size, aggregation properties and surface composition and complexity. An important section of the work was therefore dedicated to the basic characterization of both bacteria and inorganic colloid transport properties in isolation, i.e., in the absence of microbial biofilms. In terms of bacteria, it is important to understand that biofilm formation is part of an overall transport process. Biofilm formation or accumulation in the subsurface therefore cannot be regarded without taking into account the transport and initial retention of bacteria (Costerton et al., 1978).

At very low ionic strengths, i.e., deionized water, collision efficiencies for bacteria were higher than those for the inorganic clay. As the salt concentration increases, however, cells of the mucoid strain showed lower collision efficiencies as compared to LRD. In other words, *P. aeruginosa* SG81 displayed transport over a wider range of ionic strengths as compared to LRD. Even at a salt concentration of 1 M NaCl bacterial retention inside the porous medium was not complete. In flow cells although the trend was similar (Figure 3.36) bacteria were less mobile. As discussed previously (Section 4.6), this apparent discrepancy can be explained by the fact that the observation point in the CLSM method is still inside the porous medium. Most of the retained bacteria could be found in the portion of the sand-packed microscopy flow cell closest to the inlet for all three ionic strengths tested. Similarly, in the case of *P. aeruginosa* SG81R1, higher retention (higher collision efficiencies, α) was significant in intermediate salt concentrations (10 and 140 mM). This was not the case, however, at lower ionic strengths, e.g., 1 mM or higher, e.g., 1 M.

The differences on bacterial deposition for cells grown in the presence or absence of a surface confirms a phenotypical adaptation to the sessile mode of growth. This is true when fluid velocity, ionic strength, valence of dissolved ions and other external parameters remain constant or change slowly. In the case of drastic changes both in the hydrodynamic conditions of the porous medium or on the fluid chemical composition and concentration, the situation changes considerably. Figure 3.45 is a typical example where drastic changes on ionic concentration and type results in consistent remobilization patterns for a wide variety of particles including several types of microorganisms (Figure 3.46). It is evident then that drastic events might override the deposition effect of physiologically-induced cell surface heterogeneities.

The introduction of LRD at an ionic strength and concentration which would stimulate its aggregation and retention in sand columns (Figures 3.13 and 3.14) was able to stimulate remobilization of *P. aeruginosa* SG81 under conditions in which retention would generally be favorable. The influence of LRD on cellular detachment could be due to indirect interactions caused by changes of the hydrodynamic conditions inside the porous medium, leading to increased shear forces and therefore to cell detachment. Even though pH variations were apparent as the LRD was being eluted, it is very unlikely that changes of this magnitude (less than 2 pH units) could have influenced the detachment of cells (Jewett et al., 1995). Due to the reason that under lowering salt concentrations bacterial detachment was constantly decreasing (See Figures 3.17 and 3.18), it is likely that hydrodynamic alterations may play a significant role on the observed detachment. This assumption, however, was not verified quantitatively.

In biofilm literature (Stoodley et al., 1999) bacterial deposition is considered the first step on the formation of biofilms. In porous media this is also true. In this stage of development, biofilms (microbes) respond similarly as abiotic colloids do to changes in pore fluid velocity, ionic strength, pH and other physicochemical parameters. It is therefore expected that for the first stages of biofilm formation the conditions should be those that generally favor colloidal deposition. For our experiments, this was constant, low pore fluid flow and relatively high ionic strength.

The increased production of EPS which follows the initial bacterial deposition is greatly responsible for further colonization and biofilm growth. In many circumstances (e.g., contaminated environments) this can be a macroscopic event which undoubtedly will have profound effects on the deposition of many other colloids including bacteria. The present work concentrates on LRD, an inorganic clay and the influence exerted by *P. aeruginosa* SG81 biofilms. The next section deals with this main question.

4.9 Biofilm formation and colloid transport

The characterization of colloid and bacterial transport in absence of biofilms (Sections 3.3 and 3.4), was fundamental for the experiments described in this Section. First of all, it became clear that the conditions which stimulate advective movement of clay-like colloidal particles, i.e., low ionic strength conditions (less than around 5 mM) were not compatible with biofilm formation and stability in our sand columns. Biofilm growth inside the sand columns was promoted at relatively high ionic strength conditions and under an environment rich in nutrients (see Section 2.5.4) for one, two or three weeks under a constant influent. Column treatment after the biofilm growth period should minimize biofilm loss due to hydrodynamic or physicochemical effects. Drastic changes were avoided at all times. If relatively high ionic strength conditions would have been maintained during LRD colloid injection then: (i) aggregation and retention of LRD particles would have occurred both in sterile and non-sterile (biofilm forming) columns, (ii) the detection of LRD (even tagged with the fluorochrome R6G) would have been problematic in presence of numerous growth medium nutrients; (iii) Reliable discrimination between biofilm attached LRD and sand attached or suspended LRD would have been difficult. These and other consequences would have rendered LRD quantification impossible with the available equipment.

From these previous experiments it was evident that the conditions necessary for the mobility and reliable detection of our model inorganic colloid through porous media were those of very low ionic strength. In order to minimize as much as possible the effect of ionic strength decrements on biofilm stability, the strategy followed was to: (i) gradually decrease ionic strength, (ii) make the colloid transport experiments in the shortest time frame possible and (iii) keep all other parameters constant. The second point was accomplished by using shorter columns and using the short pulse breakthrough method (many BTCs took just around 20 min to complete).

The stability of biofilms grown within a sand matrix was found to be related to the type of cation dominating the influent background solution at decreasing ionic strength conditions. It was found that, as observed for colloids, the remobilization of biofilm components was drastically diminished when pore fluid was dominated by divalent cations. Preliminary experiments with LRD and biofilms in a monovalent or divalent dominated environment provided the first insights on the conceptual model shown in Figure 4.4. In the first scenario (constantly high ionic strength), colloid movement is highly dependent on “fast” deposition kinetics and colloids would be quickly filtered out both by interception or straining mechanisms. However, if colloids are infiltrated into the subsurface under these conditions, they will tend to aggregate and thus can cause clogging of pore

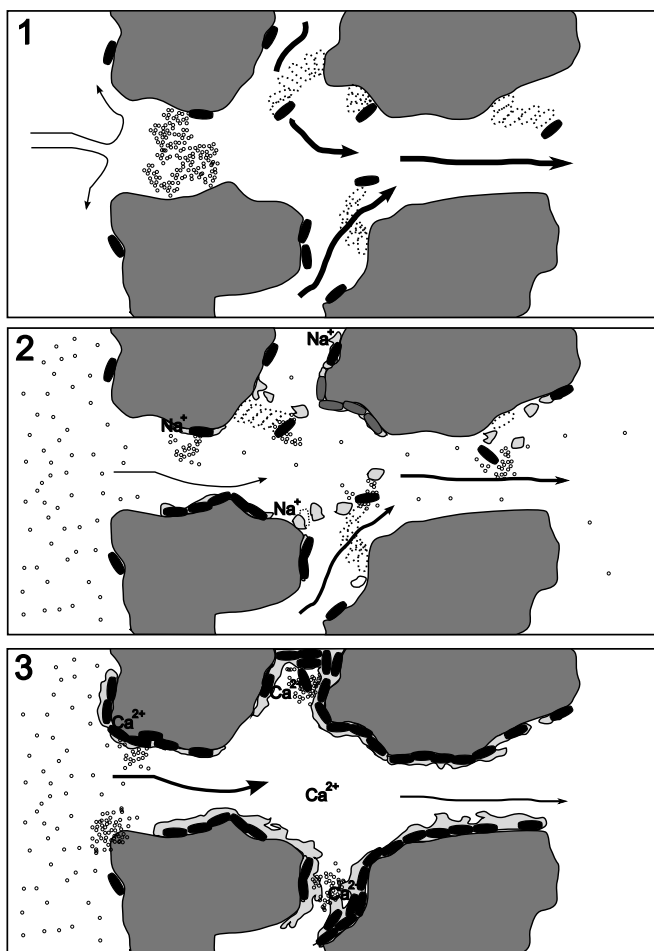


Figure 4.4: Interactions between Laponite RD and bacterial transport. First conceptual model including, 1: high ionic strength scenario in which Laponite RD aggregation promotes bacterial detachment. 2: sudden change to low ionic strength after monovalent cation dominance. 3: sudden change to low ionic strength after divalent cation dominance.

spaces (by massive straining). This will increase the flow velocity in the remaining pores which can cause detachment of adherent cells or previously adsorbed contaminants and/or colloids. The second and third scenarios, namely, at low ionic strength but after mono or divalent cation dominance are discussed later.

4.9.1 Distinguishing characteristics of sand-grown biofilms

The results (see Section 3.6.1) showed that biofilms did not grow as confluent and slimy as they normally do on the surfaces of Petri dishes. In fact, Figure 3.49 show non continuous discrete colonies which accumulate exclusively in pore throats or in regions not easily reached by the main flow vectors. Although it is arguable that most of the tridimensional EPS structure collapses during SEM sample preparation, this does not explain similar observations made with the CLSM method (Figure 3.48).

An important factor determining different biofilm architectures is the production and accumulation of EPS (Flemming and Wingender, 2001c; Kuehn et al., 2001). Extracellular polysaccharides, for example, due to their structural characteristics and production rates on many biofilms have been considered important on this respect (Sutherland, 2001).

The development and architecture of *P. aeruginosa* SG81 sand-grown biofilms are very different when compared to agar-grown biofilms or biofilms grown on other flat surfaces. When grown on agar plates, this organism formed highly mucoid microbial colonies, which developed into confluent biofilms several millimeters thick. This phenotype was not observed in fully packed sand-grown biofilms, the type used in this study. However, in separate experiments, when the biofilms were grown in columns simulating a river sediment bed, i.e., horizontally placed, half filled with sediment and with liquid flowing on top, these developed a highly mucoid state at the water body-sand interface.

The relative low amount of polysaccharides produced and the high ratio cells/EPS as found in our sand columns (Figure 3.51) may be related to the influence of the porous environment on biofilm development and architecture. It was clear from Figure 3.51 that the cells/EPS ratio increased with time of biofilm growth. This suggests a phenotypical adaptation to the physical conditions in this environment. Even in the case of low organic carbon presence, thick confluent biofilms would not be a great advantage due to the high probability of nutrient entrapment or collision inside a porous medium. Considering the fact that nutrient load was high at all times during biofilm development (see Section 2.5.4), this increasing cells/EPS ratio can instead be attributed to oxygen limitation. One should remember that oxygen quickly becomes a limiting nutrient with

column depth (distance from nutrient source). This is particularly important in the case of a highly aerobic microorganism such as *P. aeruginosa* SG81.

In contrast, it was found that despite a relatively low EPS production, biofilm development decreased the hydraulic conductivity of the sand columns up to 83 % as compared with non-inoculated columns (Figure 3.50). Even though this decrease was almost linear during the first 7-10 days of biofilm growth, a plateau was reached in which K remained stable during the rest of the observation period. In the case of the strain used for these experiments, biofilm accumulation might have been limited by nutrient availability, especially oxygen. This plateau can also be interpreted as a possible mechanism of bacterial growth control for the maintenance of nutrient transport within the system. *P. aeruginosa* SG81 is not a native organism from these types of environments so it is unlikely for it to have these growth control mechanisms already in place. It is very likely instead that with plenty of available oxygen, this organism would have clogged the system with time. In separate preliminary experiments (data not shown) constantly pumping sterile air through similar sand column systems caused massive biofilm growth and clogging. It is therefore plausible to assume oxygen limitation as responsible for the observed plateau.

The influence of biofilm architecture on how substances and particles are retained and transformed has been reported in the literature (Okabe et al., 1998; Stoodley et al., 1999; Battin et al., 2003). It has been shown that the presence of convective flow paths is important on the transport of fluorescent latex microbeads into biofilms (Okabe et al., 1998). These observations explained rapid particle transfer rates from the bulk fluid into the biofilm which were not explained in previous diffusion-only biofilm models (Characklis and Marshall, 1990).

As the results indicate, copious amounts of EPS components are not related to the influence of biofilms on the movement of colloids and colloid-bound contaminants. The results also show that an increment on EPS protein content with biofilm age coincided with colloid retention. Normally, retention processes are attributed almost exclusively to polysaccharides (Sutherland, 2001). Conditions of low EPS production with relative high extracellular protein contents are likely to be encountered in many natural and engineered subsurface environments (Flemming and Wingender, 2003).

4.9.2 LRD transport and the interaction between ionic composition and biofilm presence

For the characterization of biofilm influence on LRD transport, *P. aeruginosa* SG81 biofilms were grown in sand columns before injecting a LRD colloidal pulse. For these

experiments, biofilm age, EPS components remaining in the columns before and after the colloid transport studies, as well as, the type of cation (monovalent or divalent) dominating the influent solution were all taken into account. The use of fluorescence detection of LRD-R6G complexes allowed a more accurate determination of colloid transport patterns in the presence of biofilms. These improvements not only in the detection system but also on biofilm quantification, provided a clearer view of the interplay between biofilm formation and ionic type and strength and their influence on colloid transport in porous media.

The main technique for LRD quantification before entirely using fluorescence spectrophotometry was UV-VIS spectrophotometry. LRD detection with this setting was problematic especially when conditions were of stimulated mobility (e.g. low ionic strength). Under these conditions one expects that all eluting species such as detaching bacteria and EPS, would contribute to the absorption measurements. However, as observed in Figure 3.52 and as evidenced in other experiments (data not shown) bacterial absorbance at 535 nm would be negligible until their concentration reaches more than 1.5×10^8 cells mL^{-1} . As conditions changed, i.e., LRD pulse and reduction in subsequent influent ionic strength, bacteria were remobilized mainly after the elution of LRD (Figure 3.52A, 3.52B) was complete. The first front of bacterial detachment in this case was not sufficient to produce a measurable alteration in absorbance at 535 nm. In fact, the spectrometric monitoring of bacteria is usually done at 240 - 280 nm. Apparent from Figure 3.52B there is an alteration of LRD elution profile (early breakthrough and tailing) due probably to a reduction in the porous medium permeability (increased particle velocity), bacterial co-elution and NaCl hydrodynamic dispersion. LRD/bacteria co-elution could be the result of direct interactions between LRD and cells or cellular products such as polysaccharides. Clays are known to interact strongly with polysaccharides as reviewed by Chenu and Stotzky (2002), and polysaccharides are important components of the extracellular biofilm matrix.

Until this stage, however, accurate and clean LRD BTCs in the presence of biofilms was not possible with the UV-VIS method. The UV-VIS detection signal provided unresolved LRD BTCs due to the amount of interfering co-eluting material at Na^+ dominant conditions. It was possible to separate eluting cells by means of cell counts but LRD specific transport parameters such as collision efficiencies could not be yet quantified.

By using fluorescence spectrophotometry for LRD detection, LRD quantification became more reliable. By measuring fluorescence exclusively at the maximum emission of R6G-stained LRD, it was possible to resolve LRD regardless of any co-eluting material. This made possible the quantification of LRD transport parameters even in biofilm presence. In biofilm containing columns, the exposure to Ca^{2+} or Na^+ ions prior to decreasing

ionic strength to very low levels had a distinct impact on colloid transport as compared with sterile columns.

In sterile columns (biofilm absence experiments), it was observed that a two pore volume deionized water influent resulted in considerable transport of LRD through both Ca^{2+} and Na^+ -exposed columns. However, an increase on collision efficiency was observed in the Ca^{2+} columns (Table 3.6) as compared with the Na^+ columns when calculated from the obtained BTCs. In none of the cases there was complete colloid retention in sterile columns. This probably means that in both cases, the concentration of cations inside the sand column was not high enough to cause colloid destabilization and retention.

The influence of the ionic composition on the transport of both natural and artificial colloids has been investigated earlier (Grolimund et al., 1998; Davis et al., 2001). It has been observed that Ca^{2+} ions, in agreement with the DLVO theory, decrease the stability of colloids much more effectively than Na^+ ions (Derjaguin and Landau, 1941). This has been demonstrated for instance by comparing the electrophoretic mobility of colloids as a function of Na^+ and Ca^{2+} concentrations. Ca^{2+} counterions result much more effective in lowering particle electrokinetic charge than Na^+ counterions. In terms of retention in porous media, this can be observed for example when comparing colloid deposition rates in experiments with either type of cation (Grolimund et al., 1998). In those experiments, substantial particle deposition occurs at a much lower concentration of Ca^{2+} than for Na^+ . Remobilization patterns observed in this study confirm also this sodium-calcium effect. This was observed not only in artificial model colloids such as LRD (Section 3.3.1) but also in natural colloids (Section 3.5) such as the ones remobilized from a SFM-packed column. Considering the heterogeneity of these natural colloids it is evident that this type of ionic influence is not restricted to certain specific colloids.

In contrast, colloid retention was found to be proportional to biofilm presence and age when columns were subjected to Ca^{2+} exposure. Ca^{2+} is known to directly influence the mechanic and viscoelastic properties of biofilms (Körstgens et al., 2001). Ca^{2+} is important for the stability of the biofilm matrix acting as a bridging and stabilization factor for the EPS matrix components (Flemming et al., 2000). A decrease in biofilm detachment is therefore expected when lowering of ionic strength occurs in the presence of Ca^{2+} ions. This was the case for older than one week biofilms (Figure 3.57) and SFM (Lower images in Figure 3.45 and Figure 3.58). Biofilm stability in this case is due to the accumulation of Ca^{2+} ions and slower ion exchange processes, resulting in colloid sorption and retention. On the contrary, Na^+ ions with a less important structural role (Mayer et al., 1999) did not influence biofilm detachment processes. This resulted in the observed alteration of colloid breakthrough patterns (see Figure 3.54). Alteration of LRD breakthrough patterns after the presence of Na^+ and at low ionic strength can be observed in Figure 3.52.

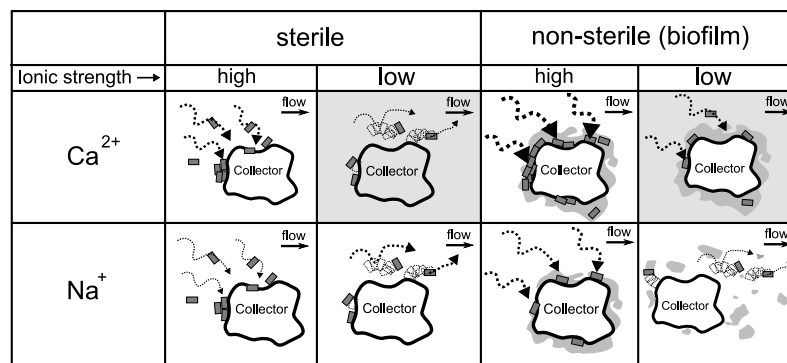


Figure 4.5: Representation of the combined effect between the presence of monovalent, divalent cations and biofilms on the transport of colloidal particles. The term collector refers to the solid phase, e.g., sand grains, to which colloids can be deposited.

The increased cell concentrations in column effluents during colloid elution as observed in this Figure, suggest a co-elution effect between the colloid and biofilm cells.

A schematic representation of the influence of ionic composition in the presence of biofilms as suggested from the findings of this study is presented in Figure 4.5. The thickness of the dotted arrows represents the intensity of particle mobilization. The combined calcium-biofilm influence on colloid transport is notorious (shaded square in non-sterile - biofilm presence section) at electrochemical conditions in which injected colloids normally would be mobile (shaded square in sterile - biofilm absence section).

4.10 Ecological perspective and concluding remarks

From these scenarios it could be concluded that under high ionic strength conditions retention of colloids within the subsurface is generally favored. Here, biofilms act as sorption site and sink for colloids and colloid-bound pollutants. However, if a decrease in ionic strength under predominance of monovalent cations or an exchange of divalent cations to monovalent cations occurs, a remobilization of colloids can be observed. In this case biofilms represent a source for colloidal or colloid-bound contaminants. Thus, environmental events which led to significant changes in ionic strength and/or ionic composition within the subsurface will drastically change the mobility of colloids and thus potentially also of contaminants. For example, this will be the case during heavy rainfalls, stormwaters, seawater infiltration, tidal processes at estuaries and infiltration of thawing salts from street run-off. The infiltration of thawing salt will change the natural ionic composition in the subsurface to a sodium-dominated system. After the thawing period the ionic strength will decrease and thus will cause a remobilization of previously retained colloids and colloid-bound pollutants from street run-off, e.g., heavy

metals and aromatic hydrocarbons.

In natural environments, the transport of colloids rarely occurs in isolated conditions. Variations in ionic strength caused by for instance sea water infiltration, torrential rain or de-icing would cause the mobility or retention of a great variety of colloidal particles. Clean bed transport studies are useful for determining fundamental transport parameters in controlled laboratory conditions. They fail, however to fully describe transport in more complex environments. As observed, bacteria have the ability to attach to surfaces, stimulated by physicochemical factors which will also stimulate the attachment of other colloidal particles including inorganic colloids. They also are remobilized by similar physicochemical factors causing detachment or release of other colloids. As consequence bacterial biofilms growing in porous materials are extremely dynamic. Their influence on colloid and therefore contaminant transport is expected to be composed of several additive effects including changes in porous medium hydrodynamics, sorption to biofilm components and co-elution with remobilized biofilm elements.

Sea water infiltration, de-icing events and contamination, e.g., caused by hydrocarbon spilling accidents or collapsing of liners in landfills can result in drastic changes on the ionic composition of ground waters. A migrating plume of organic contaminants without a constant source, i.e., in a spilling accident, will stimulate confluent biofilm development in the places through which it is moving. Biofilm presence therefore can result in considerable longer times for Ca^{2+} and other divalent cations retention and exchange. This has obvious implications on the prediction of colloid and colloid-bound contaminant transport and on the stability and detachment rates of subsurface biofilms. EPS determinations (Figures 3.56 and 3.59) and preliminary LRD transport experiments in columns packed with SFM (Figures 3.55 and 3.58) are consistent with findings in model quartz sand systems. It is hypothesized, that the effect of Ca^{2+} on the remobilization patterns of natural colloids might be importantly influenced by the presence of biofilms both in oligotrophic and contaminated environments.

Microbes are known to interact strongly with heavy metals (Brierley, 1990). In terms of colloidal metal mobility, however, the redox conditions and pH have a definitive influence. The chemical structure and evolution of subsurface environments is strongly influenced by the resident microbial community. Additionally, the expected biofilm influence on how the different electron accepting processes are distributed and delimited through the subsurface constitutes an important factor of colloidal transport in real-life situations (see Figure 4.6).

Recapitulating on the goals defined in Section 1.8, it can be said that the study of colloid transport in absence and in presence of biofilms and at changing ionic conditions, showed a clear influence of biofilms on the overall transport of environmentally relevant

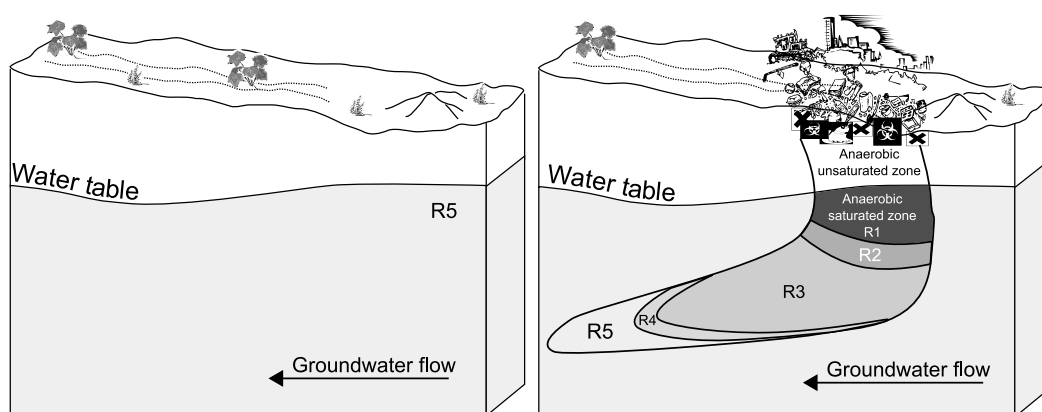


Figure 4.6: Two extreme scenarios which can lead to the presence of patchy biofilms (left) or confluent continuous films (right). Oligotrophic conditions and O_2 as main electron acceptor on the left contrasted with high organic content and several electron accepting processes on the right caused by contamination. R1: methanogenic zone, R2: Sulphate-reducing zone, R3: Iron-reducing zone, R4: Nitrate and Manganese reducing zone, R5: aerobic zone.

colloids. The significance for natural environments has been highlighted and the results from experiments with slow sand filter material showed that biofilm influence must be important, especially in contaminated environments. However, the extreme complexity of subsurface environments suggests that this influence will not be the same in every situation and in every subsurface region. In some cases biofilm influence might be of extreme importance while in others it might even be irrelevant. In contaminated environments and in some pristine environments, microbially driven redox processes are determinant on the movement of colloids and colloid-bound contaminants. In the case of heavy metal ions for example, different redox conditions will change their oxidation state which is determinant in terms of their mobility through subsurface environments. In this respect, the limitations of the study are made obvious. The migration to experimental systems in which microbially driven redox processes are better represented, including the use of other bacterial strains, is necessary for a better understanding of colloid transport processes in natural subsurface environments.

4.11 Conclusions

- Confocal microscopy was shown to be suitable for online monitoring of fluorescently-labeled microorganisms and inorganic colloidal particles in a sand-packed microscopy flow cell. This allowed the determination of deposition and transport characteristics of *P. aeruginosa* SG81 and Laponite RD as a function of ionic strength and the qualitative determination of colloidal retention inside the porous medium in a non-destructive manner.

- In clean bed columns, the mobility of Laponite RD was strongly influenced by ionic strength. Mobility was inversely correlated to NaCl concentration; NaCl concentrations of 1×10^{-2} M resulted in almost complete laponite retention within the sand columns.
- Mobility of *P. aeruginosa* SG81 was reduced predictably by NaCl concentrations up to 1 M. This effect was not as pronounced as for laponite, and some bacteria were still transported under these conditions.
- At high relative ionic strength conditions (7×10^{-2} M), introduction of laponite to a sand column containing a primary biofilm of *P. aeruginosa* SG81 resulted in remobilization of a portion of the attached cells, as indicated by effluent cell numbers. Low ionic strength (6.2×10^{-4} M NaCl) caused detachment of biofilm cells, but also an altered laponite elution profile due to co-elution or hydrodynamic effects.
- Environmental events leading to significant changes in ionic strength of the subsurface matrix will cause significant changes to the mobility of microorganisms, inorganic colloids, and colloid-borne contaminants. These events include rainfall, melting snow or ice containing dispersing salt, seawater infiltration, and tidal processes at estuaries.

Sterile/non-sterile colloid transport experiments through sand columns demonstrate that:

- Biofilm formation increased the retention of colloids after the ionic strength is decreased in Ca^{2+} presence. This also results in:
 - increased stability of biofilms in the sand matrix.
 - delayed colloid remobilization compared to sterile systems.
- Decreasing ionic strength in the presence of Na^+ resulted in:
 - decreased stability of biofilms,
 - alteration of colloid transport patterns rather than retention processes.
- Even at low EPS concentrations biofilms alter not only the hydraulic conditions but also the transport of colloidal particles in subsurface environments.
- EPS analyzes showed that the production of extracellular proteins coincided with increased colloid retention in biofilm columns.

- The role of biofilms in the subsurface has to be taken into account in the predictions of colloid transport.

4.12 Outlook

This investigation has shown that colloid transport in the presence of biofilms is a complex process dependent on many factors which are strongly interrelated. Biofilms were shown to directly influence colloid transport in conditions where colloids would be normally mobile if biofilms were absent. The specific mechanisms in terms of direct interactions between the biofilm and the migrating colloids remain, however, largely unexplored and an interesting aspect which should be taken into account in the future.

Some open questions remaining after this work and that are recommended to be tackled in future experiments include:

- What would happen if other types of organisms are used including organisms more adapted to conditions in the subsurface, e.g., facultative aerobic or anaerobic microorganisms?
- Would any other type of EPS producing organisms affect the hydraulic conductivity of subsurface environments in a different way? How?
- Which would be the consequence of taking into account the metabolic activities of microorganisms living in subsurface environments. For example, plutonium mobilization in contaminated soil has been shown to be enhanced due to fermentative microbial activity which causes dissolution of iron phases and consequent stabilization of Plutonium in colloidal form.
- Which is the real role of oxygen? Would oxygen have an impact on how and where colloidal particles are retained? How can this be related to harsh environments such as those found in contaminated sites or extreme environments?
- Which is the specific contribution of biofilms to the widely reported discrepancies in CFT? Where exactly are colloidal particles being preferentially retained? How does this change with different redox conditions?

Finally, it is clear that for the assessment of biofilm influence on colloidal transport in natural environments, a deeper understanding of the biogeochemistry involved is necessary (Figure 4.7). This knowledge must be translated into appropriate parameters to be included in models that have been developed over the years for the prediction of

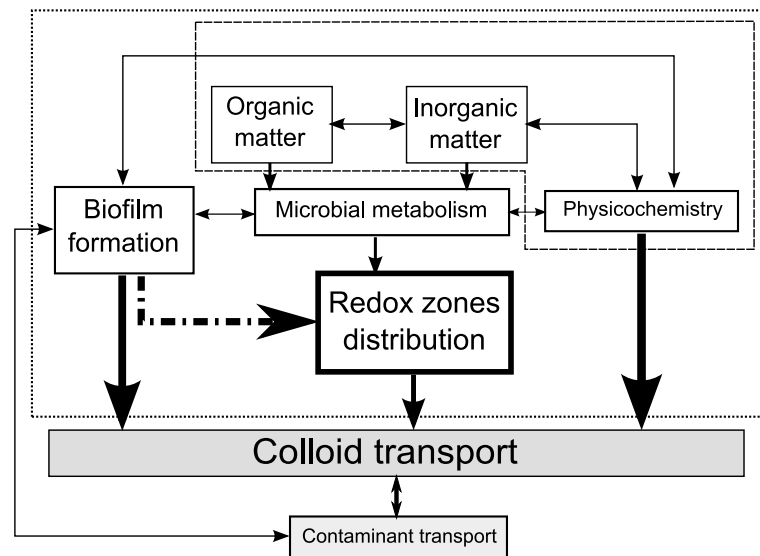


Figure 4.7: Complete overview of biogeochemical factors to be taken into account when making predictions on colloid transport in natural subsurface environments. Smaller delineated area: Factors covered by conventional studies.

colloidal transport in the subsurface. The approach should be on an environment-to-environment basis and not a generalized one. This requires perhaps laboratory simulations of different types of biofilms (aerobic, sulphate-reducing, methanogenic, etc.) and their corresponding influence on the movement of colloids. Porous medium “heterogeneities” such as biofilm formation might explain deviations from CFT which can cause some of the inconsistencies observed when predicting colloidal transport.

Literature

- Abramoff, M. D., P. J. Magelhaes, and S. J. Ram (2004). Image processing with ImageJ. *Biophotonics International* 11(7), 36–42.
- Allen, D. M. and G. P. Matsuo (2002). Results of the groundwater geochemistry study on hornby island, british columbia. Report prepared for the Islands Trust, Victoria, B.C., 119 pp.
- Allen, D. M. and M. Suchy (2001). Results of the groundwater geochemistry study on saturna island, british columbia. Report submitted to the Islands Trust, Victoria, B.C., 127 pp.
- Allison, D. (2003). The biofilm matrix. *Biofouling* 19(2), 139–150.
- Allison, L. E. (1947). Effect of microorganisms on permeability of soil under prolonged submergence. *Soil Sci.* 63, 439–450.
- Anderson, R. and D. Lovley (1997). Ecology and biogeochemistry of in situ groundwater bioremediation. *Adv. Microb. Ecol.* 15, 289–333.
- Baikun, L. and B. E. Logan (2004). Bacterial adhesion to glass and metal-oxide surfaces. *Colloids and Surfaces B: Biointerfaces* 36, 81–90.
- Balkwill, D. L., E. Murphy, D. Fair, D. Ringelberg, and D. White (1997). Microbial communities in high and low recharge environments: Implications for microbial transport in the vadose zone. *Microb. Ecol.* 35, 156–171.
- Battin, T. J., L. A. Kaplan, D. J. Newbold, and C. M. E. Hansen (2003). Contributions of microbial biofilms to ecosystem processes in stream mesocosms. *Nature* 426, 439–441.
- Bear, J. (1972). *Dynamics of fluids in porous media*. New York: American Elsevier Publishing Company.
- Becker, M., S. Collins, D. Metge, R. Harvey, and A. Shapiro (2004). Effect of cell physico-chemical characteristics and motility on bacterial transport in groundwater. *J. Contam. Hydrol.* 69, 195–213.

- Beveridge, T. J. (1989). Role of cellular design in bacterial metal accumulation and mineralization. *Annu. Rev. Microbiol.* 43, 147-171.
- Beveridge, T. J. (1999). Structures of gram-negative cell walls and their derived membrane vesicles. *J. Bacteriol.* 181(16), 4725-4733.
- Beveridge, T. J., S. A. Makin, J. L. Kadurugamuwa, and Z. S. Li (1997). Interactions between biofilms and the environment. *FEMS Microbiol. Rev.* 20(3-4), 291-303.
- Bhattacharjee, S., J. Ryan, and M. Elimelech (2002). Virus transport in physically and geochemically heterogeneous subsurface porous media. *J. Contam. Hydrol.* 57, 161-187.
- Bolster, C., A. Mills, G. Hornberger, and J. Herman (2001). Effect of surface coatings, grain size, and ionic strength on the maximum attainable coverage of bacteria on sand surfaces. *J. Contam. Hydrol.* 50, 287-305.
- Bondoc, L. L. and S. Fitzpatrick (1998). Size distribution analysis of recombinant adenovirus using disc centrifugation. *Journal of Industrial Microbiology and Biotechnology* 20, 317-322.
- Bos, R., H. C. van der Mei, and H. J. Busscher (1996). Co adhesion of oral microbial pairs under flow in the presence of saliva and lactose. *Journal of Dental Research* 75(2), 809-815.
- Bouwer, E., H. Rijnaarts, A. Cunningham, and R. Gerlach (2000). Biofilms in porous media. In J. D. Bryers (Ed.), *Biofilms II: Process analysis and applications*, pp. 123-158. Wiley-Liss.
- Brierley, C. L. (1990). Metal immobilization using bacteria. In H. L. Ehrlich and C. L. Brierley (Eds.), *Microbial mineral recovery.*, pp. 303-323. McGraw-Hill.
- Bruinsma, G. M., M. Rustema-Abbing, H. C. van der Mei, and H. J. Busscher (2001). Effects of cell surface damage on surface properties and adhesion of *Pseudomonas aeruginosa*. *Journal of Microbiological Methods* 45, 95-101.
- Bunn, R., R. Magelky, J. Ryan, and M. Elimelech (2002). Mobilization of natural colloids from an iron oxide coated sand aquifer: effect of pH and ionic strength. *Environ. Sci. Technol.* 36, 314-322.
- Busscher, H. J., G. I. Geertsema-Doornbusch, and H. C. van der Mei (1997). Adhesion to silicone rubber of yeasts and bacteria isolated from voice prostheses: Influence of salivary conditioning films. *Journal of Biomedical Materials Research* 34(2), 201-209.

- Camesano, T. A. and B. Logan (1998). Influence of fluid velocity and cell concentration on the transport of motile and nonmotile bacteria in porous media. *Environmental science and technology* 32, 1699-1708.
- Camesano, T. A., K. Unice, and B. Logan (1999). Blocking and ripening of colloids in porous media and their implications for bacterial transport. *Colloids Surf., A* 160, 291-308.
- Chapelle, F. H. (2003). Geochemistry of groundwater. *Treatise on Geochemistry* 5, 425-449.
- Characklis, W. G. and K. C. Marshall (Eds.) (1990). *Biofilms. Wiley Series in ecological and applied microbiology*. John Wiley Sons, Inc.
- Chen, B. M. and H. Kojouharov (1998). Accurate numerical simulation of biobarrier formation in porous media. In *Conference on hazardous waste research*, Snowbird, Utah, USA.
- Chen, J., C. Ko, S. Bhattacharjee, and M. Elimelech (2001). Role of spatial distribution of porous medium surface charge heterogeneity in colloid transport. *Colloids Surf., A* 191, 3-15.
- Chen-Charpentier, B. and H. Kojouharov (2001). Modeling of subsurface biobarrier formation. *J. Haz. Subs. Research* 3(1).
- Chenu, C. and G. Stotzky (2002). Interactions between microorganisms and soil particles: an overview. In P. Huang, J. Bollag, and N. Senesi (Eds.), *Interactions between soil particles and microorganisms*, pp. 3-40. John Wiley sons, Ltd.
- Cherrey, K., M. Flury, and J. Harsh (2003). Nitrate and colloid transport through coarse hanford sediments under steady state, variably saturated flow. *Water Resour. Res.* 39(6), 1-10.
- Cione, A. P. P., M. G. Neumann, and F. Gessner (1998). Time-dependent spectrophotometric study of the interaction of basic dyes with clays iii. mixed dye aggregates on swy-1 and laponite. *J. Colloid Interface Sci.* 198(1), 106-112.
- Clapp, A. R., A. G. Ruta, and R. B. Dickinson (1999). Three-dimensional optical trapping and evanescent wave light scattering for direct measurement of long range forces between a colloidal particle and a surface. *Rev Sci Instrum* 70, 2627-2636.
- Corapcioglu, M. Y., S. Jiang, and S.-H. Kim (1999). Comparison of kinetic and hybrid-equilibrium models simulating colloid-facilitated contaminant transport in porous media. *Transp. porous media* 36, 373-390.

- Costerton, J. W., G. Geesey, and G. K. Cheng (1978). How bacteria stick. *Sci. Am.* 238, 86-95.
- Cunningham, A. B., W. Characklis, F. Abedeen, and D. Crawford (1991). Influence of biofilm accumulation on porous media hydrodynamics. *Environ. Sci. Technol.* 25, 1305-1311.
- Cunningham, A. B., R. Sharp, R. Hiebert, and G. James (2003). Subsurface biofilm barriers for the containment and remediation of contaminated groundwater. *Biorem. J.* 7(3-4), 151-164.
- Davis, C., E. Eschenazi, and K. Papadopoulos (2001). Combined effects of Ca^{2+} and humic acid on colloid transport through porous media. *Colloid Polym. Sci.* 280(1), 52-58.
- Derjaguin, B. V. and L. Landau (1941). Theory of stability of strongly charged lyophobic solutions and of the adhesion of strongly charged particles in solutions of electrolytes. *Acta Physicochimica USSR* 14, 346-354.
- Deshpande, P. A. and D. R. Shonnard (1999). Modeling the effects of systematic variation in ionic strength on the attachment kinetics of *Pseudomonas fluorescens*. *Water Resources Research* 35(5), 1619-1627.
- Deziel, E., Y. Comeau, and R. Villemur (2001). Initiation of biofilm formation by *Pseudomonas aeruginosa* 57RP correlates with emergence of hyperpiliated and highly adherent phenotypic variants deficient in swimming, swarming, and twitching motilities. *J. Bacteriol.* 183(4), 1195-1204.
- Dignac, M.-F., V. Urbain, D. Rybacki, A. Bruchet, D. Snidaro, and P. Scribe (1998). Chemical description of extracellular polymers: implication on activated sludge floc structure. *Water Sci. Technol.* 38, 45-53.
- Dong, H., R. Rothmel, T. Onstott, M. Fuller, M. DeFlaun, S. Streger, R. Dunlap, and M. Fletcher (2002). Simultaneous transport of two bacterial strains in intact cores from oyster, virginia: biological effects and numerical modeling. *Appl. Environ. Microbiol.* 68, 2120-2132.
- Donlan, R. M. and J. W. Costerton (2002). Biofilms: survival mechanisms of clinically relevant microorganisms. *Clin. Microbiol. Rev.* 15(2), 167-193.
- Douglas, S. and T. J. Beveridge (1998). Mineral formation by bacteria in natural microbial communities. *FEMS Microbiol. Ecol.* 26, 79-88.

- Dubois, M., K. A. Gilles, J. K. Hamilton, P. A. Rebers, and F. Smith (1956). Colorimetric method for determination of sugars and related substances. *Anal. Chem.* 28, 350–356.
- Dutta, L., H. E. Nuttall, A. L. Cunningham, G. James, and R. Hiebert (2005). In situ biofilm barriers: Case study of a nitrate groundwater plume, albuquerque, new mexico. *Remediation Journal* 15(4), 101–111.
- El-Masry, M., M. Hassouna, N. El-Rakshy, and E. I. Mousa (1995). Bacterial populations in the biofilm and non-biofilm components of a sand filter used in water treatment. *FEMS Microbiol. Lett.* 131(3), 263–269.
- Elimelech, M., J. Chen, and Z. Kuznar (2003). Particle deposition onto solid surfaces with micropatterned charge heterogeneity: the "hydrodynamic bump" effect. *Langmuir* 19(17), 6594–6597.
- Elimelech, M., J. Gregory, X. Jia, and R. A. Williams (1995). *Particle deposition and aggregation*. Colloid and Surface Engineering: Applications in the process industries. Butterworth-Heinemann.
- Elimelech, M., M. Nagai, C. Ko, and J. N. Ryan (2000). Relative insignificance of mineral grain zeta potential to colloid transport in geochemically heterogeneous porous media. *Environ. Sci. Technol.* 34, 2143–2148.
- Fang, Y. and B. Logan (1999). Bacterial transport in gas-sparged porous medium. *J. Envir. Engrg.* 125(7), 668–673.
- Ferris, F. G. (2000). Microbe-metal interactions in sediments. In R. Riding and S. Awramik (Eds.), *Microbial sediments*, pp. 121–126. Berlin: Springer.
- Fetter, C. (1998). *Contaminant hydrogeology* (2nd edition ed.). Prentice Hall.
- Flemming, H. C. (1995). Sorption sites in biofilms. *Water Sci. Technol.* 32(8), 27–33.
- Flemming, H. C., T. Griebe, and G. Schaule (1996). Antifouling strategies in technical systems - a short review. *Water Science Technology* 34(5-6), 517–524.
- Flemming, H. C. and A. Leis (2002). Sorption properties of biofilms. In G. Bitton (Ed.), *Encyclopedia of Environmental Microbiology*, Volume 5, pp. 2958–2967. New York: John Wiley Sons, Inc.
- Flemming, H. C., A. Leis, M. Strathmann, and C. Leon Morales (2005). The matrix reloaded - an interactive milieu. In A. McBain, D. Allison, J. Pratten, D. Spratt, M. Upton, and J. Verran (Eds.), *Biofilms: persistence and ubiquity*, pp. 67–81. Manchester: The biofilm club.

Flemming, H. C. and G. Schaule (1998). Biofouling on membranes - a microbiological approach. *Desalination* 70, 95-119.

Flemming, H. C., J. Schmitt, and K. C. Marshall (1996). Sorption properties of biofilms. In W. Calmano and U. Förstner (Eds.), *Environmental behaviour of sediments*, pp. 115-157. Chelsea, Michigan: Lewis Publishers.

Flemming, H.-C. and J. Wingender (2001a). Biofilme - die bevorzugte lebensform der bakterien. *Biologie in unserer Zeit* 31, 169-180.

Flemming, H. C. and J. Wingender (2001b). Relevance of microbial extracellular polymeric substances (EPS) - part I: Structural and ecological aspects. *Water Sci. Technol.* 43(6), 1-8.

Flemming, H. C. and J. Wingender (2001c). Relevance of microbial extracellular polymeric substances (EPS) - part II: Technical aspects. *Water Sci. Technol.* 43(6), 9-16.

Flemming, H. C. and J. Wingender (2003). The crucial role of extracellular polymeric substances in biofilms. In S. Wuertz, P. Bishop, and P. Wilderer (Eds.), *Biofilms in wastewater treatment. An interdisciplinary approach*, pp. 401. London: IWA Publishing.

Flemming, H.-C., J. Wingender, C. Mayer, V. Körstgens, and W. Borchard (2000). Cohesiveness in biofilm matrix polymers. In D. G. Allison, P. Gilbert, H. M. Lappin-Scott, and M. Wilson (Eds.), *Community Structure and Cooperation in Biofilms*, pp. 87-105. Cambridge: Cambridge University Press.

Flury, M. and N. Wai (2003). Dyes as tracers for vadose zone hydrology. *Reviews of Geophysics* 41(1).

Frølund, B., R. Palmgren, K. Keiding, and P. H. Nielsen (1996). Extraction of extracellular polymers from activated sludge using a cation exchange resin. *Water Res.* 30(8), 1749-1758.

Gannon, J. T., V. B. Manilal, and M. Alexander (1991). Relationship between cell surface properties and transport of bacteria through soil. *Appl. Environ. Microbiol.* 57(1), 190-193.

Gehrke, T., J. Telegdi, D. Thierry, and W. Sand (1998). Importance of extracellular polymeric substances from *Thiobacillus ferrooxidans* for bioleaching. *Appl. Environ. Microbiol.* 64(7), 2743-2747.

Gerlach, R., A. Cunningham, and F. Caccavo (1998, May). Formation of redox-reactive subsurface barriers using dissimilatory metal-reducing bacteria. In *Conference on Hazardous Waste Research*, Snow Bird, Utah, USA.

- Gottenbos, B., H. C. van der Mei, and H. J. Busscher (1999). Initial adhesion and surface growth of *Pseudomonas aeruginosa* on negatively and positively charged poly(methacrylates). *J Mater Sci* 10, 853-855.
- Grobe, S., J. Wingender, and H. Truper (1995). Characterization of mucoid *Pseudomonas aeruginosa* strains isolated from technical water systems. *J. Appl. Bacteriol.* 79, 94-102.
- Grolimund, D., M. Borkovec, K. Bartmettler, and H. Sticher (1996). Colloid-facilitated transport of strongly sorbing contaminants in natural porous media: a laboratory column study. *Environ. Sci. Technol.* 30, 3118-3123.
- Grolimund, D., M. Elimelech, and M. Borkovec (2001). Aggregation and deposition kinetics of mobile colloidal particles in natural porous media. *Colloids Surf., A* 191, 179-188.
- Grolimund, D., M. Elimelech, M. Borkovec, K. Barmettler, R. Kretzschmar, and H. Sticher (1998). Transport of in situ mobilized colloidal particles in packed soil columns. *Environ. Sci. Technol.* 32, 3562-3569.
- Gross, M. J., O. Albinger, D. G. Jewett, B. E. Logan, R. C. Bales, and R. G. Arnold (1995). Measurement of bacterial collision efficiencies in porous media. *Water Res.* 29(4), 1151-1158.
- Habash, M. B., H. C. van der Mei, G. Reid, and H. J. Busscher (1997). Adhesion of *Pseudomonas aeruginosa* to silicone rubber in a parallel plate flow chamber in the absence and presence of nutrient broth. *Microbiology-Uk* 143, 2569-2574.
- Harvey, R. (1997). Microorganisms as tracers in groundwater injection and recovery experiments: a review. *FEMS Microbiology Reviews* 20, 461-472.
- Hendricks, S. K., C. Kwok, M. C. Shen, T. A. Horbett, B. D. Ratner, and J. D. Bryers (2000). Plasma-deposited membranes for controlled release of antibiotic to prevent bacterial adhesion and biofilm formation. *Journal of Biomedical Materials Research* 50(2), 160-170.
- Hess, K. (2002). Multispecies reactive tracer test in an aquifer with spatially variable chemical conditions, cape cod, massachusetts: dispersive transport of bromide and nickel. *Water Resources Research* 38(8), 1-17.
- Holliger, C., S. Gaspard, G. Glod, C. Heijman, W. Schumacher, R. Schwarzenbach, and F. Vazquez (1997). Contaminated environments in the subsurface and bioremediation: organic contaminants. *FEMS Microbiol. Rev.* 20, 517-523.

- Holmqvist, P., J. K. G. Dhont, and P. R. Lang (2007). Colloidal dynamics near a wall studied by evanescent wave light scattering: Experimental and theoretical improvements and methodological limitations. *J Chem Phys* 126, 10.
- Horwath, W. R. (2002). Biomass: soil microbial biomass. In G. Bitton (Ed.), *Encyclopedia of environmental microbiology*, Volume 2, pp. 663-670. John Wiley & Sons, Inc.
- Hu, M. Z. C., J. M. Norman, B. D. Faison, and M. E. Reeves (1996). Biosorption of uranium by *Pseudomonas aeruginosa* strain CSU: Characterization and comparison studies. *Biotechnol. Bioeng.* 51(2), 237-247.
- Huettel, M., H. Roy, E. Precht, and S. Ehrenhauss (2003). Hydrodynamical impact on biogeochemical processes in aquatic sediments. *Hydrobiologia* 494, 231-236.
- Huettel, M. and A. Rusch (2000). Transport and degradation of phytoplankton in permeable sediment. *Limnol. Oceanogr.* 45(3), 534-549.
- Jahn, A. and P. H. Nielsen (1995). Extraction of extracellular polymeric substances (EPS) from biofilms using a cation exchange resin. *Water Sci. Technol.* 32(8), 157-164.
- Janssen, F., M. Huettel, and U. Witte (2005). Pore-water advection and solute fluxes in permeable marine sediments (ii): benthic respiration at three sandy sites with different permeabilities (german bight, north sea). *Limnol. Oceanogr.* 50(3), 779-792.
- Jaruwong, P., J. Aumpush, and R. Kiattikomol (2005). Uptake of cationic and azo dyes by montmorillonite in batch and column systems. *Thammasat Int. J. Sc. Techn.* 10(1), 47-56.
- Jewett, D. G., T. Hilbert, B. Logan, R. Arnold, and R. Bales (1995). Bacterial transport in laboratory columns and filters: influence of ionic strength and ph on collision efficiency. *Water Res.* 29(7), 1673-1680.
- Jewett, D. G., B. E. Logan, R. G. Arnold, and R. C. Bales (1999). Transport of *Pseudomonas fluorescens* strain P17 through quartz sand columns as a function of water content. *J. Contam. Hydrol.* 36(1-2), 73-89.
- Johnson, P., N. Sun, and M. Elimelech (1996). Colloid transport in geochemically heterogeneous porous media: modeling and measurements. *Environ. Sci. Technol.* 30, 3284-3293.
- Johnson, W., M. Martin, M. Gross, and B. Logan (1996). Facilitation of bacterial transport through porous media by changes in solution and surface properties. *Colloids and Surfaces A: Physicochemical and Engineering Aspects* 107, 263-271.

- Kieft, T. and T. Phelps (1997). Life in the slow lane: activities of microorganisms in the subsurface. In P. Amy and D. Haldeman (Eds.), *The microbiology of the terrestrial deep subsurface*, pp. 356. New York: Lewis publishers.
- Kim, S. and M. Corapcioglu (1997). The role of biofilm growth in bacteria-facilitated contaminant transport in porous media. *Transp. porous media* 26, 161-181.
- Knapp, E., J. Herman, G. Hornberger, and A. Mills. The effect of distribution of iron-oxyhydroxide grain coatings on the transport of bacterial cells in porous media. *Environmental Geology* 33(4), 243-248.
- Körstgens, V., H. C. Flemming, J. Wingender, and W. Borchard (2001). Influence of calcium ions on the mechanical properties of a model biofilm of mucoid pseudomonas aeruginosa. *Water Science and Technology* 43(6), 49-57.
- Kretzschmar, R., K. Barmettler, D. Grolimund, Y.-d. Yan, M. Borkovec, and H. Sticher (1997). Experimental determination of colloid deposition rates and collision efficiencies in natural porous media. *Water Resour. Res.* 33(5), 1129-1137.
- Kretzschmar, R., M. Borkovec, D. Grolimund, and M. Elimelech (1999). Mobile subsurface colloids and their role in contaminant transport. *Advances in Agronomy* 66, 121-193.
- Kretzschmar, R. and H. Sticher (1998). Colloid transport in natural porous media: influence of surface chemistry and flow velocity. *Phys. Chem. Earth* 23(2), 133-139.
- Kuehn, M., M. Mehl, M. Hausner, H.-J. Bungartz, and S. Wuerty (2001). Time-resolved study of biofilm architecture and transport processes using experimental and simulation techniques: the role of eps. *Water Science Technology* 43(8), 143-151.
- Laegdsmand, M., P. Moldrup, and L. de Jonge (2003). Colloid mobilization in an aggregated soil system as affected of organic matter and solution chemistry. *EGS - AGU - EUG Joint assembly, abstracts from meeting hold in Nice, France 6-11 April 2003*.
- Langley, S. and T. J. Beveridge (1999). Metal binding by *Pseudomonas aeruginosa* PAO1 is influenced by growth of the cells as a biofilm. *Can. J. Microbiol.* 45(7), 616-622.
- Leis, A., S. Schlicher, H. Franke, and M. Strathmann (2005). Optically transparent porous medium for nondestructive studies of microbial biofilm architecture and transport dynamics. *Appl. Environ. Microbiol.* 71(8), 4801-4808.
- Leon Morales, C. F., A. P. Leis, M. Strathmann, and H. C. Flemming (2004). Interactions between laponite and microbial biofilms in porous media: implications for colloid transport and biofilm stability. *Water Res.* 38(16), 3614-26.

- Leon Morales, C. F., M. Strathmann, and H. Flemming (2007). Influence of biofilms on the movement of colloids in porous media. implications for colloid facilitated transport in subsurface environments. *Water Res.* 41, 2059–2068.
- Li, Q. and B. Logan (1999). Enhancing bacterial transport for bioaugmentation of aquifers using low ionic strength solutions and surfactants. *Water Res.* 33(4), 1090–1100.
- Liu, D., P. Johnson, and M. Elimelech (1995). Colloid deposition dynamics in flow through porous media: role of electrolyte concentration. *Environ. Sci. Technol.* 29, 2963–2973.
- López Arbeloa, F., J. Herrán Martínez, T. López Arbeloa, and I. López Arbeloa (1998). The hydrophobic effect on the adsorption of rhodamines in aqueous suspensions of smectites. the rhodamine 3B/laponite B system. *Langmuir* 14, 4566–4573.
- López Arbeloa, F., M. Tapia Estévez, T. López Arbeloa, and I. López Arbeloa (1996). Spectroscopic study of the adsorption of rhodamine 6G on clay minerals in aqueous suspensions. *Clay Miner.* 32, 97–106.
- Lowry, O. H., N. J. Rosenbrough, A. L. Farr, and R. J. Randall (1951). Protein measurement with the folin phenol reagent. *J. Biol. Chem.* 193, 265–275.
- Ludvigsen, L., H.-J. Albrechtsen, G. Heron, P. Bjerg, and T. Christensen (1998). Anaerobic microbial redox processes in a landfill leachate contaminated aquifer (Grindsted, Denmark). *J. Contam. Hydrol.* 33, 273–291.
- Majone, M., M. P. Papini, and E. Rolle (1998). Influence of metal speciation in landfill leachates on kaolinite sorption. *Water Res.* 32(3), 882–290.
- Margulies, L., H. Rozen, and S. Nir (1988). Model for competitive adsorption of organic cations on clays. *Clays and Clay Minerals* 36, 270–276.
- Martin, M., B. Logan, W. Johnson, D. Jewett, and R. Arnold (1996). Scaling bacterial filtration rates in different sized porous media. *Journal of Environmental Engineering-ASCE* 122(5), 407–415.
- Martin, R. E., L. M. Hanna, and E. J. Bouwer (1991). Determination of bacterial collision efficiencies in a rotating disk system. *Environ Sci Technol* 25, 2075–2082.
- Mayer, C., R. Moritz, C. Kirschner, W. Borchard, R. Maibaum, J. Wingender, and H. C. Flemming (1999). The role of intermolecular interactions: studies on model systems for bacterial biofilms. *International Journal of Biological Macromolecules* 26(1), 3–16.

- McCarthy, J. and L. McKay (2004). Colloid transport in the subsurface: past, present, and future challenges. *Vadose Zone Journal* 3, 326-337.
- McCarthy, J., L. McKay, and D. Bruner (2002). Influence of ionic strength and cation charge on transport of colloidal particles in fractured shale saprolite. *Environmental science and technology* 36(17), 3735-3743.
- Neu, T. R. (1996). Significance of bacterial surface-active compounds in interaction of bacteria with interfaces. *Microbiol. Rev.* 60(1), 151-166.
- Neville, A., T. Hodgkiess, and A. P. Morizot (1999). Electrochemical assessment of calcium carbonate deposition using a rotating disc electrode (rde). *J Appl Electrochem* 29(4), 455-462.
- Nicolai, T. and S. Cocard (2001). Dynamic light-scattering study of aggregating and gelling colloidal disks. *J. Colloid Interface Sci.* 244, 51-57.
- Nielsen, P. H., A. Jahn, and R. Palmgren (1997). Conceptual model for production and composition of exopolymers in biofilms. *Water Sci. Technol.* 36(1), 11-19.
- Nivens, D. E., R. A. Palmer, and D. C. White (1995). Continuous nondestructive monitoring of microbial biofilms: a review of analytical techniques. *J. Ind. Microbiol.* 15, 263-276.
- Ogata, A. (1970). Theory of dispersion in a granular medium. *U.S. Geological Survey Paper 411-I*, 1-34.
- Ohman, D. E. and A. M. Chakrabarty (1981). Genetic mapping of chromosomal determinants for the production of the exopolysaccharide alginate in a *Pseudomonas aeruginosa* cystic fibrosis isolate. *Infect. Immun.* 33(1), 142-148.
- Okabe, S., H. Kuroda, and Y. Watanabe (1998). Significance of biofilm structure on transport of inert particulates into biofilms. *Water Sci. Technol.* 38(8-9), 163-170.
- O'Toole, G. A. and R. Kolter (1998). Flagellar and twitching motility are necessary for *Pseudomonas aeruginosa* biofilm development. *Mol. Microbiol.* 30(2), 295-304.
- Pang, L., M. E. Close, M. J. Noonan, M. J. Flintoft, and P. van den Brink (2005). A laboratory study of bacteria-facilitated cadmium transport in alluvial gravel aquifer media. *J. Environ. Qual.* 34(1), 237-247.
- Parker, D. L., B. R. Schram, J. L. Plude, and R. E. Moore (1996). Effect of metal cations on the viscosity of a pectin-like capsular polysaccharide from the *Cyanobacterium Microcystis flos-aquae* C3-40. *Appl. Environ. Microbiol.* 62(4), 1208-1213.

- Petalas, C. P. and I. B. Diamantis (1999). Origin and distribution of saline groundwaters in the upper miocene. *Hydrogeology Journal* 7, 305–316.
- Powelson, D. and A. Mills (2001). Transport of *Escherichia coli* in sand columns with constant and changing water contents. *J. Environ. Qual.* 30, 238–245.
- Raiders, R. A., R. M. Knapp, and M. J. McInerney (1989). Microbial selective plugging and enhanced oil recovery. *J. Ind. Microbiol.* 4, 215–230.
- Rashid, M. H. and A. Kornberg (2000). Inorganic polyphosphate is needed for swimming, swarming, and twitching motilities of *Pseudomonas aeruginosa*. *Proc. Natl. Acad. Sci. U. S. A.* 97(9), 4885–4890.
- Redman, J., S. Walker, and M. Elimelech (2003). Bacterial adhesion and transport in porous media: role of the secondary energy minimum. *Environ. Sci. Technol.*
- Ren, J., A. Packman, and C. Welty (2000). Correlation of colloid collision efficiency with hydraulic conductivity of silica sands. *Water Resour. Res.* 36(9), 2493–2500.
- Rijnaarts, H. H. M. (1994). *Interactions between bacteria and solid surfaces in relation to bacterial transport in porous media*. Phd, Wageningen.
- Rijnaarts, H. H. M., W. Norde, J. Lyklerna, and A. Zehnder (1999). Dvvo and steric contributions to bacterial deposition in media of different ionic strengths. *Colloids Surf., B* 14, 179–195.
- Rittmann, B. E. (1993). The significance of biofilms in porous media. *Water Resour. Res.* 29(7), 2195–2202.
- Rogers, B. and B. Logan (2000). Bacterial transport in NAPL-contaminated porous media. *J. Envir. Engrg.* 126(7), 657–666.
- Ryan, J. and M. Elimelech (1996). Colloid mobilization and transport in groundwater. *Colloids Surf., A* 107, 1–56.
- Ryan, J., M. Elimelech, R. Ard, R. Harvey, and P. Johnson (1999). Bacteriophage PRD1 and silica colloid transport and recovery in an iron oxide-coated sand aquifer. *Environ. Sci. Technol.* 33, 63–73.
- Saiers, J. and J. Lenhart (2003). Ionic-strength effects on colloid transport and interfacial reactions in partially saturated porous media. *Water Resour. Res.* 39(9), 1–13.
- Sambrook, J., E. F. Fritsch, and T. Maniatis (1989). *Molecular cloning: a laboratory manual*. New York: Cold Spring Harbor Laboratory Press.

- Sauer, K. and A. K. Camper (2001). Characterization of phenotypic changes in *Pseudomonas putida* in response to surface-associated growth. *J. Bacteriol.* 183(22), 6579-6589.
- Sauer, K., A. K. Camper, G. D. Ehrlich, J. W. Costerton, and D. G. Davies (2002). *Pseudomonas aeruginosa* displays multiple phenotypes during development as a biofilm. *J. Bacteriol.* 184(4), 1140-1154.
- Schmitt, J. and H. C. Flemming (1999). Water binding in biofilms. *Water Sci. Technol.* 39(7), 77-82.
- Schmitt, J., D. Nivens, D. C. White, and H. C. Flemming (1995). Changes of biofilm properties in response to sorbed substances - an FTIR-ATR study. *Water Sci. Technol.* 32(8), 149-155.
- Schultze-Lam, S., D. Fortin, B. S. Davis, and T. J. Beveridge (1996). Mineralization of bacterial surfaces. *Chem. Geol.* 132, 171-181.
- Shaw, D. J. (1980). *Introduction to Colloid and Surface Chemistry* (3rd ed.). London: Butterworth-Heinemann Ltd.
- Shaw, J. C., B. Bramhill, N. C. Wardlaw, and J. W. Costerton (1985). Bacterial fouling in a model core system. *Appl. Environ. Microbiol.* 49(3), 693-701.
- Skoog, D., D. West, and F. Holler (1996). *Fundamentals of analytical chemistry* (7th ed.). Saunders college publishing.
- Smets, B. F., D. Grasso, M. Engwall, and B. Machinist (1999). Surface physicochemical properties of *Pseudomonas fluorescens* and impact on adhesion and transport through porous media. *Colloids Surf., B* 14(1-4), 121-139.
- Song, L. and M. Elimelech (1993). Dynamics of colloid deposition in porous media: modeling the role of retained particles. *Colloids Surfaces, A: Physicochemical and Engineering Aspects* 73, 49-63.
- Späth, R., H. C. Flemming, and S. Wuertz (1998). Sorption properties of biofilms. *Water Science and Technology* 37(4-5), 207-210.
- Stoodley, P., J. D. Boyle, D. DeBeer, and H. M. Lappin-Scott (1999). Evolving perspectives of biofilm structure. *Biofouling* 14(1), 75-90.
- Stoodley, P., D. deBeer, and Z. Lewandowski (1994). Liquid flow in biofilm systems. *Appl. Environ. Microbiol.* 60(8), 2711-2716.

- Stoodley, P., I. Dodds, D. de Beer, H. LappinScott, and J. D. Boyle (2005). Flowing biofilms as a transport mechanism for biomass through porous media under laminar and turbulent conditions in a laboratory reactor system. *Biofouling* 21(3/4), 161-168.
- Strauss, J. and C. Bolster (2004). Detachment of bacteria from porous media in laboratory columns. *American Geophysical union, spring meeting 2004*.
- Sutherland, I. (2001). Biofilm exopolysaccharides: a strong and sticky framework. *Microbiology* 147(Pt 1), 3-9.
- Sutherland, I. W. (1994). Structure-function relationships in microbial exopolysaccharides. *Biotechnol. Adv.* 12, 393-448.
- Tapia Estévez, M., F. López Arbeloa, T. López Arbeloa, and I. López Arbeloa (1993). Absorption and fluorescence properties of rhodamine 6g adsorbed on aqueous suspensions of wyoming montmorillonite. *Langmuir* 9, 3629-3634.
- Tapia Estévez, M., F. López Arbeloa, T. López Arbeloa, I. López Arbeloa, and R. Schoonheydt (1994). Spectroscopic study of the adsorption of rhodamine 6G on laponite b for low loadings. *Clay Miner.* 29, 105-113.
- Tatalovich, M., K. Lee, and C. Chrysikopoulos (2000). Modeling the transport of contaminants originating from the dissolution of DNAPL pools in aquifers in the presence of dissolved humic substances. *Transp. porous media* 38, 93-115.
- Taylor, S. W. and P. R. Jaffe (1990a). Biofilm growth and the related changes in the physical properties of a porous medium. 1. experimental investigation. *Water Resour. Res.* 26(9), 2153-2159.
- Taylor, S. W. and P. R. Jaffe (1990b). Biofilm growth and the related changes in the physical properties of a porous medium. 3. dispersivity and model verification. *Water Resources Research* 26(9), 2171-2180.
- Tielker, D., S. Hacker, R. Loris, M. Strathmann, J. Wingender, S. Wilhelm, F. Rosenau, and K.-E. Jaeger (2005). *Pseudomonas aeruginosa* lectin LecB is located in the outer membrane and is involved in biofilm formation. *Microbiology* 151, 1313-1323.
- Tong, M., X. Li, C. Brow, and W. Johnson (2005). Detachment-influenced transport of an adhesion-deficient bacterial strain within water-reactive porous media. *Environmental science and technology* 39, 2500-2508.
- Tsuneda, S., H. Aikawa, H. Hayashi, and A. Hirata (2004). Significance of cell electrokinetic properties determined by soft-particle analysis in bacterial adhesion onto a solid surface. *J Colloid Interface Sci* 279, 410-417.

- Tsuneda, S., H. Aikawa, H. Hayashi, A. Yuasa, and A. Hirata (2003). Extracellular polymeric substances responsible for bacterial adhesion onto solid surface. *FEMS Microbiology Letters*, 287-292.
- Tufenkji, N. and M. Elimelech (2004). Deviation from the classical colloid filtration theory in the presence of repulsive dlvo interactions. *Langmuir* 20, 10818-10828.
- Tufenkji, N. and M. Elimelech (2005). Breakdown of colloid filtration theory: role of the secondary energy minimum and surface charge heterogeneities. *Langmuir* 21, 841-852.
- Tufenkji, N., J. Ryan, and M. Elimelech (2002). The promise of bank filtration. *Environ. Sci. Technol.*, 423-428.
- van der Mei, H. C., B. van de Belt-Gritter, G. Reid, H. Bialkowska-Hobrzanska, and H. J. Busscher (1997). Adhesion of coagulase-negative staphylococci grouped according to physico-chemical surface properties. *Microbiology-Uk* 143, 3861-3870.
- Vandevivere, P. and P. Baveye (1992). Effect of bacterial extracellular polymers on the saturated hydraulic conductivity of sand columns. *Appl. Environ. Microbiol.* 58(5), 1690-1698.
- Verwey, E. J. W. and J. T. G. Overbeek (1948). *Theory of the stability of lyophobic colloids*. Elsevier.
- Vogt, M., H. C. Flemming, and W. S. Veeman (2000). Diffusion in *Pseudomonas aeruginosa* biofilms: a pulsed field gradient NMR study. *J. Biotechnol.* 77(1), 137-146.
- Walker, S. L., J. E. Hill, J. A. Redman, and M. Elimelech (2005). Influence of growth phase on adhesion kinetics of *Escherichia coli* d21g. *Appl Environ Microbiol* 71(6), 3093-3099.
- Wanner, O., A. B. Cunningham, and R. Lundman (1995). Modeling biofilm accumulation and mass-transport in a porous-medium under high substrate loading. *Biotechnol. Bioeng.* 47(6), 703-712.
- Weerkamp, A. H., H. M. Uyen, and H. J. Busscher (1988). Effect of zeta potential and surface energy on bacterial adhesion to uncoated and saliva-coated human enamel and dentin. *J Dent Res* 67(12), 1483-1487.
- Westbrook, S. J., J. L. Rayner, G. B. Davis, T. P. Clement, P. L. Bjerg, and S. J. Fisher (2005). Interaction between shallow groundwater, saline surface water and contaminant discharge at a seasonally and tidally forced estuarine boundary. *Journal of Hydrology* 302, 255-269.

- Wingender, J. and K.-E. Jaeger (2002). Extracellular enzymes in biofilms. In G. Bitton (Ed.), *Encyclopedia of Environmental Microbiology*, Volume 3, pp. 1207–1223. New York: John Wiley Sons, Inc.
- Wingender, J., T. R. Neu, and H.-C. Flemming (1999). What are bacterial extracellular polymeric substances? In J. Wingender, T. R. Neu, and H.-C. Flemming (Eds.), *Microbial Extracellular Polymeric Substances*, pp. 1–19. Berlin: Springer-Verlag.
- Wingender, J., M. Strathmann, A. Rode, A. Leis, and H.-C. Flemming (2001). Isolation and biochemical characterization of extracellular polymeric substances from *Pseudomonas aeruginosa*. *Meth. Enzymol.* 336(25), 302–314.
- Wolfaardt, G. M., J. R. Lawrence, R. D. Robarts, and D. E. Caldwell (1998). In situ characterization of biofilm exopolymers involved in the accumulation of chlorinated organics. *Microb. Ecol.* 35(3), 213–223.
- Yang, J. L., R. Bos, G. F. Belder, J. Engel, and H. J. Busscher (1999). Deposition of oral bacteria and polystyrene particles to quartz and dental enamel in a parallel plate and stagnation point flow chamber. *Journal of Colloid Interface Science* 220(2), 410–418.
- Yao, K., M. Habibian, and C. O'Melia (1971). Water and waste water filtration - concepts and applications. *Environ. Sci. Technol.* 5, 1105–1112.
- Yariv, S., M. Müller Vonmoos, G. Kahr, and A. Rub (1989). Thermal analytic study of the adsorption of acridine orange by smectite minerals. *Journal of Thermal Analysis and Calorimetry* 35(6), 1997–2008.
- Yermiyahu, Z., I. Lapidés, and S. Yariv (2003). Visible absorption spectroscopy study of the adsorption of congo red by montmorillonite. *Clay Miner.* 38(4), 483–500.
- Zhang, W., E. Bouwer, L. Wilson, and N. Durant (1995). Biotransformation of aromatic-hydrocarbons in subsurface biofilms. *Water Sci. Technol.* 31(1), 1–14.
- Zobell, C. E. (1943). The effect of solid surfaces upon bacterial activity. *J. Bacteriol.* 46, 39–56.

Curriculum Vitae

Carlos Felipe Leon Morales
Peterstal 11, 47051 Duisburg

Personal Data

- Date of birth 23.11.1975
- Place of birth Santafé de Bogotá, Colombia
- Marital status Married
- Nationality Colombian

High School and Undergraduate Studies

- 1986-1992 Colegio Cooperativo Champagnat, Palmira, Colombia. High School Degree.
- 1993-1999 Pontificia Universidad Javeriana, Bogotá, Colombia. Final project: Antagonic effect of lactic acid bacteria isolated from diary products over *Salmonella enteritidis* (spanish). BSc. Industrial Microbiology.

Graduate Studies

- 1999-2001 Saxion Hogeschool Ijselland, The Netherlands / University of Greenwich, United Kingdom. Final project: Assessment of substances that may enhance the anaerobic biodegradation of BTEX in contaminated groundwater environments. A distinction mark was obtained for this final work. MSc. Environmental Technology.
- Since 2002 Biofilm Centre, University of Duisburg-Essen. PhD student. Supervision: Prof. Hans-Curt Flemming.

Practical and Training periods

- 1998-1999 Sucromiles S.A. A fermentation based alcohol and citric acid producing plant. Cali, Colombia. Practicing student of Microbiology in the ethanol production plant.
- July-November 2001 Wageningen University. The Netherlands. Research-training period. Laboratory of Microbiology. Supervisor: Dr. Gosse Schraa and Dr. Miriam van Eeckert. Quinone use by some anaerobic microorganisms.
- January-February 2002 University of Portsmouth. School of Pharmacy and Biomedical Sciences. United Kingdom. Research-training period. Applied Microbiology Laboratory. Supervisor: Dr. Iwona Beech. Growth of microbial biofilms *in situ*. Assessment of different anaerobic techniques and media for the growth of Sulfate Reducing Bacteria (SRB).

Erklärung / Declaration

Hiermit erkläre ich, die vorliegende Arbeit selbständig verfasst zu haben. Es wurden nur die angegebenen Hilfsmittel genutzt. Alle Stellen, die im Wortlaut oder dem Sinn nach anderen Arbeiten entnommen wurden, habe ich unter Angabe der Quelle als Entlehnung kenntlich gemacht.

Herewith I declare that this thesis is the result of my independent work. All sources and auxiliary materials used by me in this thesis are cited completely.

Duisburg, 21.12.2007

(C.F. Leon Morales)